THE UNIVERSITY OF ALBERTA

PERFORMANCE AND ANALYSIS OF A 45 MB/S FIBER OPTIC SYSTEM USING DFSK WITH OPTICAL SELF-HETERODYNE DETECTION

by

SUNIT LOHTIA ©

A THESIS
SUBMITTED TO THE FACULTY OF GRADUATE STUDIES AND RESEARCH
IN PARTIAL FULFILMENT OF THE REQUIREMENTS FOR THE DEGREE
OF **MASTER OF SCIENCE**

DEPARTMENT OF ELECTRICAL ENGINEERING

EDMONTON, ALBERTA
FALL 1989

THE UNIVERSITY OF ALBERTA

RELEASE FORM

NAME OF AUTHOR: SUNIT LOHTIA

TITLE OF THESIS: PERFORMANCE AND ANALYSIS OF A 45 MB/S FIBER OPTIC SYSTEM USING DFSK WITH OPTICAL SELF-HETERODYNE DETECTION.

DEGREE: MASTER OF SCIENCE

YEAR THIS DEGREE GRANTED: FALL 1989

Permission is hereby granted to THE UNIVERSITY OF ALBERTA LIBRARY to reproduce single copies of this thesis and to lend or sell such copies for private, scholarly or scientific research purposes only.

The author reserves other publication rights, and neither the thesis nor extensive extracts from it may be printed or otherwise reproduced without the author's written permission.

(SIGNED) Sunit Lohtia

PERMANENT ADDRESS:

# BA-5,
REGIONAL ENGINEERING COLLEGE,
KURUKSHETRA, HARYANA
INDIA 132119

DATED: SEP. 27, 1989

THE UNIVERSITY OF ALBERTA

FACULTY OF GRADUATE STUDIES AND RESEARCH

The undersigned certify that they have read, and recommend to the Faculty of Graduate Studies and Research for acceptance, a thesis entitled PERFORMANCE AND ANALYSIS OF A 45 MB/S FIBER OPTIC SYSTEM USING DFSK WITH OPTICAL SELF-HETERODYNE DETECTION submitted by SUNIT LOHTIA in partial fulfilment of the requirements for the degree of MASTER OF SCIENCE in Electrical Engineering.

Co-supervisor

C. G. Englefield

Co-supervisor

G. D. Cormack

Date Sept 8th 1989

DEDICATED TO

my father Rajinder Paul Lohtia, my mother Chand Lohtia and my brother Anit Lohtia who have been encouraging and caring for me.

ABSTRACT

A 45 Mb/s optical differential frequency shift keying (DFSK) system is developed and its characteristics are studied. It is observed that, even when the transmitting laser has a broad linewidth, a bit error rate (BER) of less than 10^{-9} can be obtained. The effect of the broad linewidth is to produce a wide linewidth IF signal, which increases the bandwidth requirement for the IF filter. For a 45 Mb/s data rate and a laser with 22 MHz linewidth, the optimum bandwidth of the IF filter is 650 MHz. This value of the required bandwidth agrees well with the existing theoretical results. If the bandwidth of the IF filter is reduced, part of the IF spectrum is lost, and a degradation in the error rate performance is observed. Also, the BER is found to be pattern dependent; for example, for three consecutive '1' bits and '0' bits in a row, an error rate floor develops at 10^{-8}. This BER floor for data with a relatively high low frequency content is due mainly to the non-uniform frequency modulation (FM) response of the laser diode (LD). To compensate for this effect, the NRZ data is Manchester encoded. With Manchester encoding, a BER of less than 10^{-9} is achieved for a pseudo-random bit sequence of length 2^{23}-1. This suggests that, for a DFSK system, the transmitted signal should have neither dc nor low frequency content.

The characteristics of the DFSK system are also studied for the case when two channels are transmitted simultaneously. The interference caused by the phase noise in the second channel is very small and causes a negligible power penalty. A theoretical calculation of the signal to interference ratio as a function of the channel spacing is also presented. For a DFSK system with an IF linewidth-to-bit-rate ratio of 1.0, the desired channel spacing for minimum interference should be 15 times the bit-rate to achieve a signal to interference ratio of 20 dB.

ACKNOWLEDGEMENTS

I would like to express my sincere thanks and respect to Dr. Paul A. Goud and Dr. Colin G. Englefield for their inspiring guidance, help and encouragement. I am also grateful to Dr. George D. Cormack for the loan of equipment for this project. My special thanks are also due to Ms. Azmina Somani and Dr. Jann Binder for several technical suggestions and stimulating discussions. This project benefitted greatly from the preliminary work carried out by Dr. Goud and Ms. Azmina Somani at the Alberta Telecommunications Research Centre (ATRC) under Bell-Northern Research (BNR) sponsorship. I am indebted to ATRC for providing a Graduate Scholarship and the facilities during the course of this work. Further I wish to extend my gratitude to the members of the examining committee for reviewing this work.

In addition, I would like to acknowledge the following:

- Mr. Bert Telder for building the Manchester encoder and decoder.
- Mr. George Fraser (ATRC) for his valuable suggestions concerning high frequency circuit design.
- Mr. Kevin Jacobsen, Mr. Marc Veilleux and Mr. Yan Loke for their co-operation in the optics lab at ATRC.
- Mr. Joseph Ip (BNR) for providing DFB laser diodes.
- Mr. Stephen Vandenbrink, Ms. Chen Zhijing and Mr. V.A. Anand for sharing the data generator and the error detector.

My appreciation is due to my uncle Vinod and his family for their love and for inviting me over for supper on several fine evenings. I should also convey thanks to my friends, teachers, and everyone who has helped me in one way or another in completing the work reported in this thesis.

TABLE OF CONTENTS

CHAPTER PAGE

1. INTRODUCTION 1
- 1.1 INTENSITY MODULATION DIRECT DETECTION SYSTEMS 3
- 1.2 COHERENT OPTICAL SYSTEMS 5
- 1.3 MODULATION/DEMODULATION FORMATS 10
- 1.4 THESIS OBJECTIVES AND ORGANISATION 13
  - 1.4.1 Thesis organisation 15

2. DFSK PRINCIPLE AND EXPERIMENTAL SETUP 16
- 2.1 DFSK PRINCIPLE 16
  - 2.1.1 Differential encoding and decoding 17
  - 2.1.2 Advantages 21
  - 2.1.3 Limitations 22
    - 2.1.3.1 Receiver sensitivity 22
    - 2.1.3.2 Power penalty 22
    - 2.1.3.3 Bandwidth limitations 23
- 2.2 DFSK FOR MULTI-CHANNEL TRANSMISSION 23
- 2.3 EXPERIMENTAL SETUP 27
- 2.4 SUMMARY 31

3. THEORETICAL ANALYSIS FOR A DFSK SYSTEM 32
- 3.1 REQUIRED OPTICAL SOURCE CHARACTERISTICS 32
  - 3.1.1 Laser linewidth 33
  - 3.1.2 Frequency modulation characteristics 34
- 3.2 POWER SPECTRAL ANALYSIS 38
- 3.3 BIT ERROR RATE CALCULATIONS 42
- 3.4 CROSS-TALK PENALTY IN TWO-CHANNEL TRANSMISSION 48
- 3.5 RECEIVER NOISE ANALYSIS 50
- 3.6 SUMMARY 53

4. TRANSMITTER DESIGN 56
- 4.1 TRANSMITTER COMPONENTS 56
  - 4.1.1 DFB laser diode 56
  - 4.1.2 GRIN rod lens 59
  - 4.1.3 Optical isolator 59
  - 4.1.4 Manchester encoder 60
  - 4.1.5 Differential encoder 61
  - 4.1.6 Laser driver circuit 65
  - 4.1.7 Cooling circuit 68
- 4.2 EXPERIMENTAL MEASUREMENTS 68
  - 4.2.1 Wavelength measurements 68
  - 4.2.2 Linewidth and frequency deviation measurements 71
- 4.3 MEASURING/MONITORING EQUIPMENT 76
  - 4.3.1 Scanning monochromator and Fabry Perot interferometer 76
  - 4.3.2 Self-heterodyne setup 78
- 4.4 SUMMARY 80

5. RECEIVER DESIGN 82
  5.1 PINFET RECEIVER 82
  5.2 BAND PASS FILTER 89
  5.3 HIGH FREQUENCY AMPLIFIER 90
  5.4 ENVELOPE DETECTOR 94
  5.5 LOW PASS FILTER 96
  5.6 MANCHESTER DECODER 98
  5.7 SUMMARY 99

6. SYSTEM MEASUREMENTS 100
  6.1 POWER SPECTRUM MEASUREMENTS 100
    6.1.1 Received signal at pre-amplifier 101
    6.1.2 Received signal at bandpass filter 101
  6.2 RECEIVED SIGNAL WAVEFORMS 103
  6.3 BIT ERROR RATE MEASUREMENTS 107
    6.3.1 Single channel DFSK system 107
    6.3.2 Manchester-differential encoded signal 110
    6.3.3 Two-channel transmission 113
  6.4 SUMMARY 117

7. SUMMARY AND CONCLUSIONS 118

8. REFERENCES 122

APPENDIX A 127

APPENDIX B 133

LIST OF TABLES

TABLE PAGE

1 Receiver sensitivities for various modulation techniques 9

2 Frequency state table for differentially encoded signal 17

LIST OF FIGURES

FIGURE PAGE

1.1 Progress in the bit-rate distance product in optical communication systems during recent years 2

1.2 Block diagram of a sub-carrier multiplexing system 4

1.3 Block diagram of a coherent optical fiber transmission system 7

1.4 A star configuration for local area networks 12

2.1 A general dual detector receiver 16

2.2 Differential encoding and delay line detection 19

2.3 A 4-level coding and dual filter detection for DFSK system 24

2.4 a) A topology for multi-channel optical DFSK system.
b) Electrical power spectrum at the receiver 25

2.5 Multi-channel DFSK system using tunable optical filter at the receiver 28

2.6 Experimental setup for DFSK system 29

3.1 Frequency modulation characteristics of DFB laser diodes.
a) Conventional DFB.
b) Phase tunable DFB 37

3.2 Laser output spectrum for a DFSK system with no modulation signal 41

3.3 Theoretical BER as a function of the received signal to noise ratio 47

3.4 BER as a function of the received optical power for different IF linewidths and a filter bandwidth of $5R_b$ 47

3.5 SIR as a function of the normalised channel spacing for a DFSK system 51

3.6 Receiver noise components as a function of the filter bandwidth.
a) IF linewidth = $0.3R_b$.
b) IF linewidth = $0.4R_b$.
c) IF linewidth = $0.5R_b$ 54

4.1 Detailed diagram of single channel DFSK transmitter 57

4.2 Manchester encoder and clock doubler circuit 60

4.3 Timing diagram for
  a) Manchester encoder.
  b) Clock doubler 62

4.4 Signal waveforms at the transmitter.
  a) The NRZ data (upper trace) and the Manchester encoded signal (lower trace) for a data pattern of 111101100001110 The differentially encoded signal is delayed by two bit periods as compared to input signal.
  b) The clock signal for a 45 Mb/s data rate (upper trace) and the clock signal at the output of the clock doubler circuit 63

4.5 Circuit diagram of the differential encoder 64

4.6 The input signal (upper trace) and the differential encoded output signal (lower trace) for a data pattern of 111101100001110... The differentially encoded signal is delayed by two bit periods as compared to the input signal 64

4.7 Circuit diagram of laser driver circuit 66

4.8 Optical pulses received from the LD 67

4.9 Circuit diagram of the laser cooler circuit 69

4.10 Laser output spectrum of the LDs measured by a scanning monochromator.
  a) NEC quarter wave shifted DFB laser.
  b) Fujitsu DFB laser 70

4.11 Output power spectrum of the LDs measured by a Fabry-Perot interferometer 72

4.12 Linewidth of the NEC quarter wave shifted DFB LD for different bias currents measured by the delayed self-heterodyne setup 73

4.13 Linewidth of the Fujitsu DFB LD for different bias currents measured by the delayed-self-heterodyne setup 74

4.14 Scanning monochromator setup for laser wavelength measurements 77

4.15 Fabry-Perot interferometer setup for laser spectrum measurements 77

4.16 Delayed self-heterodyne system for high resolution linewidth measurements 79

5.1 Block diagram of the experimental DFSK receiver 83

5.2 Most commonly used receivers for optical fiber systems 85

5.3 Circuit diagram of the single detector PINFET receiver 86

5.4 Frequency response of the PINFET amplifier.
a) GaAs FET pre-amplifier without PIN photodiode.
b) PIN photodiode and FET pre-amplifier.................................... 88

5.5 Configuration of a dual detector receiver.................................... 89

5.6 Bandpass filter with a passband of about 650 MHz.
a) Schematic diagram.
b) Frequency response.................................... 91

5.7 Frequency response of filter 2 (Telonic TBP-1000-300-8SS).................................... 92

5.8 Schematic diagram of high frequency power amplifier.................................... 92

5.9 Frequency response of high frequency amplifiers.
a) Amplifier 1 with a gain of 22 dB.
b) Amplifier 2 with a gain of 33 dB.................................... 93

5.10 Schottky diode square law detector.
a) Circuit diagram.
b) Frequency response.................................... 95

5.11 Low pass filter.
a) Circuit diagram.
b) Frequency response.................................... 97

5.12 Circuit diagram of the Manchester decoder.................................... 98

6.1 Power spectrum of the received signal.
a) No modulation signal applied to the LD.
b) For 1.6 mA peak to peak modulation current.................................... 102

6.2 Power spectrum of the IF signal at the output of the filter 1.
a) With modulation signal applied to the LD.
b) Without modulation signal.................................... 104

6.3 The transmitted signal waveforms (upper traces) and the received signal waveforms (lower traces) for different data patterns.
a) Bit pattern: 101010........
b) Bit pattern: 1000001010101010.... 105

6.4 The transmitted signal waveforms (upper traces) and the received signal waveforms (lower traces) after Manchester encoder and the decoder were implemented.
a) Bit pattern: 1111000001001010.......
b) Bit pattern: 1111111101111110....... 106

6.5 BER as a function of the received average optical power. The bandwidth of the IF filter was 650 MHz.
a) Bit pattern: 101010.......
b) Bit pattern: 11001100.....
c) Bit pattern: 111000111000.................................... 108

6.6 BER as a function of the received average optical power with an IF filter of 300 MHz bandwidth.
a) Bit pattern: 101010......
b) Bit pattern: 11001100 109

6.7 Filter bandwidth requirements as a function of the IF linewidth to bit-rate ratio 111

6.8 BER as a function of the received average optical power for a Pseudo random bit sequence of 2^{23}-1 . These measurements were carried out after the Manchester encoder was incorporated in the experimental system 112

6.9 BER as a function of the received average optical power for two channel transmission.
a) Second channel off.
b) Average optical power in second channel = 10 μW.
c) Average optical power in second channel = 20 μW 115

6.10 Power spectrum of the interference signal caused by the second channel (upper trace). The lower trace corresponds to the receiver noise when both the channels are off.
a) Average optical power in second channel = 10 μW.
b) Average optical power in second channel = 20 μW 116

B.1 Optical power output as a function of the bias current for NEC DFB LD 133

B.2 Optical power output as a function of the bias current for Fujitsu DFB LD 134

B.3 Thermistor resistance calibration 135

B.4 Equivalent circuit of the GaAs FET 136

LIST OF ABBREVIATIONS

AGC:	Automatic gain control.
APD:	Avalanche photodiode.
ASK:	Amplitude shift keying.
BER:	Bit error rate.
BPF:	Band pass filter.
DFB:	Distributed feedback.
DFSK:	Differential frequency shift keying.
FDM:	Frequency division multiplexed.
FSK:	Frequency shift keying.
IMD:	Intermodulation distortion.
IMDD:	Intensity modulation direct detection system.
LD:	Laser diode.
LED:	Light emitting diode.
LO:	Local oscilllator
NRZ:	Non return to zero.
PDF:	Probability density function.
PSK:	Phase shift keying.
SCM:	Subcarrier multiplexing.
SIR:	Signal to interference ratio.
SMSR:	Side mode suppression ratio.
TDM:	Time division multiplexing.
WDM:	Wavelength division multiplexing.

CHAPTER 1 - INTRODUCTION

In the past decade, there has been a tremendous growth in the technology and deployment of optical fiber communication systems, which is still continuing apace. This can be attributed to the many advantages of optical fiber cables over coaxial cables, such as low loss, low cost, high bandwidth, high security, small size and lack of RF (radio frequency) interference. Since the advent of fiber optic systems, there has been a continuing advance in the ability to transmit increasingly high data rates over ever longer distances. Fig. 1.1 shows the trend of the increasing bandwidth-distance product from 1976 to 1989 [1], [2], [3]. With single mode fiber having a very low attenuation (0.2 dB/km), it has been possible to achieve large repeater spacings as compared to the repeater spacings in conventional systems using metallic transmission lines [4]. At the same time, there has been a significant improvement in the optical devices as well. Today's technology provides single mode laser diodes (LDs) which can be modulated at very high bit rates (10 Gb/s) [2]. Also, PIN photodiodes having a bandwidth in excess of 100 GHz have been reported in the literature [5], [6]. As a result of rapid developments in the technology of optical devices, today's optical fiber systems can transmit at higher bit rates (10 Gb/s range) than any other guided wave transmission system.

Optical transmission systems can be divided into two categories; namely, intensity modulation direct detection (IMDD) systems and coherent optical systems. Following a brief description of IMDD systems, the principles and modulation/demodulation formats for coherent optical systems are discussed in this chapter. A discussion on the objectives and the organisation of this thesis concludes this chapter.

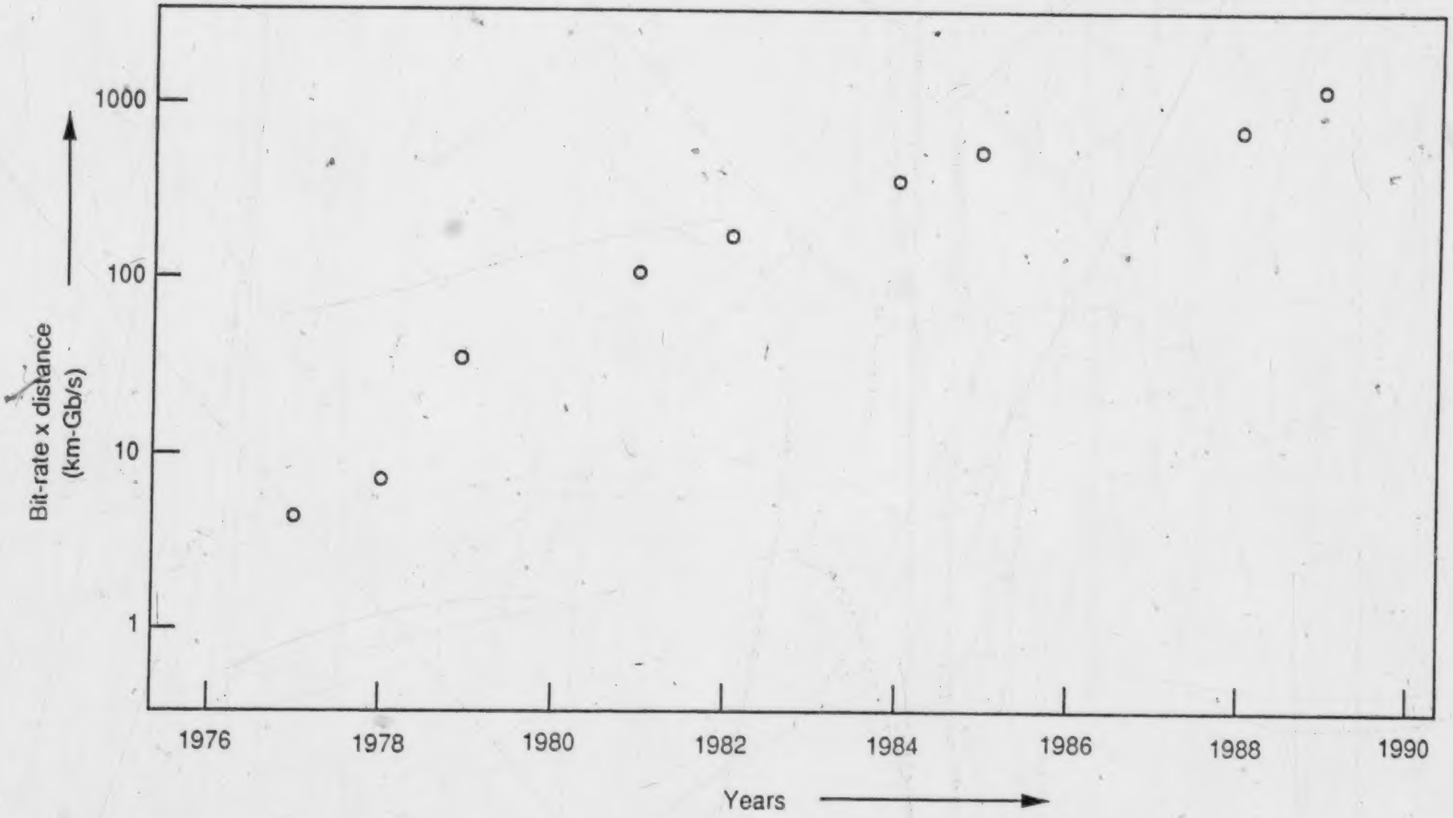

Fig. 1.1 Progress in the bit-rate distance product in optical communication systems during recent years.

1.1 INTENSITY MODULATION DIRECT DETECTION SYSTEMS

In IMDD systems, the optical power or the intensity of the optical source is changed according to the transmitted data. The optical source for such systems can be either a LD or a light emitting diode (LED). For an ideal transmission system, the received pulse at the receiver should be exactly the same as the transmitted pulse. In practice, however, the transmitted pulse becomes progressively attenuated and distorted with increasing distance due to scattering, absorption and dispersion effects. For single mode fibers, the main source of dispersion is chromatic or intramodal dispersion, which is wavelength dependent. Hence, to reduce the effects of chromatic dispersion, the spectral width (band of wavelengths over which the source emits) of the source should be narrow. LDs in general have a narrower spectral spread than LEDs and hence are better optical sources for IMDD systems. At the receiver, the received optical signal is directly converted to the baseband signal by a photo-diode. Electric current generated by the photo-diode is directly proportional to the received optical power. Since the shot noise in the photo-detector depends upon the signal current, the shot noise is very small compared to the receiver thermal-noise for weak received signals. Hence, the thermal noise dominates the shot noise, and the detection process is thermal noise limited. The receiver sensitivity of such systems is typically of the order of 10-20 dB above the theoretical quantum limit (10 photons/bit) [7].

Several microwave sub-carriers can be multiplexed and used to intensity modulate a LD. This technique is known as sub-carrier multiplexing (SCM). As shown in Fig. 1.2, in SCM systems, each channel has its own microwave carrier, which is modulated (e.g. ASK, FSK or PSK) by the respective data. These sub-carriers, from different channels, are then multiplexed in the microwave frequency domain. The multiplexed signal is superimposed on the bias current of the LD, to

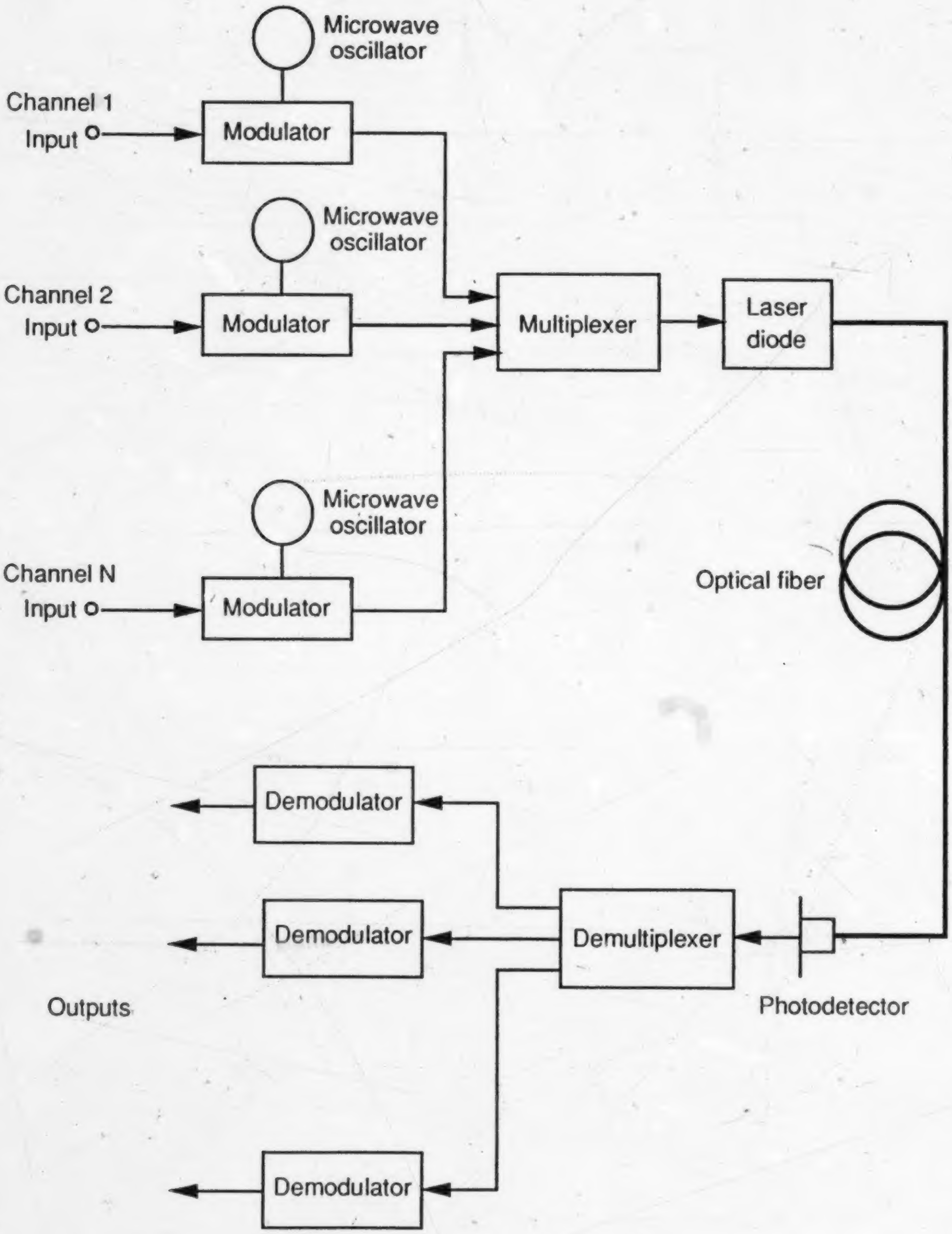
Microwave oscillator
Channel 1 Input
Modulator
Microwave oscillator
Channel 2 Input
Modulator
Multiplexer
Laser diode
Microwave oscillator
Channel N Input
Modulator
Optical fiber
Demodulator
Demodulator
Demultiplexer
Outputs
Photodetector
Demodulator

Fig. 1.2 Block diagram of a sub-carrier multiplexing system.

generate an intensity modulated optical signal. The photodiode at each receiver detects all the sub-carrier channels over the total receiver bandwidth. The desired channel can be selected, amplified and demodulated by using conventional microwave techniques. By itself, this system makes relatively inefficient use of the available fiber bandwidth, because the maximum transmitted bandwidth is equal to the frequency modulation bandwidth of the laser, which lies in the range of 5 GHz to 10 GHz. Also, intermodulation distortion (IMD) adversely affects the performance of these systems. IMD occurs when two or more carrier frequencies interact in a non-linear medium and generate 2nd order and 3rd order intermodulation frequencies, which interfere with the transmitted channel [8], [9]. This distortion can be severe when an optical amplifier is used in the system [10].

The main advantages of IMDD systems are simplicity in system design and low cost. As a result, most of the commercial optical fiber systems that exist today are based on IMDD techniques.

1.2 COHERENT OPTICAL SYSTEMS

Coherent lightwave systems, similar to coherent radio communication systems, are based on the principle of transmitting signals by modulating the amplitude, phase or frequency of the optical carrier. In such systems, the weak received optical signal is mixed with a strong local oscillator (LO) signal to obtain an intermediate frequency (IF) equal to f_S-f_{LO}, where f_S is the received optical signal and f_{LO} is the LO signal. If the IF is 0 Hz, then these systems are referred to as homodyne optical systems while, if the difference frequency is other than 0 Hz, then these systems are called heterodyne optical systems. An optical system with heterodyne detection was demonstrated as early as 1967 [11] but, due to the non-availability of narrow linewidth LDs at that time, research in this area was discontinued. However, by the late 1970s, progress in semiconductor optical device technology began to provide LDs which could operate in a single mode and were capable of producing very narrow linewidths (a few MHz). These advances encouraged researchers to again study coherent optical transmission systems. As a result, several experiments were reported in the 1980s [12], which demonstrated the improved performance of heterodyne/homodyne detection over direct detection systems. Today, optical coherent systems are being studied in major communications laboratories worldwide.

A block diagram of a coherent optical transmission system is shown in Fig. 1.3. The transmitter typically transmits an optical signal which uses either amplitude shift keying (ASK), frequency shift keying (FSK) or phase shift keying (PSK). Basically, an optical transmitter for a coherent system consists of an optical oscillator (a LD) and a modulator. The amplitude and/or the frequency modulation of the output light of a LD can be accomplished either by using an external modulator or by modulating the bias current by the transmitted data (internal modulation). For phase modulation of the optical signal an external modulator is required. At the receiver, mixing between the received optical signal and the relatively strong LO wave occurs at the photodiode. The IF, obtained as a result of the adding of two optical signals prior tc detection, typically lies in the microwave region. This IF band is then filtered out and demodulated to baseband to retrieve the desired received signal. On the other hand, in a homodyne detection system, the baseband signal is obtained directly after the optical mixing process.

Coherent systems are very sensitive to the polarisation of the received signal and the LO signal. The polarisation of the received signal must be aligned with the polarisation axis of the LO signal. Since deformities in the optical fiber randomly change the polarisation of the received signal, the matching of the polarisation states becomes difficult. Normally, the mismatch between the two

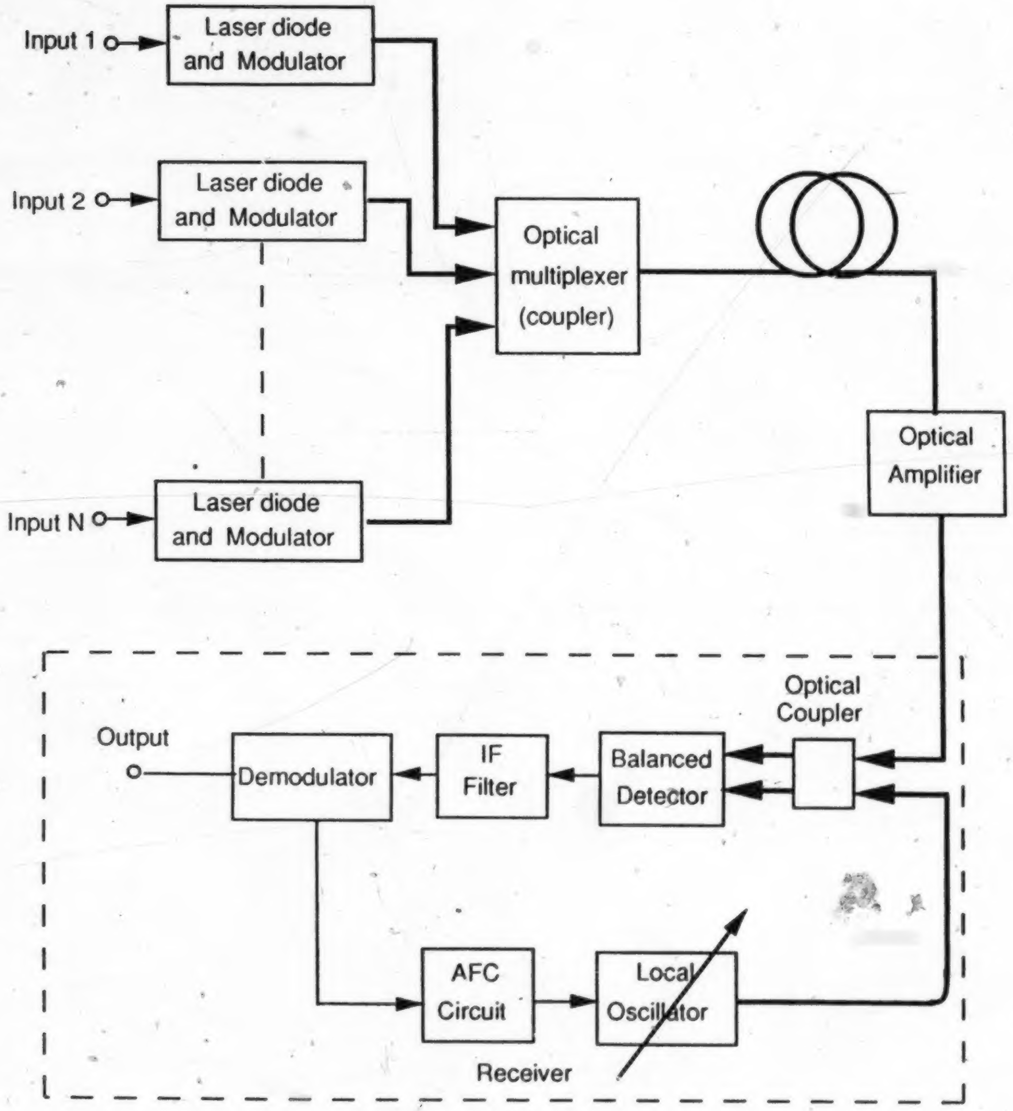

Input 1
Laser diode and Modulator
Input 2
Laser diode and Modulator
Input N
Laser diode and Modulator
Optical multiplexer (coupler)
Optical Amplifier
Optical Coupler
Output
Demodulator
IF Filter
Balanced Detector
AFC Circuit
Local Oscillator
Receiver

Fig. 1.3 Block diagram of a coherent optical fiber transmission system.

polarisation states is compensated for by means of a polarisation controller at the receiver [12]. Recently, polarisation diversity receivers have been demonstrated which minimise the degradation due to polarisation mismatching [13], [14]. Such receivers divide the signal equally between the two orthogonal polarisations, and detect them separately. A polarisation maintaining fiber, which maintains the polarisation state of the propagating signal, can also be utilised, but these fibers are very expensive.

There are basically two advantages of using coherent transmission techniques over the direct detection scheme. These are:

1. **Improved receiver sensitivity**: In coherent systems, the received optical power at the detector is directly proportional to the product of the electric field of the weak received optical signal and the strong LO signal. Because of this conversion gain, a coherent receiver can detect very weak optical signals (less than -55 dBm), whereas in IMDD systems, the minimum detectable power is in the range of -35 dBm. Further, the shot noise generated by the LO signal is usually larger than the receiver thermal noise. Therefore, the detection process is shot noise limited and hence an improved signal to noise ratio is obtained. Table 1 compares the receiver sensitivities of various modulation/demodulation schemes in coherent systems and direct detection systems [15]. Due to their greater receiver sensitivity, the repeater spacing of coherent systems can be larger than that needed in direct detection systems.
2. **Channel Selectivity**: Coherent systems are very attractive for the transmission of several optical channels using optical frequency division multiplexing. The demultiplexing of the received multiplexed channels is accomplished by means of a tunable LO. As the LO can be tuned to a wide range of optical frequencies, this scheme makes efficient use of the

Table 1 Receiver sensitivities for various modulation techniques.

Modulation technique	Theoretical quantum noise limit (photons/bit)	Minimum detectable power to achieve a BER of 10^{-9} (photons/bit)
PSK (homodyne)	9	34
PSK (heterodyne)	18	69
Differential phase shift keying (DPSK)	20	45
FSK	36	203
ASK (homodyne)	18	69
ASK (heterodyne)	36	137
Direct detection	10	500

available fiber bandwidth. Receiver bandwidth requirements for coherent systems is independent of the number of transmitted channels, because the LO frequency can be tuned to obtain the desired IF.

1.3 MODULATION/DEMODULATION FORMATS

In optical fiber communication systems, the three most commonly used modulation schemes are: amplitude shift keying (ASK), phase shift keying (PSK) and frequency shift keying (FSK).

In the ASK modulation scheme, the amplitude of the LD output is modulated by the baseband signal. An amplitude modulated signal can be obtained by direct modulation of the LD current at the transmitter. After the received optical signal is mixed with the optical LO signal, the electrical IF can be demodulated by means of an envelope detector. For ASK systems, a LD of linewidth about 0.1 times the data rate can be employed at the transmitter, without any significant penalty in error rate performance [16].

For systems using PSK, an external modulator is needed to modulate the phase of the optical carrier. Typically, a $LiNbO_3$ travelling wave modulator is used for this purpose. PSK systems are very sensitive to the phase noise of the LD at the transmitter as well as at the receiver and hence require LDs with a linewidth equal to less than 1% of the data rate [17].

In the FSK modulation scheme, the desired information is transmitted by modulating the frequency of the optical carrier. As for the case of amplitude modulation, frequency modulation of the LD at the transmitter can be achieved either by superimposing the signal on the bias current or by using an acousto-optic modulator. At the receiver, the IF can be demodulated by one of the following three methods:

a. Frequency discrimination detection

b. Single filter detection

c. Dual filter detection

The output voltage of a frequency discriminator is a function of the input frequency. Therefore, the two intermediate frequencies corresponding to a '1' bit and a '0' bit generate different voltages at the output of the discriminator. In this detection scheme, the received baseband signal contains AM noise which results from conversion of the FM noise of the LDs (source and LO) to AM noise by the frequency discriminator [18].

Single filter detection is similar to the ASK detection of signals. In this scheme, one of the IF signals, either corresponding to a '1' bit or corresponding to a '0' bit is selected using a bandpass filter and the output of the bandpass filter is then demodulated using an envelope detector. This method gives the poorest sensitivity compared to that of frequency discrimination and dual filter detection, because there is a 3 dB loss of power due to the rejection of one of the IF signals [19]. On the other hand, this detection scheme is simplest to implement and allows a wide spectral spread of the transmitting laser (0.5 times the data rate) [20].

Dual filter detection of a FSK signal is accomplished using two band-pass filters. One of the filters allows the IF corresponding to the '1' bit to pass, while the other filter allows the IF corresponding to the '0' bit to go through. The outputs of these two filters are converted to baseband by means of two envelope detectors, which are then combined to obtain the received signal.

Recent advances in high speed and narrow linewidth LDs and highly sensitive receivers have encouraged the study of the feasibility of coherent optical systems for use in long haul as well as in inter-office applications [21], [22]. A star network topology is shown in Fig. 1.4, in which each station has its own transmitter and receiver. The operating wavelengths of the transmitting LDs at each station are selected to space the optical channels sufficiently apart in order to minimize inter-channel interference. At each station, a tunable LD (LO) is provided to select the desired channel.

In spite of the obvious advantages of coherent optical systems over direct detection systems, telecommunications industries are still deploying direct detection systems because IMDD is a proven technology with existing products. Further, the following three limitations, which add to the cost of coherent systems have so far hindered their use in commercial applications:

a. Requirement of narrow linewidth LDs.

b. Frequency stabilisation of the LO.

c. Need for a tunable optical LO.

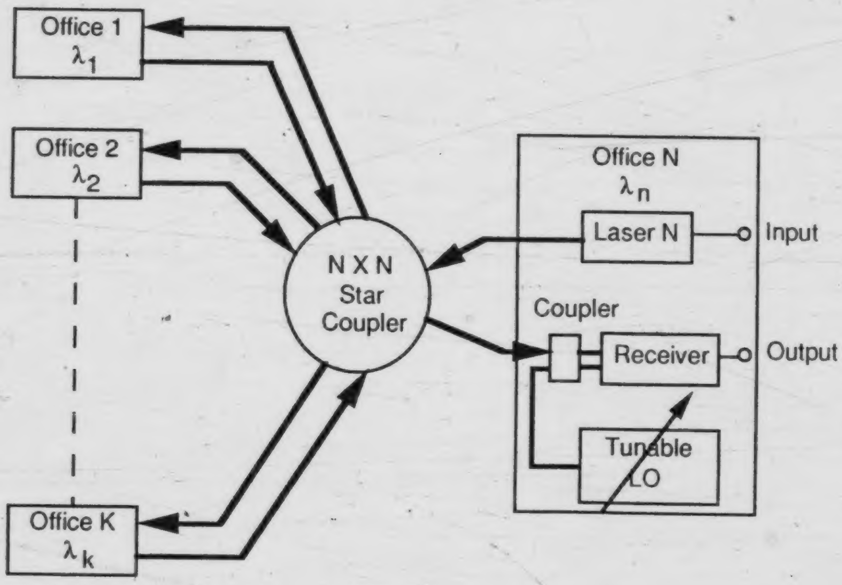
Office 1
λ_1
Office 2
λ_2
Office K
λ_k
N X N
Star
Coupler
Office N
λ_n
Laser N
Input
Coupler
Receiver
Output
Tunable
LO

Fig 1.4 A Star configuration for local area networks.

Coherent systems, as described in an earlier section, require narrow linewidth LDs at the transmitter and at the receiver. Also, precise control of the frequency of the source and of the LO are needed, in order to obtain a stable IF. This requirement becomes increasingly difficult to implement when several optical FDM channels are transmitted, because now one requires not only a tunable LD at the receiver, but also several frequency-locked LDs at the transmitter. These factors add to the cost and complexity of coherent systems.

In this thesis, a novel optical differential frequency shift keying (DFSK) system with self-heterodyne detection (SHD) has been studied. A DFSK system is based on the principle of coherent detection to transmit several optical FDM channels, each with a different frequency deviation, and at the same time is very simple to implement. In this system, the signal is transmitted by shifting or modulating the optical frequency of the LD. The frequency modulated signal is converted to an amplitude modulated signal using a delay line detection technique. This technique involves mixing of the received optical signal with its delayed version and hence down-converting the optical frequencies into the microwave frequency range. These frequencies can then be detected by a simple electronic receiver circuit. The DFSK scheme allows optical frequency division multiplexing of the several channels without any need for a tunable LO at the receiver. Demultiplexing of the received signal occurs at the detector and the channels are separated in the RF frequency domain. A detailed description of the operation of the optical DFSK system is presented in Chapter 2.

1.4 THESIS OBJECTIVES AND ORGANISATION

The main objective of this research project was to demonstrate a DFSK system with SHD and to evaluate its capability to transmit several channels using optical frequency division multiplexing. An experimental system, operating at a

DS-3 data rate (44.7 Mb/s), has been developed and investigated. The effect of crosstalk when two channels are simultaneously transmitted has also been studied.

To achieve this objective, the following tasks were performed:

1. Characterise the laser diodes to be used in the transmitter; i.e., measure the spectral linewidth, and measure the operating wavelength of the LDs.
2. Calculate the minimum required channel spacing for desirable operation of a DFSK system.
3. Design a laser diode transmitter which consists of a temperature stabilisation circuit for the laser, the laser driver circuit, the differential encoder and the Manchester encoder.
4. Build a high speed and high input impedance PINFET receiver, high frequency amplifiers, an envelope detector and the Manchester decoder.
5. Evaluate the performance of the system by measuring bit error rate (BER) as a function of received optical power and determine the effect of the bandwidth of the bandpass filter on the BER.
6. Measure the power penalty in receiver sensitivity for two-channel transmission, which arises due to phase noise of the LD and shot noise in the second channel.
7. Study the effect of linewidth on performance for both single channel and two channel DFSK systems, and compare the experimental results with existing theoretical results.

1.4.1 THESIS ORGANIZATION

In Chapter 1, IMDD systems and coherent systems have been discussed. Following an introduction to differential encoding and delay line detection, the experimental DFSK system is presented in Chapter 2. In coherent optical systems, the linewidth of the LD at the transmitter and at the receiver are very critical from a system performance point-of-view. In Chapter 3, the effect of laser linewidth on the performance of the DFSK system is analysed. A computer model is developed to analyse the inter-channel interference and to measure the signal-to-interference ratio. In Chapter 4, a detailed description of various transmitter components is presented and is followed by a brief description of the experimental setup for measuring the characteristics of the two LDs. Chapter 5 discusses the receiver that was designed and constructed for this project. Chapter 6 presents the results obtained for single channel- and two-channel transmission. The power spectrum of the received signal is presented and its dependence on the linewidth of the LD is discussed. Chapter 7, the concluding chapter, summarizes the results and suggests some related important problems for future investigation.

CHAPTER 2 - DFSK PRINCIPLE AND EXPERIMENTAL SYSTEM

In optical differential frequency shift keying (DFSK) systems, as the name implies, the transmitted data is first differentially encoded and is then transmitted by modulating the optical frequency of the LD. At the receiver, decoding of the received signal is carried out using delay line detection, which basically converts the FSK to ASK. In this chapter, the principle of differential encoding and of delay line detection are presented first. Following a discussion of some network configurations for DFSK systems, the chapter ends with a brief description of the block diagram of the experimental system designed and built for this thesis.

2.1 DFSK PRINCIPLE

A balanced DFSK receiver, as shown in Fig. 2.1, basically consists of two 3 dB optical fiber couplers, an optical delay line, two photo-detectors, a BPF and

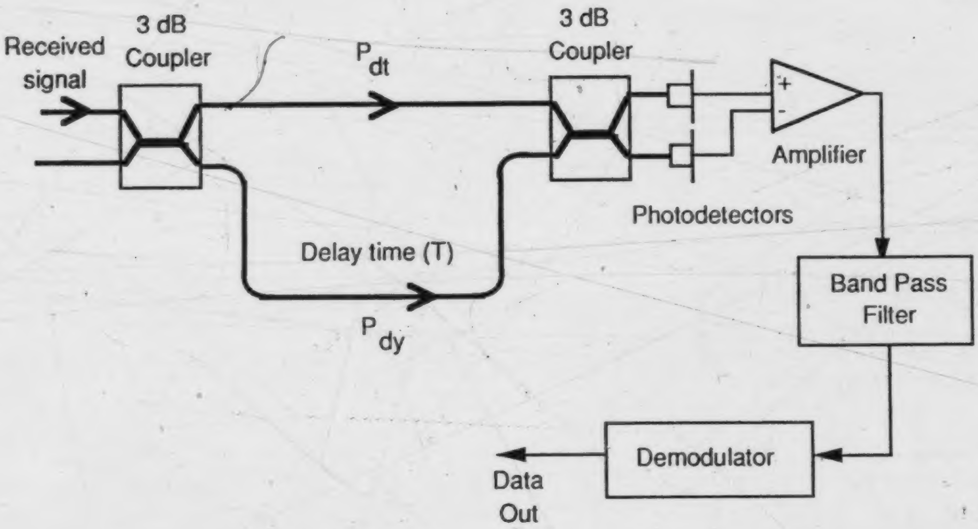
Received signal
3 dB Coupler
P_{dt}
3 dB Coupler
+
-
Amplifier
Photodetectors
Delay time (T)
P_{dy}
Band Pass Filter
Demodulator
Data Out

Fig. 2.1 A general dual detector DFSK receiver.

an envelope detector. The first optical fiber coupler splits the signal into two equal parts, while the second optical fiber coupler recombines the direct and the delayed signal (P_{dt} and P_{dy}). At the photo-detector, the two optical signals mix together and generate an IF. Because the received signal beats with itself, this type of detection is most commonly referred to as self-heterodyne or self-homodyne detection.

2.1.1 DIFFERENTIAL ENCODING AND DECODING

In conventional optical FSK systems, the transmitter transmits two frequencies, f_1 and f_2, for a '1' bit and a '0' bit, respectively. The received signal, at the receiver, is mixed with a LO signal of frequency f_{LO}, and as a result the two difference frequencies, also known as IFs, are generated. One of the IF frequencies (f_{LO}-f_1) corresponds to a '1' bit, while the other IF frequency (f_{LO}-f_2) corresponds to a '0' bit. These IFs can then be detected by a single filter or dual filter receiver.

On the other hand, in DFSK systems, as shown in Table 2, a transition in

Table 2 Frequency state table for differentially encoded signal.

Transmitted bit	Transmitted frequency (in previous bit)	Transmitted frequency (present bit)
0	f_1	f_1
0	f_2	f_2
1	f_1	f_2
1	f_2	f_1

the transmitted frequency occurs only when a '1' bit is transmitted. Therefore the transmitted bit can be obtained by comparing the frequency of the signal in two successive bit periods. If the frequency of the received signal is the same as in the previous bit period then a '0' bit was transmitted and if the frequencies are different then a '1' bit was transmitted. The frequencies of the received signal during two adjoining bit periods may be compared using a delay line detection technique. In this technique, the received differential encoded signal is split in two paths having different lengths. The received signal in one path is delayed with respect to the signal in the other path by one bit period (T). These two signals (direct and delayed) are then recombined and detected by a detector. Detection of the received signal in a photo-diode causes the direct signal to beat with the delayed signal. When a '1' bit is received, the frequency of the signal in the direct path is different from that in the delayed path. Hence, optical frequency f_2 beats with the other optical frequency f_1 and an IF equal to f_2-f_1 (say Δf) is obtained. For the case when a '0' bit is transmitted, the frequencies of the signals in the two paths are equal and no IF is obtained. In other words, as shown in Fig. 2.2, an IF is obtained at the output of the photo-detector whenever a '1' bit is received, and no output is obtained when a '0' bit is received. In the practical case however, because of random frequency fluctuations (known as phase noise or FM noise) and the finite response time of the LD, a low frequency noise is observed when a '0' bit is transmitted. To filter out the IF, a band pass filter is used at the receiver. This converts the frequency modulated signal at the transmitter to an amplitude modulated signal at the receiver. The IF is then demodulated by means of an envelope detector.

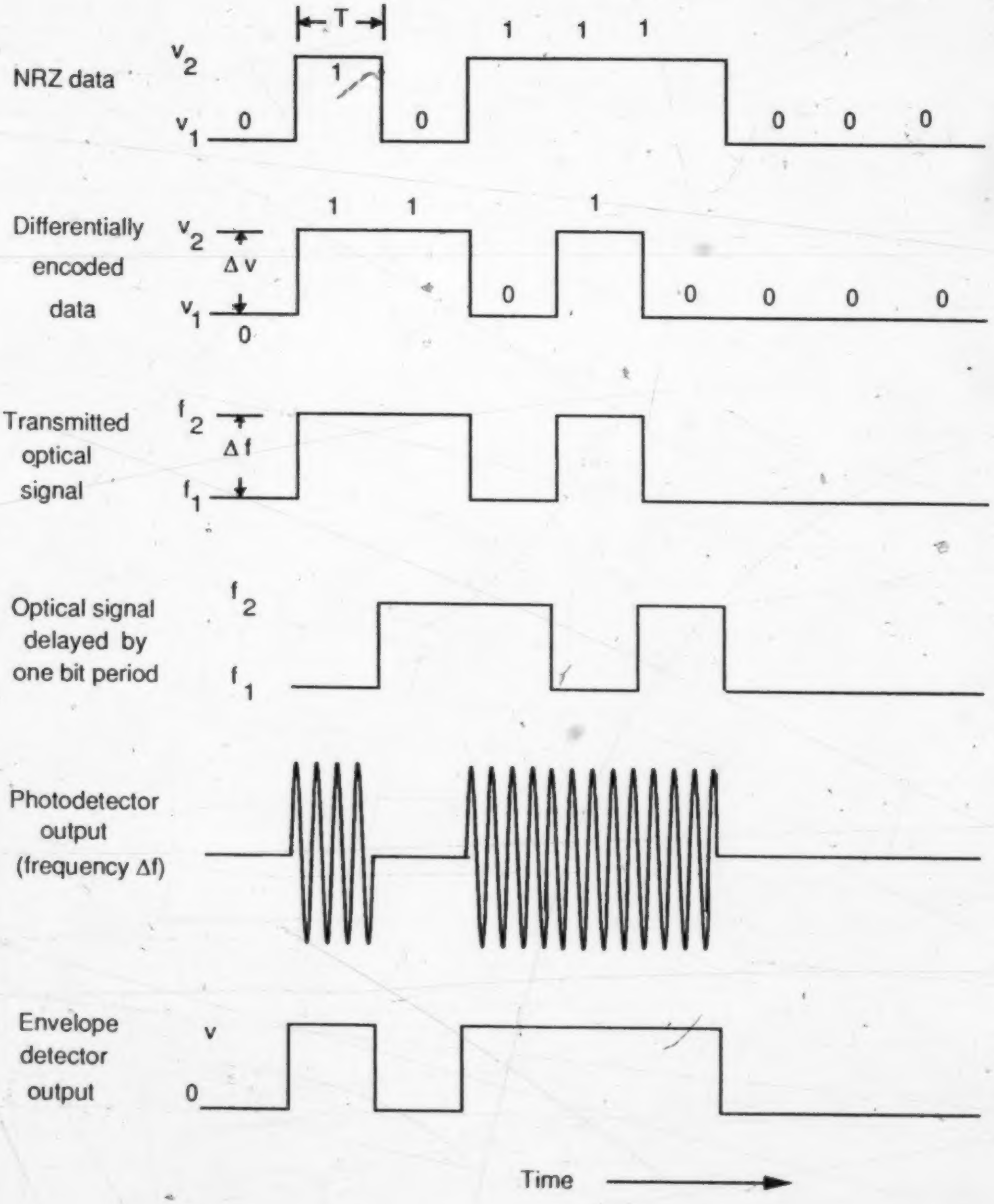
T
NRZ data
v_2
v_1
0
1
0
1 1 1
0 0 0
Differentially encoded data
v_2
Δv
v_1
0
1 1
0
1
0 0 0 0
Transmitted optical signal
f_2
Δf
f_1
Optical signal delayed by one bit period
f_2
f_1
Photodetector output (frequency Δf)
Envelope detector output
v
0
Time

Fig. 2.2 Differential encoding and delay line detection.

In a DFSK system, the signal power in the direct (P_{dt}) and the delayed (P_{dy}) path can be represented as

$$P_{dt} = A\cos\{2\pi f(t)t + \phi_n(t)\} \tag{2.1}$$

and

$$P_{dy} = A\cos\{2\pi f(t-T)t + \phi_n(t-T)\} \tag{2.2}$$

where A is a constant, ϕ_n is the phase of the signal, and $f(t)$ $(= f_1$ or $f_2)$ is the frequency of the signal at time t.

After P_{dy} and P_{dt} are mixed, the output of the photodetector is given by

$$I_{out}(1) = RP_{dy}P_{dt}\cdot\cos\{2\pi\Delta ft + \Delta\phi_n(T)\} \tag{2.3}$$

for a received '1' bit and for a received '0' bit,

$$I_{out}(0) = RP_{dy}P_{dt}\cdot\cos\{\Delta\phi_n(T)\} \tag{2.4}$$

where R is the responsivity of photodetector, $\Delta\phi_n(T)$ $(= \phi_n(t) - \phi_n(t-T) = \Delta\omega T)$ is the phase error, and Δf $(= f_2 - f_1)$ is the difference frequency.

$\Delta\omega$ is called the FM quantum noise of the LD and can be expressed as a zero mean Gaussian noise. It can be inferred from Eq. 2.4 that the output of the photodetector will have a random frequency noise associated with it even when a '0' bit is received. This noise is distributed around d.c. and has a Lorentzian power spectrum [23].

To obtain maximum signal current, the signal power in the direct path and the delayed path should be equal. This can be easily shown by a simple calculation. If P_{rec} is the total received optical power at the output of the second coupler, then

$$P_{rec} = P_{dt} + P_{dy} \quad \text{or} \quad P_{dy} = P_{rec} - P_{dt}\,. \tag{2.5}$$

Substituting this relationship in Eq. 2.3 and differentiating with respect to P_{dt} we obtain

$$\frac{d\, I_{out}(1)}{d\, P_{dt}} = R \cdot (P_{rec} - 2P_{dt}) \cdot \cos\,(2\pi\Delta ft + \Delta\phi_n(T)) \ . \qquad (2.6)$$

To obtain maximum output power at the IF, the right hand expression in Eq. 2.6 should equal 0. This implies

$$P_{rec} - 2P_{dt} = 0 \quad \text{or} \quad P_{dt} = 0.5P_{rec} \ . \qquad (2.7)$$

Therefore, $P_{dy} = P_{rec} - P_{dt} = 0.5P_{rec}$. (2.8)

Hence, the two optical couplers should have coupling ratios of 0.5 (or 3 dB) to obtain maximum power at the output of the second coupler.

2.1.2 ADVANTAGES

There are several advantages of using the DFSK scheme for transmitting signals in optical fiber systems. These are as follows:

1. Unlike other coherent optical systems, there is no need for an additional laser LO at the receiver. This results in a simple receiver design and low system cost because wavelength stabilisation and the AFC circuit at the receiver end are no longer required.
2. The absolute laser frequency at the transmitter is not critical for DFSK systems, as the information is contained within the relative frequency between the two successive bit periods. Hence, the wavelength of the transmitting LD need not be stabilised.
3. The receiver operates independently of the polarisation of the incoming signal as long as the delay line does not change the relative polarisation between the delayed and the direct signals.
4. A laser diode of moderate linewidth (0.5 times the bit-rate) can be employed at the transmitter. This requirement is far less than that in other coherent systems such as PSK and continuous-phase FSK (CPFSK).

5. The present multi-channel fiber optic networks are based on time division multiplexing (TDM) techniques using high speed electronic multiplexers and demultiplexers. Since the optical channels in a DFSK system are wavelength division multiplexed using optical fiber couplers, one no longer requires high speed electronic multiplexers. Also, unlike subcarrier multiplexing, there is no need for microwave modulators/demodulators.
6. The frequency of the laser can be directly modulated by modulating the bias current; hence no external modulator is needed.
7. There is no intermodulation distortion because the carrier frequencies are in the optical range and their intermodulation products are outside the bandwidth of the receiver. This allows the use of optical amplifiers for long distance transmission.

2.1.3 LIMITATIONS

2.1.3.1 RECEIVER SENSITIVITY:

The best receiver sensitivity that can be achieved in DFSK systems with SHD detection is about equal to that of a direct detection scheme because the detection process is thermal noise limited. Thus, such a DFSK system is not very attractive for long distance transmission. On the other hand, in coherent systems with an independent LO at the receiver, since the LO power is large (around 0 dBm) conversion gain takes place. Therefore, the receiver can detect very weak received signals, which allows larger repeater spacings.

2.1.3.2 POWER PENALTY:

In the detection process, the receiver detects only the binary '1' since the photocurrent for binary '0' is rejected by the BPF. This loss of one half the power can be avoided by using a four level coding scheme [24], in which both the '1' bit and the '0' bit are actively transmitted. Such a coding scheme, as illustrated in Fig. 2.3, uses four absolute frequency transitions to obtain two distinct IFs, which can be detected separately by a dual filter receiver. This coding scheme introduces a significant coding complexity at the transmitter and increases the bandwidth requirement for each channel and hence was not considered suitable for this project.

2.1.3.3 BANDWIDTH LIMITATIONS:

The maximum usable bandwidth of the DFSK systems depends upon the detector bandwidth. On the other hand, in coherent systems using a tunable LO, the usable bandwidth depends upon the LD at the receiver. Since the tunable LDs can be tuned to several wavelengths, the maximum usable bandwidth for coherent systems is larger than that for DFSK systems.

2.2 DFSK SCHEME FOR MULTI-CHANNEL TRANSMISSION

The DFSK scheme can be implemented to transmit more than one optical channel. A system configuration for a multi-channel DFSK system is shown in Fig. 2.4, where the channels are multiplexed optically using optical fiber couplers. Each transmitter, in this configuration, produces a unique frequency shift equal to $\Delta f = (f_2 - f_1)$, which is different for each optical channel. Also, the operating wavelengths of the LDs at the transmitters should be different so that the transmitted optical frequencies are separated significantly. At the receivers, the IFs corresponding to all the transmitted stations are received. Because every transmitter has a unique frequency shift associated with it, the receiver can select the desired transmitter by tuning its band pass filter to the IF corresponding to that particular station.

The frequency of a LD, as mentioned in the previous chapter, can be modulated either by modulating the bias current or by using an external

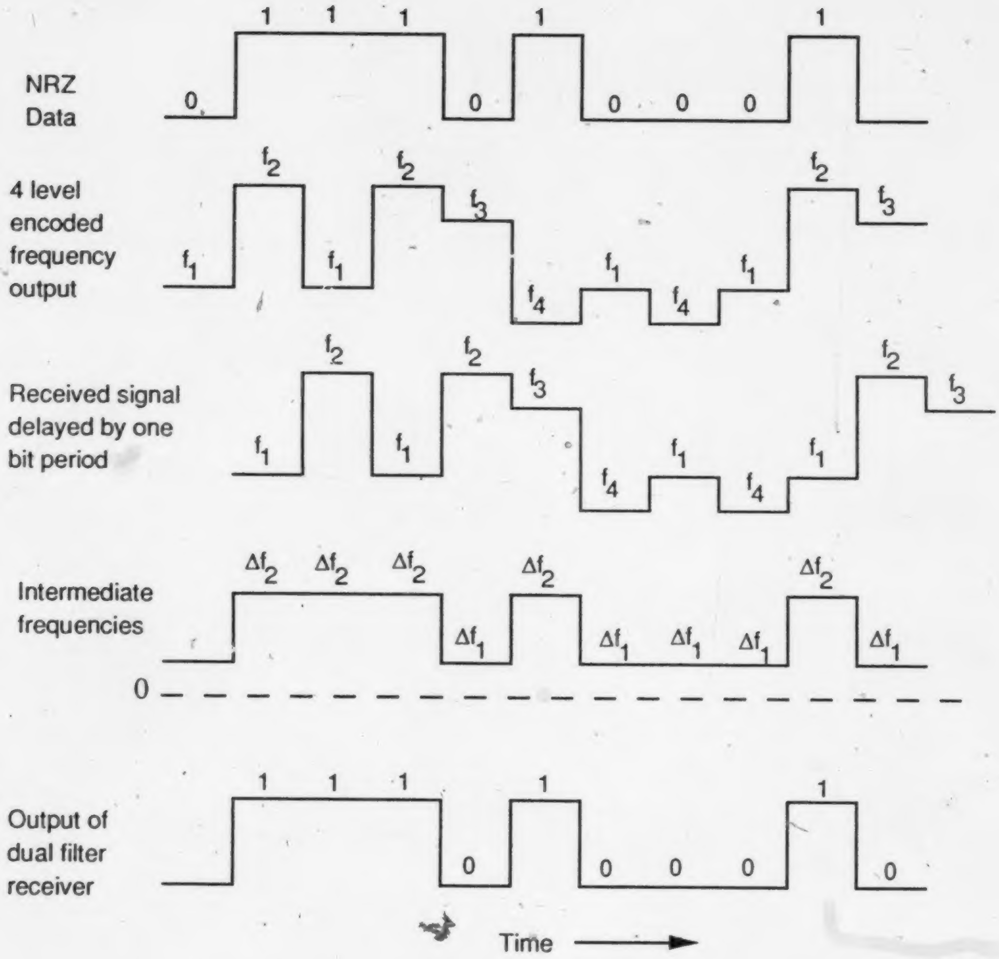
NRZ Data
0
1 1 1
0
1
0 0 0
1
4 level encoded frequency output
f1 f2 f1 f2 f3 f4 f1 f4 f1 f2 f3
Received signal delayed by one bit period
f1 f2 f1 f2 f3 f4 f1 f4 f1 f2 f3
Intermediate frequencies
Δf2 Δf2 Δf2 Δf1 Δf2 Δf1 Δf1 Δf1 Δf2 Δf1
0
Output of dual filter receiver
1 1 1 0 1 0 0 0 1 0
Time

$$f_3 - f_4 = f_2 - f_1 = \Delta f_1$$

$$f_2 - f_3 = f_1 - f_4 = \Delta f_2$$

Fig. 2.3 A 4-level coding and dual filter detection for DFSK system.

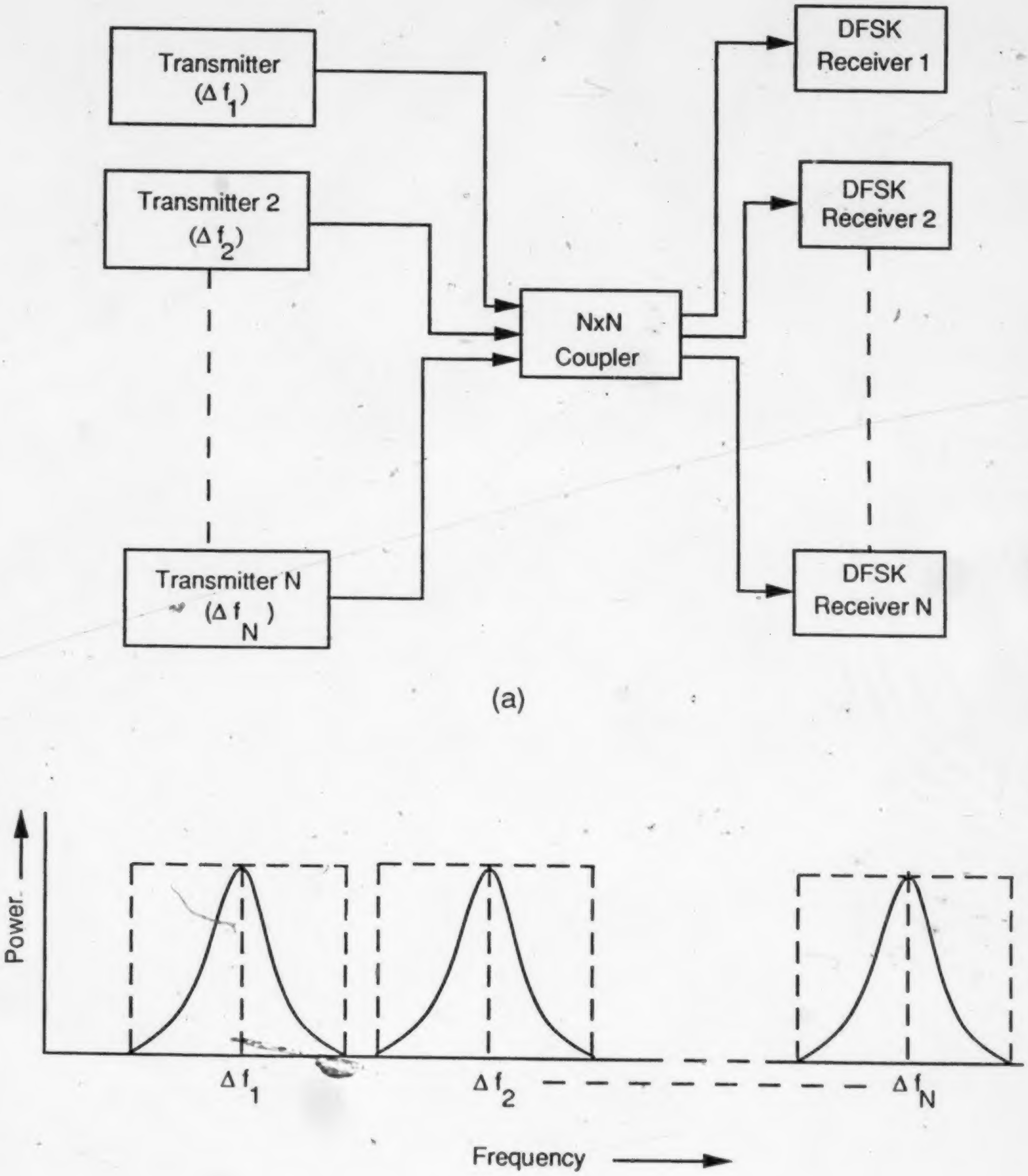
Transmitter
(Δ f1)
Transmitter 2
(Δ f2)
Transmitter N
(Δ fN)
NxN
Coupler
DFSK
Receiver 1
DFSK
Receiver 2
DFSK
Receiver N
Power
Δ f1
Δ f2
Δ fN
Frequency

(a)

(b)

Fig. 2.4 a) A topology for a multi-channel optical DFSK system.
b) Electrical power spectrum at the receiver.

modulator. A change in the bias current to obtain frequency shift also causes the intensity of the light to change. If there are several transmitting stations, the amplitude of the modulating current should be large to obtain large frequency shifts. Typically, the frequency deviation constant for LDs, which is expressed in terms of frequency shift per unit current, is about 300 MHz/mA for modulation frequencies higher than 15 MHz [25]. Hence, to achieve a frequency shift of about 5 GHz, the peak to peak amplitude of the modulating current should be more than 10 mA. Such a large modulating signal can produce a significant AM or intensity noise and can also damage the LD. For such cases, an external modulator should be used to frequency modulate the optical carrier. The other alternative is to use phase tunable DFB lasers. This type of laser structure is discussed in Section 3.1.2.

In DFSK systems, the IF needs to be amplified before it is selected by a band pass filter. For multi-channel transmission, the receiver receives all the channels and hence it is essential that the photo-diode and the pre-amplifier should have sufficiently large bandwidth to accommodate all the channels. While high speed GaAs photo-detectors (100 GHz) have been developed [5], high speed amplifiers with very low noise figure are still to be developed. In order to utilise the photo-detector bandwidth completely without any need for high frequency amplifiers, the received optical signal should be down-converted to lower frequencies at the photodetector. The down-conversion process is based on beating the received IF with another microwave signal (say f_m) to obtain a new difference frequency (say f_N), which is equal to IF-f_m. The mixing process takes place at the detector and can be achieved by superimposing the microwave signal on the bias current of the photo-detector [26]. A microwave signal from a tunable microwave oscillator is applied to the photo-detector and the required channel is selected by tuning the oscillator. Hence, a tunable band pass filter is no longer required at the receiver.

Another possible configuration in which a DFSK system can be used is shown in Fig. 2.5. In this configuration, a tunable optical filter pre-selects the channels before the receiver receives them. This system allows assignment of the same frequency shift to two or more channels as long as the optical filter selects only one of these channels. The pre-filtering of the transmitted channels in the optical domain can significantly increase the number of allowable channels in DFSK systems.

2.3 EXPERIMENTAL SETUP

The experimental setup for this project is shown in Fig. 2.6. The project was carried out in three stages and the experimental system was modified after every stage.

During the first stage, a single channel DFSK system was implemented. The optical source for this channel consists of a NEC distributed feedback (DFB) LD with spectral linewidth equal to about 22 MHz. This optical source is then frequency modulated by differentially encoded NRZ data at a data rate of 45 Mb/s. For the experimental system, the frequency of the optical source is modulated internally. The output of the LD is then launched into 8 km of single mode fiber with a core diameter of 5 μm and a loss of 0.25 dB/km at a wavelength of 1300 nm.

At the receiver, an optical fiber coupler splits the received signal into two parts. A delay line is added to one of the paths, which introduces a delay of one bit period as compared to the direct path. For 45 Mb/s, one bit period is equal to 22.2 ns and hence the length of the delay line should be 4.44 meters (T x C, T is the bit period, C is the velocity of light in optical fiber). In order to match the polarisation of the signal in the direct path to that of the signal in the delayed path,

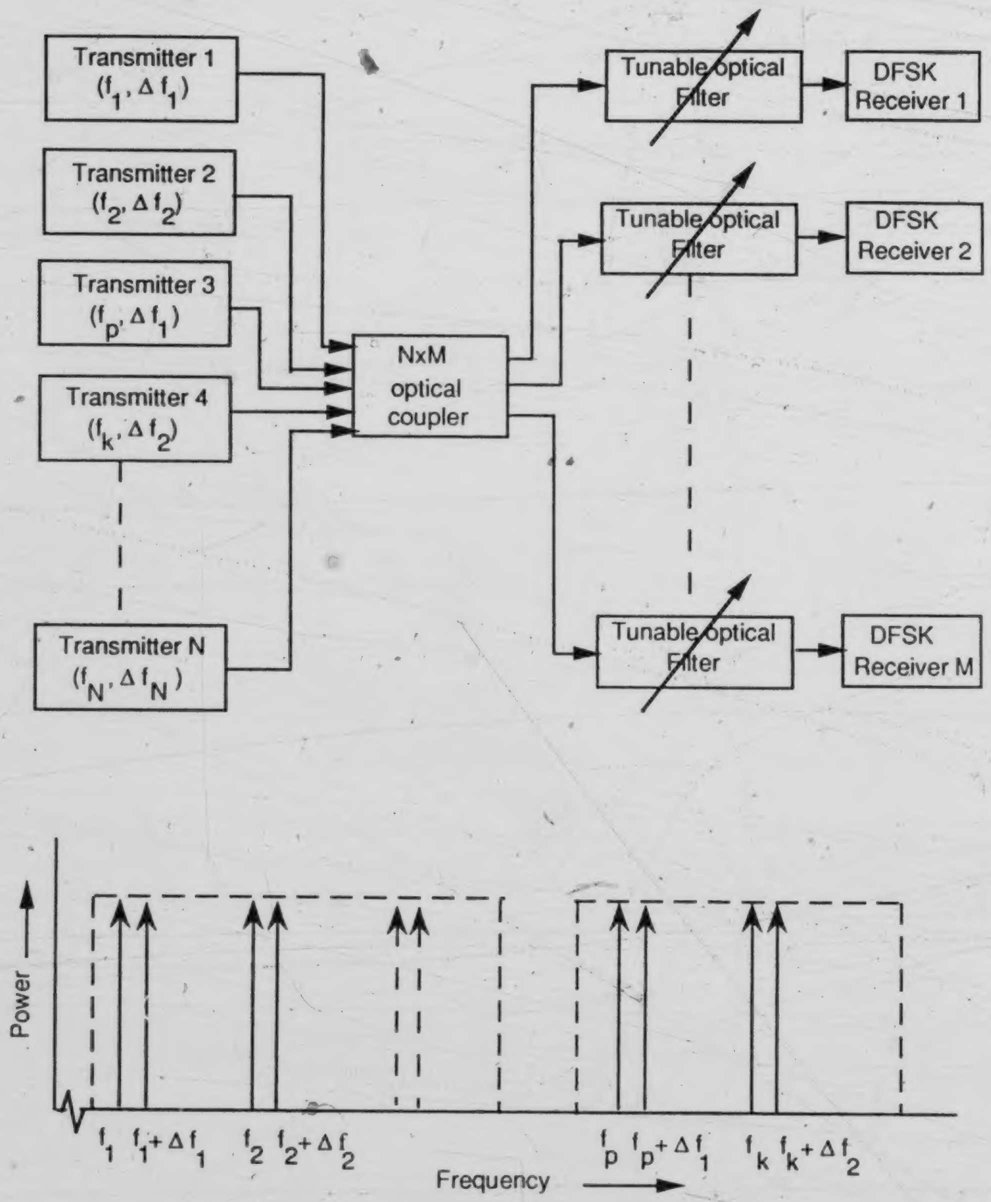
Transmitter 1 (f_1, Δf_1)
Transmitter 2 (f_2, Δf_2)
Transmitter 3 (f_p, Δf_1)
Transmitter 4 (f_k, Δf_2)
Transmitter N (f_N, Δf_N)
NxM optical coupler
Tunable optical Filter
Tunable optical Filter
Tunable optical Filter
DFSK Receiver 1
DFSK Receiver 2
DFSK Receiver M
Power
f_1
$f_1+\Delta f_1$
f_2
$f_2+\Delta f_2$
f_p
$f_p+\Delta f_1$
f_k
$f_k+\Delta f_2$
Frequency

(Optical power spectrum)
(not to scale)

Fig. 2.5 Multi-channel DFSK system using tunable optical filter at the receiver.

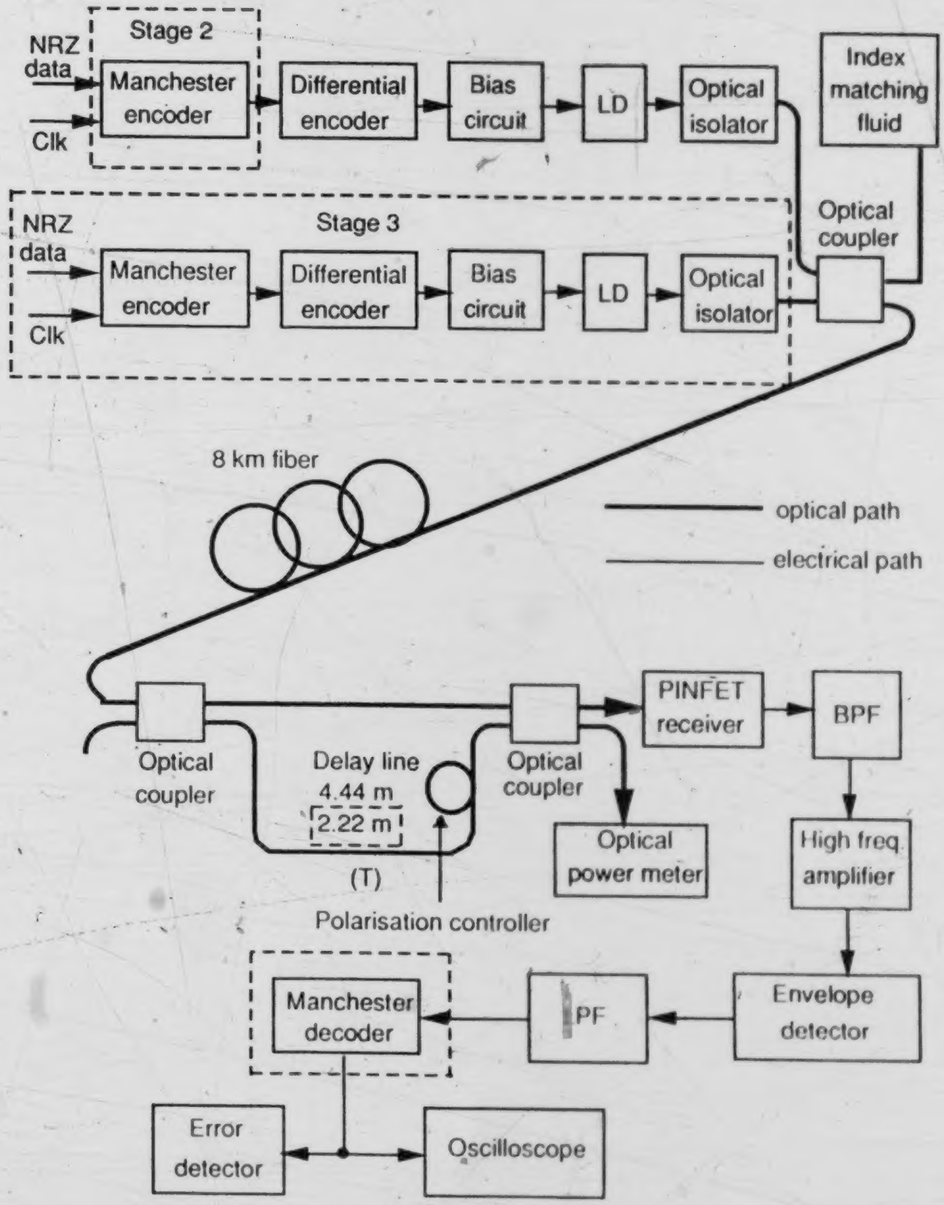
Stage 2
NRZ data
Clk
Manchester encoder
Differential encoder
Bias circuit
LD
Optical isolator
Index matching fluid
Stage 3
NRZ data
Clk
Manchester encoder
Differential encoder
Bias circuit
LD
Optical isolator
Optical coupler
8 km fiber
optical path
electrical path
Optical coupler
Delay line
4.44 m
2.22 m
(T)
Polarisation controller
Optical coupler
PINFET receiver
BPF
Optical power meter
High freq. amplifier
Envelope detector
PF
Manchester decoder
Error detector
Oscilloscope

Fig. 2.6 Experimental setup for DFSK system.

a polarisation controller is used in the delay path. This polarisation controller consists of a fiber loop. The fiber loop is rotated to obtain maximum power at the output of the coupler. The output of the photo-detector is passed through a BPF and is demodulated using an envelope detector.

The characteristics of a single channel DFSK system were studied and it was observed that more than two 1's or 0's in a row caused an error rate floor occurrence at higher than 10^{-9}. This effect is due to base line wander caused by non-uniform frequency modulation characteristics and heating effects of the LD. Hence, Manchester encoding was considered in order to reduce the detrimental effects of the non-uniform frequency modulation characteristics of the LD. In Manchester encoding, each NRZ bit is represented by two successive pulses of one half the bit duration, having binary values of 1 and 0. Therefore, the number of consecutive '1's and '0's in the encoded data is limited to 2. The increase in the number of transitions in the data stream reduces the baseline wander effect. This also relaxes the requirements for the linewidth of the LD. Hence, a Manchester encoder and a decoder were incorporated in the experimental system during the second stage. As the effective bit period is reduced by half, the length of the delay line at this stage was reduced to 2.22 meters (one-half of its previous value), as depicted in Fig. 2.6. At the transmitter, a Manchester encoder was implemented before the differential encoder and at the receiver, a Manchester decoder was used at the output of the low pass filter.

In the third stage, a second channel was incorporated in the system. For channel 2, a Fujitsu DFB LD with 13 MHz linewidth acts as an optical source. The other transmitter components in the second channel are the same as in the first channel (channel 1). Channel 1 and channel 2 were optically frequency division multiplexed using an optical coupler. A more detailed description on the transmitter design and the receiver design can be found in subsequent chapters.

2.4 SUMMARY

In this chapter, an introduction to the basic principles of the operation of a DFSK system have been presented. Further, the advantages and limitations of DFSK systems have been discussed and a few network configurations for multi-channel transmission have been proposed. Finally, a brief description of the system block diagram was given. The simplicity and low cost of the receiver make DFSK systems attractive for future local area network applications.

CHAPTER 3 - THEORETICAL ANALYSIS OF DFSK SYSTEM

For earlier low bit rate IMDD optical fiber communication systems, the linewidth of the optical source was not of major concern. But in the early 80's, when optical fiber systems operating at high bit rates were designed, the system performance was limited by the inter-symbol interference caused by the chromatic dispersion in optical fiber cables. This chromatic dispersion depends upon the spectral linewidth of the optical source at the transmitter. In order to reduce this dispersion to a minimum, narrow linewidth LDs were required. During the same period, coherent optical transmission systems were developed and the requirement of narrow linewidth LDs was even more stringent in these systems. As a result, several techniques were and are being developed to obtain narrow linewidth LDs.

In this chapter, a brief discussion about the linewidth and the frequency modulation response of a DFB LD is presented. The effect of the phase noise or linewidth of the LD on the power spectrum of the received signal for the DFSK system is calculated next. The calculated power spectrum is then used to obtain the signal to interference ratio (SIR) for a two channel DFSK system. At the end of the chapter, a brief analysis of the receiver noise is included.

3.1 REQUIRED OPTICAL SOURCE CHARACTERISTICS

As the information is contained in the frequency of the optical carrier, it is essential that the output of the optical source is stabilised and that it oscillates in a single mode. For such applications, DFB LDs are very attractive. They have a well stabilised frequency output and exhibit a very high side mode suppression ratio (SMSR). SMSR is defined as the ratio of the intensity in the dominant mode to that in the next most intense mode. Apart from a well stabilised frequency output, the optical source should also exhibit narrow linewidth and a flat frequency modulation characteristic.

3.1.1 LASER LINEWIDTH

The output of a well stabilised LD is typically affected by the quantum amplitude noise and the quantum phase noise. When the laser is operated well above threshold, the quantum phase noise dominates over the quantum amplitude noise. This quantum phase noise causes the oscillation frequency of the LD to wander about its mean value and therefore it is also referred to as quantum FM noise. The random frequency fluctuations in a LD cause a Lorentzian output power spectrum and the 3 dB full width half maximum of this power spectrum is known as spectral linewidth or the lineshape of the LD.

The fluctuations in the frequency or the phase of the LD are caused by the spontaneous emission of photons. This spontaneous emission causes the phase and the intensity of the optical field to change [27]. In order to restore the steady state intensity, the LD undergoes a relaxation oscillation and there is a change in the real and the imaginary part of the refractive index of the active medium. The ratio of the two parts (real and the imaginary) of the refractive index, is called the linewidth enhancement factor, α, and is equal to

$$\alpha = \frac{\Delta n'}{\Delta n''} \tag{3.1}$$

where $\Delta n'$ is the real part of the refractive index, and $\Delta n''$ is the imaginary part of the refractive index.

The coupling of the phase noise to the amplitude noise increases the linewidth by a factor of $1+\alpha^2$. The linewidth of a LD can be expressed as [28]

$$\Delta\upsilon = \frac{v_g^{2} h\upsilon g \eta_{SP} \alpha_m}{8\pi P_o} \cdot (1 + \alpha^{2}) \tag{3.2}$$

where v_g is group velocity of the light, g is the threshold gain, h is Plank's constant (= $3.384 \cdot 10^{-34}$ J-s), υ is the optical frequency, η_{SP} is the spontaneous emission factor, P_o is the output power of the facet, $\alpha_m = g - a_L$, and a_L is waveguide loss of the laser.

The above equation also applies to the DFB LDs but in that case, the definition of α_m changes [28]. Eq. 3.2 also suggests that the linewidth of a LD is directly proportional to $P_0{}^{-1}$. However, for semiconductor lasers, it is not possible to obtain negligible linewidths for large mode power. Later studies have revealed that the linewidth is not completely power dependent and can be expressed as [29], [30].

$$\Delta\upsilon = \Delta\upsilon_P + \Delta\upsilon_0 \tag{3.3}$$

where $\Delta\upsilon_P$ is the power dependent term and $\Delta\upsilon_0$ is the power independent term. $\Delta\upsilon_0$ is proportional to the third power of the side mode intensity. This term has not been explained fully as yet [23].

3.1.2 FREQUENCY MODULATION CHARACTERISTICS

A change in the bias current of a LD causes the oscillation frequency to shift. This direct frequency modulation capability of semiconductor LDs has been the key factor in the development of tunable optical local oscillator and coherent FSK systems.

The propagation constant of the gain medium can be expressed as [31]

$$k = u + jv = \frac{\omega n}{c} \cdot \left[1 - \frac{(\omega_0 - \omega) \cdot c}{\Delta\omega n \omega} \cdot S(I_0) \right] + j \frac{1}{2cn} \cdot \left[S(I_0) \cdot nc - \frac{\sigma}{\epsilon_0} \right] \tag{3.4}$$

where n is the refractive index, c is the velocity of light, σ is the conductivity of the laser medium, ϵ_0 is the electric permeability of vacuum, $\Delta\omega$ is the linewidth, ω_0 is the operating frequency of laser, I_0 is the DC bias current, and S is the susceptibility of the medium.

When the bias current (I_0) is changed, the susceptibility (γ) changes. The change in susceptibility alters the real (u) and the imaginary (v) part of the propagation constant. The change in u causes the amplitude or intensity to change, while the change in v causes a shift in the frequency output of the LD [31].

Basically, a change in bias current causes the carrier density as well as the temperature of the active layer to change. Both the thermal variation and the carrier density change are responsible for the frequency modulation of the LD. In the low modulation frequency region, the frequency shift occurs mainly due to the temperature variations caused by the modulating current. The normalised frequency deviation due to thermal effects can be written in the form [25]

$$\frac{\Delta F_t}{F_0} = -(\alpha_L + \alpha_n)\cdot\Delta T_{eff} \tag{3.5}$$

where

$$\alpha_L = \frac{1}{L}\cdot\frac{dL}{dT} \quad \text{and} \quad \alpha_n = \frac{1}{n}\cdot\frac{dn}{dT} \tag{3.6}$$

where α_L is the linear thermal expansion coefficient, and α_n is the thermal refractive index constant.

However, at high modulating frequencies, the thermal effect is smaller, and the carrier density modulation is mainly responsible for the frequency shift.

The frequency modulation capability of a LD is expressed in terms of the frequency deviation per unit current (frequency deviation constant). For a conventional DFB LD, the frequency deviation constant as a function of the modulation frequency has the behaviour shown in Fig. 3.1 [32]. As can be seen from this Figure, the frequency shift per unit current is not the same for different modulation frequencies. The dip in the frequency modulation characteristics occurs where the cause of the frequency shift changes from the thermal effect to the carrier density effect. This non-flat frequency response of LDs is responsible for waveform distortion as well as IF broadening.

Recently, a phase tunable DFB laser was reported, which has a flat frequency response from 1 kHz to about 450 MHz (refer to Fig. 3.1) [32]. Such lasers consist of two regions; namely, a DFB region and a modulation region. The DFB region, which contains a second order grating, acts as a DFB laser, while the modulation region is used for the frequency modulation of the LD. If the dc offset of the modulating current is less than the threshold current of the LD, the carrier density effect in the modulating region is 5-20 times greater than the temperature effect. Hence, the frequency modulation response is caused by the carrier density effect at low, as well as at high modulation frequencies.

Another alternative to obtain a flat frequency modulation response is to introduce carrier density non-uniformity along a semiconductor laser cavity. Non-uniformity in the carrier density can be achieved by partitioning the electrode into a number of sections and electrically isolating these sections. The carrier density can then be artificially controlled by applying different dc bias to these electrodes. The frequency modulation response of a three electrode DFB LD was measured by Y. Yoshikuni et. al. [33]. They reported that these LDs can be tuned over a range of 30 GHz and exhibit a flat frequency response from 1 kHz to about 300 MHz. Phase tunable and multi-electrode DFB lasers have a flat frequency response up to 1GHz. For high bit-rates, the non-uniform FM response can be

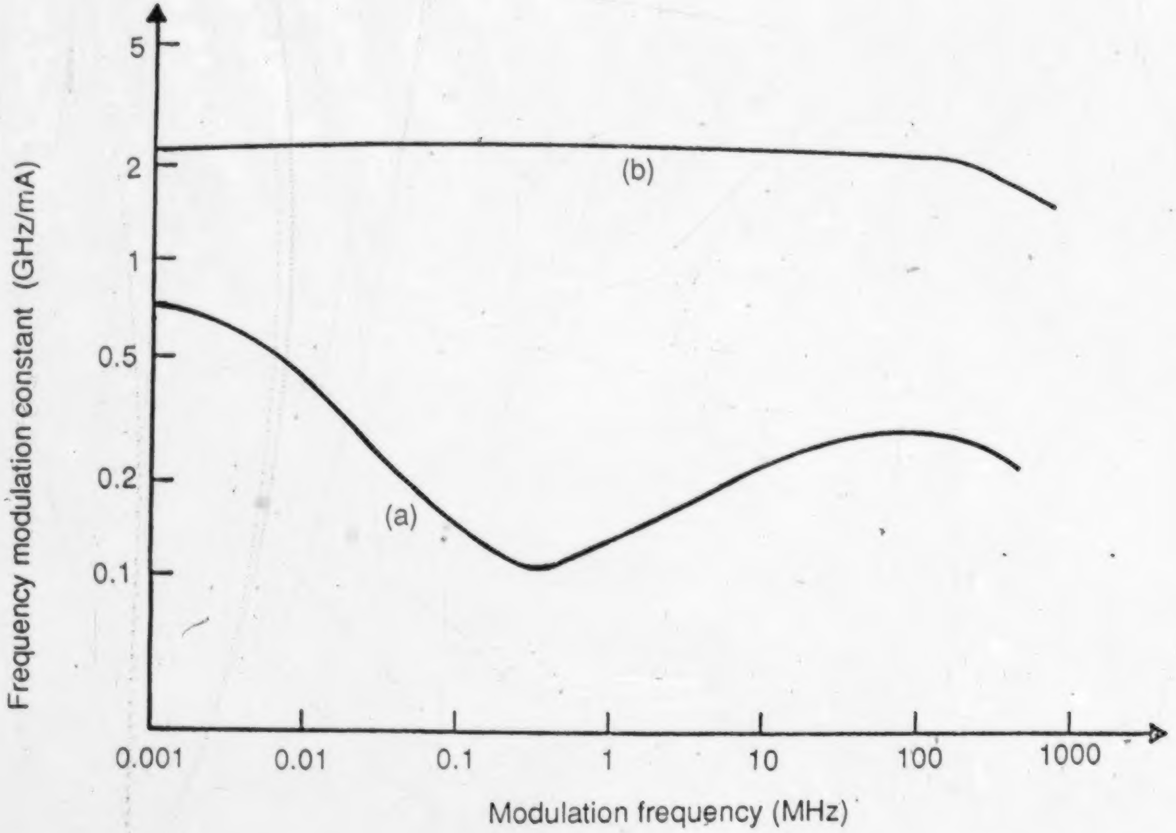

Fig. 3.1 Frequency modulation characteristics of DFB laser diodes.
(a) Conventional DFB.
(b) Phase tunable DFB.

compensated for by pre-equalisation of the modulation signal with a passive RC network. This technique however, reduces the frequency deviation constant of the LD [34].

At low modulating frequencies, the frequency modulation constant is independent of the bias current. However, at high modulation frequencies (above 10 MHz), the frequency modulation constant changes with the bias current. At modulation frequencies near the relaxation oscillation of the LD, a resonance peak occurs in the FM response. This peak frequency deviation decreases and the relaxation oscillation resonant frequency increases with an increase in bias current. Hence, there is a steep decrease in frequency deviation constant at very high modulation frequencies (around 5 GHz) [33].

At relatively low modulation frequencies (from 10 MHz to few GHz), the quasi-Fermi level (carrier density) is clamped by the gain saturation effect and hence the carrier density modulation is suppressed in the core region. At these modulation frequencies, carrier density change takes place at the outside of the effective core region, where the quasi-Fermi level is not clamped by the gain saturation due to weak optical intensity. However, as the bias current is increased, due to the stronger effect of gain saturation, carrier density modulation is restrained and the frequency deviation constant decreases [25]. This explains the low frequency deviation constant for large bias current.

3.2 POWER SPECTRAL ANALYSIS

When the light beam is divided into two parts and is then recombined, one part delayed with respect to the other, the FM noise of the LD is converted into intensity fluctuations. The power spectrum of this signal can be obtained analytically by calculating the Fourier transform of the autocorrelation function.

For DFSK systems, the effect of the laser linewidth on the IF broadening can be estimated by calculating the power spectrum of the self-heterodyned optical signal at the detector. From Eq. 2.4, the optical power arriving at the photodetector surface is

$$P_{out} = E_{dy}E_{dt}\cdot\cos\{\omega(t) + \Delta\phi(t)\}\cdot\cos\{\omega(t + T) + \Delta\phi(t + T)\} \ . \qquad (3.7)$$

Neglecting the terms at optical frequencies, we obtain the detector output current

$$I_{out} = RE_{dy}E_{dt}\cdot\cos\{\omega\tau + \Delta\phi(t) - \Delta\phi(t + T)\} \qquad (3.8)$$

where $\omega\tau$ is a constant and can be neglected. Therefore,

$$I_{out} = A\cdot\cos\{\Delta\phi(t)\} \qquad (3.9)$$

where $A = RE_{dy}E_{dt}$ and $\Delta\phi(t) = \phi(t) - \phi(t + T)$.

T is the relative delay in one of the paths and $\Delta\phi$ is known as the phase error. This phase error, which is caused by the random frequency fluctuations in the LD, has been analysed both theoretically and experimentally [35], [36]. It has a gaussian probability density function (PDF) with a zero mean and a variance of $\sigma_\phi{}^2$. The phase noise variance, $\sigma_\phi{}^2$, depends on the time over which the phase fluctuations are measured, and can be expressed as

$$\sigma_\phi{}^2 = 2\pi\Delta f T \ . \qquad (3.10)$$

Δf being the linewidth of the LD and T being the time over which the phase error is accumulated.

The auto-correlation of the received optical signal in Eq. 3.9 is equal to

$$R(t') = E\,[A^2\cdot\cos\{\Delta\phi(t)\}\cdot\cos\{\Delta\phi(t + t')\}] \ . \qquad (3.11)$$

Expressing the above equation in exponential form, we obtain

$$R(t') = \frac{A^2}{4}\cdot E\left[\,[\exp\{j\Delta\phi(t)\} + \exp\{-j\Delta\phi(t)\}]\cdot [\exp\{j\Delta\phi(t + t')\} + \exp\{-j\Delta\phi(t + t')\}]\right] . \qquad (3.12)$$

where $E[x]$ denotes the expected value of the argument x.

The above expression can be solved analytically (see Eq. A.11) and the auto-correlation can be written in the form

$$R(t') = \begin{cases} \frac{A^2}{4} \cdot \left[\exp(-2\pi\Delta f |t'|) + \exp(-4\pi\Delta f T) \cdot \exp(2\pi\Delta f |t'|) \right] & \text{for } |t'| \le T, \\ A^2 \cdot \exp(-2\pi\Delta f T) & \text{for } |t'| > T. \end{cases} \tag{3.13}$$

The normalised Fourier transform of the above equation is equal to (see Eq. A.22)

$$S(f) = \exp(-2\pi\Delta f T) \cdot \delta(f) + \left[1 - \exp(-4\pi\Delta f T) - \frac{2\Delta f}{f} \cdot \sin(2\pi f T) \cdot \exp(-2\pi\Delta f T) \right] \cdot \frac{1}{2\pi} \cdot \frac{\Delta f}{\Delta f^2 + f^2} . \tag{3.14}$$

This power spectrum has a Lorentzian shape with 3 dB bandwidth equal to twice the linewidth of the laser.

Fig. 3.2 shows the power spectrum calculated from Eq. 3.14 for a linewidth of 22 MHz and delay times of 1 ns and 22 ns. Curve (b) in this graph represents the power spectrum that applies to our experimental system. When the delay time in Eq. 3.14 is smaller than the coherence time[1], τ_c of the LD, the first term (delta function) dominates and the magnitude of the power spectrum is small at high frequencies. As this power spectrum represents the carrier signal in a DFSK system, it should have very narrow spectral linewidth if a narrow linewidth IF is desired. IF linewidth is defined as the linewidth of the beat signal (I_{out} in Eq. 3.8). For coherent systems using LDs with Lorentzian lineshape, the IF linewidth can

---

[1] Coherence time is defined to be equal to 1/(linewidth) [55].

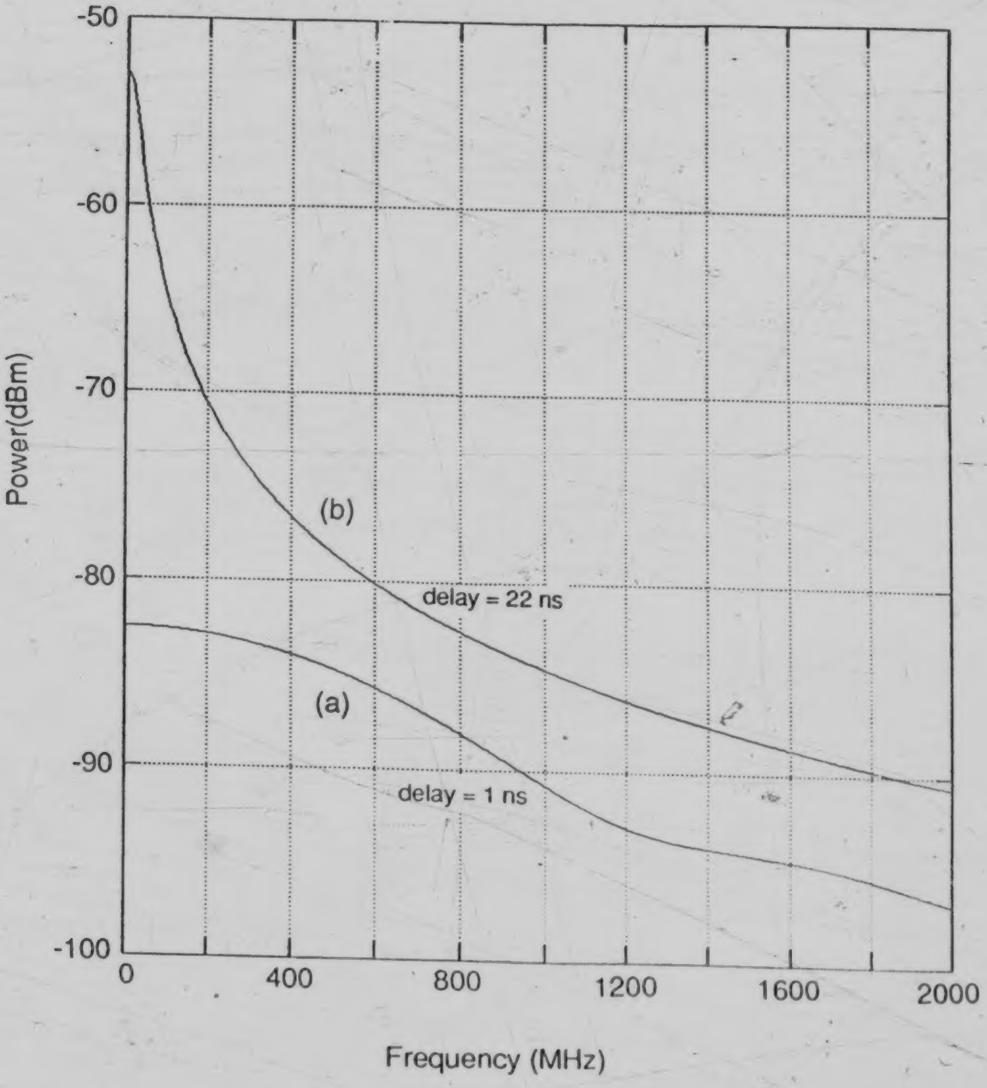

Fig. 3.2 Laser output spectrum for a DFSK system with no modulation signal. Linewidth of the LD = 22 MHz.

be expressed as [37], [38]

$$\Delta\nu_{IF} = \Delta\nu_s + \Delta\nu_{LO} \tag{3.15}$$

where $\Delta\nu_{IF}$ is the IF linewidth, $\Delta\nu_s$ is the source LD linewidth and $\Delta\nu_{LO}$ is the LO linewidth. The relation shown in Eq. 3.15 is true only when the received signal and the LO signals are uncorrelated. However for the self-heterodyned laser output spectrum, as shown in Fig. 3.2, the IF linewidth depends upon the delay time in the delay path.

It should be noted that the power spectrum in Eq. 3.14 also represents the received signal spectrum when a '0' bit is received (this has been and will be referred to in this thesis, as low frequency phase noise). The intersymbol interference, caused by the overlapping of the IF signal and the tail of the low frequency phase noise, will depend upon the magnitude of the low frequency phase noise in the IF band. Since the magnitude of the low frequency phase noise is small for delay times less than the coherence time of the LD, the ratio of the linewidth to the bit rate should be small.

3.3 BIT ERROR RATE CALCULATIONS

It can be assumed that, for a band pass filter with a rectangular pass band, the low frequency phase noise at the receiver will be rejected by the IF filter. Hence, the received signal current can be represented as

$$I_1(t) = A\cdot\cos\,(2\pi f_{IF}t + \Delta\phi(t)) \qquad \text{for a '1' bit,}$$

and

$$I_0(t) = 0 \qquad \text{for a '0' bit.} \tag{3.16}$$

These expressions for the received signal power are similar to those in ASK systems and hence, the theoretical calculations for coherent optical ASK systems should also predict the performance of the DFSK system. At the receiver, shot noise and thermal noise are added to the received signal. If the system is assumed to be linear and the receiver noise is assumed to be independent of the phase noise, then the output current is given by

$$I_1(t) = A\cdot[\cos(2\pi f_{IF}t + \Delta\phi(t)) + n(t)] ,$$

and $$I_0(t) = n(t) . \tag{3.17}$$

The receiver noise, $n(t)$, has a gaussian PDF which can be written as

$$p_n(n) = \frac{1}{\sqrt{2\pi\sigma_n^2}}\cdot\exp\left[-\frac{n^2}{2\sigma_n^2}\right]. \tag{3.18}$$

where σ_n^2 is the variance of the receiver noise, which has been explained in section 3.4. If we assume that the probability of transmitting a '1' bit is equal to that of transmitting a '0' bit, the total probability of error can be expressed as

$$P_e = \frac{1}{2}\cdot(P_{e1} + P_{e0}). \tag{3.19}$$

where P_{e1} is the Probability of error when a '1' bit is received and P_{e0} is the Probability of error when a '0' bit is received.

In other words, if I_{th} is the threshold value of the current at the output of the receiver, the error probabilities are equal to

$$P_{e1} = \mathrm{Prob}[I_1(t)<I_{th})] ,$$

and $$P_{e0} = \mathrm{Prob}[I_0(t)>I_{th})] . \tag{3.20}$$

The theoretical expressions for these probabilities are developed next.

$$P_{e1} = \mathrm{Prob}[(A\cdot\cos(\Delta\phi(t)) + n(t)) < I_{th}]$$
$$= \iint \mathrm{PDF}(I_1)\ d\Delta\phi\cdot dn . \tag{3.21}$$

Substituting $m = A\cdot\cos(\Delta\phi(t))$, and let $p_m(m)$ and $p_n(n)$ denote the PDFs of random variables m and n respectively. It is well known that the PDF of the sum of two independent gaussian random variables is equal to the convolution of their individual PDFs [39]. Hence,

$$\mathrm{PDF}(I_1) = p_x(x) = p_m(m) * p_n(n) \tag{3.22}$$

or

$$\mathrm{PDF}(I_1) = \int_{-\infty}^{\infty} p_m(z)\cdot p_n(x-z)\cdot dz \tag{3.23}$$

$p_{\Delta\phi}(\Delta\phi)$, as explained earlier, has a gaussian form and can be written as

$$p_{\Delta\phi}(\Delta\phi) = \frac{1}{\sqrt{2\pi\sigma_\phi^2}}\cdot\exp\left[-\frac{\sigma_\phi^2}{2\sigma_\phi^2}\right] \tag{3.24}$$

where $\sigma_\phi^2 = 2\pi\Delta f\tau$ and τ is the integration time which depends upon the filter bandwidth and is approximately equal to 1/B (B being the IF filter bandwidth) [40].

The PDF of m can be expressed in terms of the PDF of $\Delta\phi$ as in [41]

$$p_m(m) = p_{\Delta\phi}(m)\cdot\frac{1}{\left|\dfrac{d[A\cdot\cos(\Delta\phi)]}{d(\Delta\phi)}\right|} \tag{3.25}$$

where A is a constant.

The above expression has been simplified in [41] and the resulting expression is

$$p_m(m) = \frac{1 + r(m)}{\sqrt{2\pi\cdot(A^2-m^2)}\cdot\sigma_\phi}\cdot\exp\left[-\frac{\arccos(m/A)}{2\sigma_\phi^2}\right] \tag{3.26}$$

where

$$r(m) = \sum_{i=1}^{\infty} \exp\left[-\frac{2i^2\pi^2}{\sigma_\phi^2}\right]\cdot\left\{\exp\left[\frac{2\pi i\cdot\arccos(m/A)}{2\sigma_\phi^2}\right]\right.$$

$$\left. + \exp\left[\frac{-2\pi i\cdot\arccos(m/A)}{2\sigma_\phi^2}\right] . \qquad (3.27)\right.$$

It follows from Eq. 3.23 that

$$p_x(x) = \frac{1}{\pi\sigma_\phi\sigma_n}\int\frac{1 + r(z)}{\sqrt{A^2 - z^2}}\cdot\exp\left[-\frac{\arccos\ (z/A)}{2\sigma_\phi^2}\right]\cdot\exp\left[-\frac{(x-z)^2}{\sigma_\phi^2}\right]\cdot dz . \qquad (3.28)$$

Substituting

$\gamma = \frac{A^2}{2\sigma_n^2}$ and $k = \arccos(z/A)$ in Eq. 3.28 yields

(γ is the signal to receiver noise ratio)

$$P_x(x) = \frac{\sqrt{2\gamma}}{A\pi\sigma_\phi}\cdot\int\sqrt{1 - \cos^2(k)}\cdot\exp\left[-\frac{k^2}{2\sigma_\phi^2}\right]\cdot\exp\left[-\gamma\cdot\left\{\frac{x}{A} - \cos(k)\right\}\right]\cdot dk . \qquad (3.29)$$

In the above derivation it has been assumed that $\sigma_\phi<1$ and therefore, $r(z)=0$. From this equation P_{e1} can be obtained as

$$P_{e1} = \int_{-\infty}^{I_{th}} p_x(x)\cdot dx . \qquad (3.30)$$

Also,

$$P_{e0} = \int_{I_{th}}^{\infty}\frac{1}{\sqrt{2\pi\sigma_n^2}}\cdot\exp\left[-\frac{x^2}{2\sigma_n^2}\right]\cdot dx . \qquad (3.31)$$

Substituting

$$\frac{x2}{2\sigma_n^{\;2}} = t^2 \qquad \text{and} \qquad dx = \sqrt{2\sigma_n^{\;2}}\cdot dt$$

yields

$$P_{e0} = \int_{I_{th}/\sqrt{2\sigma_\nu}}^{\infty} \frac{1}{\sqrt{\pi}}\cdot \exp\,(-t^2)\cdot dt \tag{3.32}$$

or

$$P_{e0} = \frac{1}{2}\cdot\left[1 - \mathrm{erf}(b\cdot\sqrt{\gamma})\right] = \frac{1}{2}\cdot\left[\mathrm{erfc}(b\cdot\sqrt{\gamma})\right]. \tag{3.33}$$

In the above equation, $b = I_{th}/A$, is the normalised threshold level

The total probability of error as a function of signal to noise ratio can be computed numerically and is shown in Fig. 3.3 [42]. These curves clearly indicate that the value of σ_ϕ should be less than 0.2 to achieve a BER of 10^{-9}. Similar results have been obtained by Kikuchi and Okoshi [43]. Substituting the required value of σ_ϕ and τ, the required source linewidth to IF filter bandwidth ratio should be 0.0063 to obtain a BER of 10^{-9}. However, in practical systems it has been shown that with a linewidth to IF filter bandwidth ratio of 0.04, a BER of 10^{-9} can be obtained [44]. This discrepancy between the theoretical and the experimental results is due to the assumption that the effect of the IF filter on the PDF of the phase noise is negligible. Recently, Garrett and Jacobsen developed a computer model to calculate the effect of laser phase noise on the performance of coherent systems [45]. They obtained results for different values of the IF linewidth to bit rate ratio and these results are shown in Fig. 3.4 [46]. In these curves, $\Delta\nu_{IF}$ represents the IF linewidth, which is equal to the sum of the transmitter and the LO laser linewidths [45]. It can be inferred from the graph that, by selecting a proper bandwidth for the IF filter, the detrimental effects due to the phase noise of the LD can be compensated. However, an increase in the bandwidth of the filter

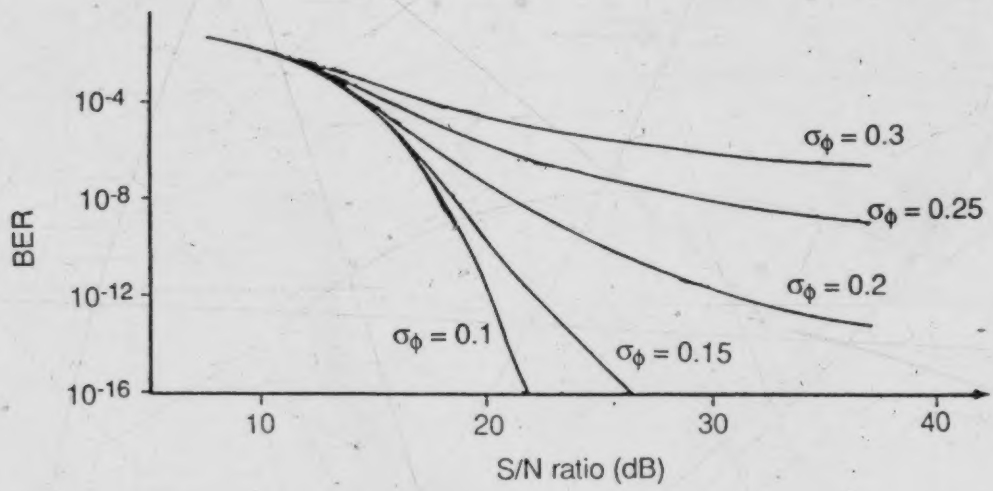

Fig. 3.3 Theoretical BER as a function of the received signal to noise ratio.

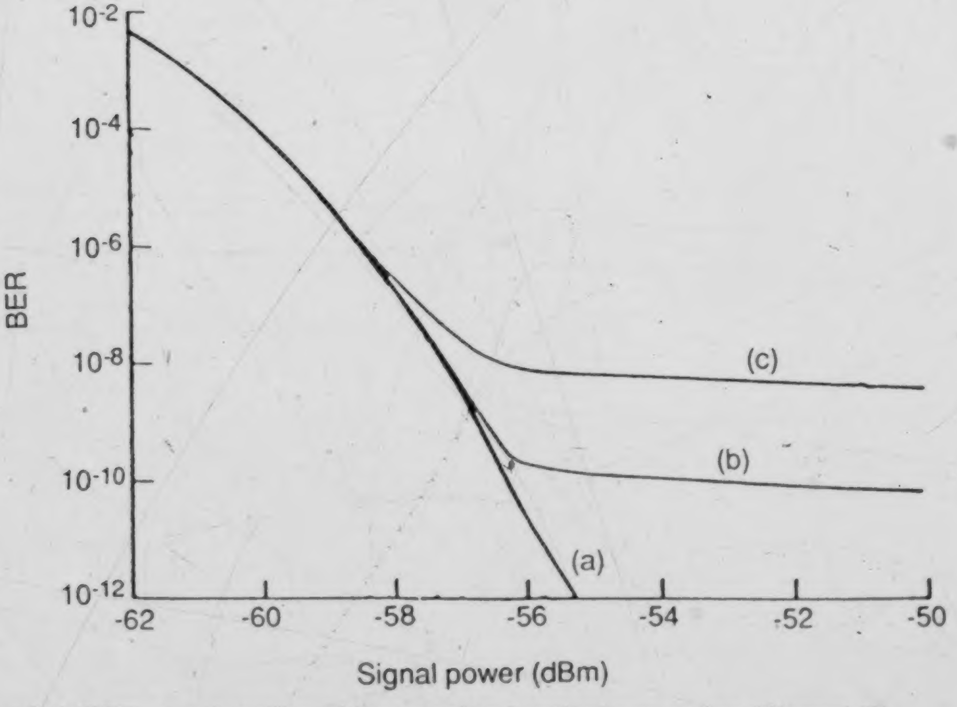

Fig. 3.4 BER as a function of the received optical power for different IF linewidths and a filter bandwidth of $5R_b$.

(a) IF linewidth = $0.3R_b$.
(b) IF linewidth = $0.4R_b$.
(c) IF linewidth = $0.5R_b$.

will also increase the noise in the receiver and hence will result in poor receiver sensitivity.

3.4 CROSS-TALK PENALTY IN TWO CHANNEL DFSK SYSTEM

When two channels are received at the receiver, the power spectrum of one channel may overlap that of the other channel. This inter-channel interference depends upon the channel spacing, the bit-rate and the linewidth of the transmitting LDs. For a multi-channel optical fiber transmission system, two types of interference occur:

1. Intermodulation distortion (IMD)
2 Inter-channel interference

Intermodulation distortion occurs due to the non-linear response of the photodetector, which causes the different carrier frequencies to mix with each other and yield intermodulation frequencies [47]. This effect is more serious in IMDD systems than in coherent systems. In coherent optical systems, if the LO power is sufficiently large, then the intermodulation frequencies will be very small in amplitude as compared to the desired signal. However, in DFSK systems, since the LO signal is very weak, the amplitude of the intermodulation frequencies can be comparable to that of the received signal. But if the optical carrier frequencies for different channels are spaced sufficiently apart, then the intermodulation frequencies will be rejected by the receiver bandwidth.

After the received optical signal is converted into the electrical domain, the power in one channel may extend into the frequency domain of the other channel and hence cause interchannel interference. This interference depends upon the spectral spread of each channel and the spacing of the IFs. Inter-channel interference for coherent optical communication systems has been analysed by Kazovsky [48]. In his analysis, he assumes that the linewidth of the LDs are very small as compared to the data rate and hence do not have any significant effect on the IF. This assumption is not true in our case.

In this section, the signal to interference ratio (SIR) as a function of the normalised channel spacing (normalised to the bit rate) has been calculated for a DFSK system, taking the laser linewidth into account. The intermodulation distortion due to mixing of the optical carriers is assumed to be negligible. SIR is defined as [49]

$$\mathrm{SIR} = \frac{P_0}{P_{int}} = \frac{A_1 \cdot \int |H(f)|^2 \cdot G(f) \cdot df}{A_2 \cdot \int |H(f)|^2 \cdot G_{int}(f) \cdot df} \tag{3.34}$$

where G(f) is the power in the main channel, $G_{int}(f)$ is the power in the interfering channel, and H(f) is the transfer function of the filter defined as follows

$$\begin{aligned} H(f) &= 1 && \text{for } |f_{IF} - B| < |f| < |f_{IF} + B| \\ &= 0 && \text{otherwise.} \end{aligned} \tag{3.35}$$

The bandwidth of the IF filter is 2B.

Further, it has been assumed that the IF frequency (f_{IF}) is very large and hence the interference due to the low frequency phase noise of the LD is ignored.

The power spectrum of the IF signal can be represented by the following [50]

$$G(f) = G_c(f) * G_b(f) \tag{3.36}$$

where * denotes convolution.

$G_c(f)$ is the power spectrum of the carrier, which has been calculated in Eq. 3.14 and $G_b(f)$ is the normalised power spectrum of the NRZ modulating signal. For a NRZ signal

$$G_b(f) = \frac{1}{4R_b} \cdot \mathrm{sinc}^2 \left[\frac{f}{R_b} + \frac{1}{4} \cdot \delta(f) \right] . \tag{3.37}$$

Further, it has been assumed that the two channels contain equal power and are identical, so that $A_1 = A_2$ and $G(f) = G_{int}(f)$.

Hence, if S is the channel spacing, the SIR can be represented as

$$SIR(S) = \frac{\int_{f_{IF} - B}^{f_{IF} + B} (G(f - f_{IF}) \, df}{\int_{f_{IF} - B}^{f_{IF} + B} (G(f - f_{IF} - S) \, df} . \qquad (3.38)$$

This equation has been evaluated numerically using a computer program and the results are shown in Fig. 3.5. To achieve a BER of 10^{-9}, the signal to noise ratio should be about 18 dB for an ASK or FSK system [43]. Therefore a suitable channel spacing for a DFSK system would be about $15R_b$. In the above analysis, we have not considered the receiver noise. As the receiver noise is independent of the channel spacing, its effect would be to lower the graph, and hence to further increase the required channel spacing to obtain the desired signal to noise ratio. Hoffstetter [51] has calculated the signal to noise and crosstalk ratio for a multi-channel DFSK system, assuming negligible linewidth of LDs. His results suggest that, with a channel spacing of $12R_b$, a signal to noise ratio of 18 dB can be achieved. The difference between his results and our results can be attributed to the linewidth factor.

3.5 RECEIVER NOISE ANALYSIS

The major noise sources in the receiver arise from the random nature of the photon to electron conversion process and the thermal noise associated with the amplifier. These noise sources determine the receiver sensitivity, which is defined as the minimum required optical power at the photodetector, to achieve a BER of 10^{-9}. Receiver noise can be categorised as follows:

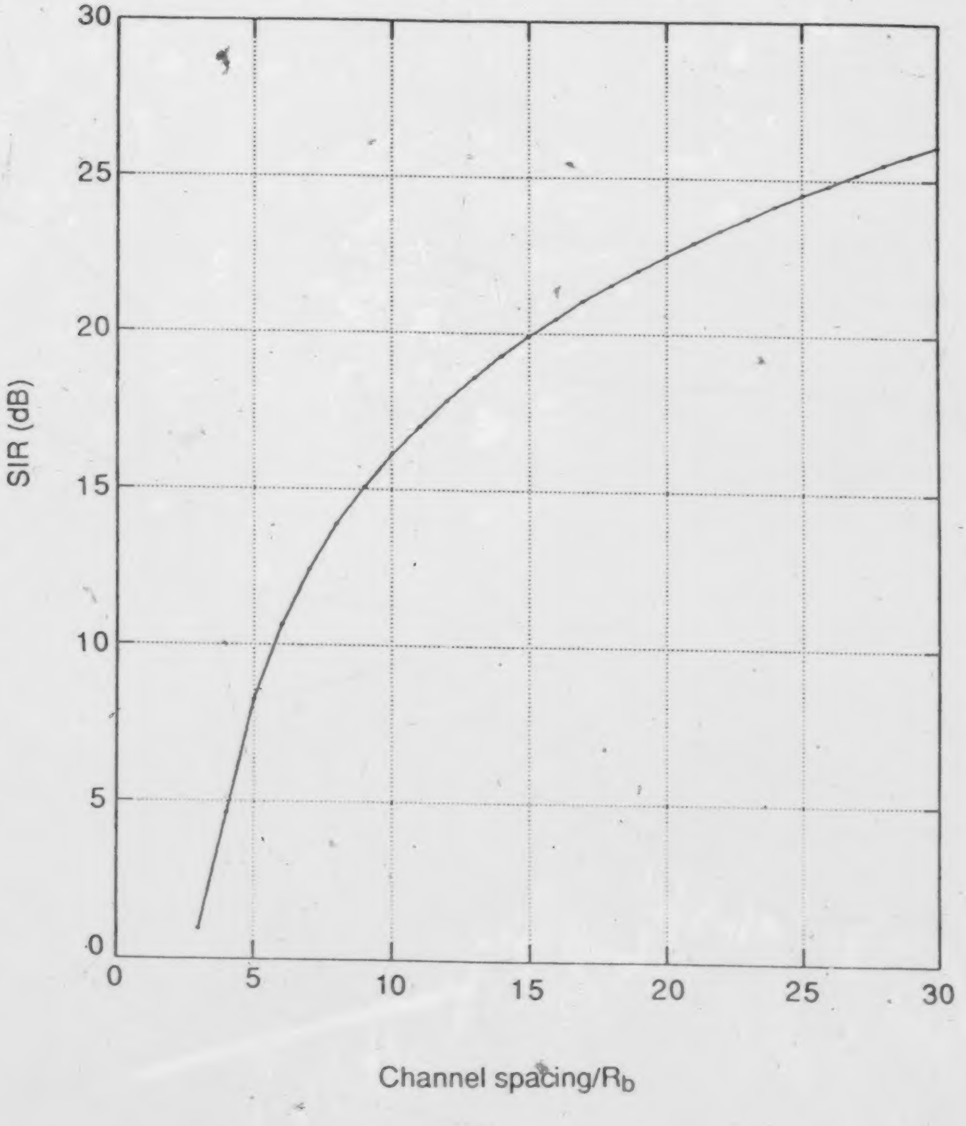

Fig. 3.5 SIR as a function of the normalised channel spacing for a DFSK system.

1. **Shot Noise**:

Shot noise in an optical receiver is signal dependent and depends upon the rate of arrival of photons at the receiver. In a given time, the number of electron-hole pairs generated is a random variable with a Poisson's distribution [52], [53]. The mean square value of this noise current can be expressed as

$$\langle I_s^2 \rangle = 2eR_pP_{opt}B \qquad (3.39)$$

where R_p is the responsivity of the photodetector, P_{opt} is the optical power, and B is the receiver bandwidth.

2. **Dark Current Noise**:

Dark current is defined as the reverse current which flows when no light is incident on the photodetector. This current is caused by the generation of hole and electron pairs in the depletion region, due to the thermal effects. The mean square value of the dark current noise can be expressed as [54]

$$\langle I_d^2 \rangle = 2eI_DB \qquad (3.40)$$

where I_D is the detector dark current, e is the electronic charge, and B is the filter bandwidth.

3. **Thermal Noise**:

Thermal noise occurs due to random motion of the charge carriers (electrons) in a conducting medium due to temperature. The thermal noise current in a resistance R can be expressed as

$$\langle I_t^2 \rangle = 4kTB/R \ . \qquad (3.41)$$

For a high input impedance amplifier, the load resistance is much smaller than the amplifier input resistance. Therefore, to minimise the thermal noise, the load resistance should be large. However, a large bias resistance limits the receiver bandwidth.

For a FET front end amplifier, the total noise current due to the amplifier can be expressed as [54]

$$\langle I_a{}^2\rangle = \frac{4kT}{R_L}\cdot\left[1 + \frac{\Gamma}{g_m R_L}\right]\cdot B + 2eI_{gate}B + 4kT\Gamma\cdot\frac{(2\pi C_T)^2}{g_m}\cdot B^3 \tag{3.42}$$

where R_L is the load resistance, Γ is a constant given by FET material (≈ 1.1 for GaAs), C_T is the total capacitance, g_m is the transconductance of FET, I_{gate} is the gate leakage current, and B is the IF filter bandwidth.

The receiver noise sources described above are plotted as a function of the filter bandwidth and are shown in Fig. 3.6. For the experimental receiver, R_L is 5kΩ, C_T is equal to the sum of the PIN diode (C_p) and FET gate to source (C_{gs}) capacitances and equals 0.8 pF, g_m is equal to 0.048 mho and I_{gate} is equal to 1 mA. From Fig. 3.6, it is clear that the thermal noise is greater than the shot noise and the dark current noise in the detector, and therefore largely determines the receiver noise. The three noise sources are completely independent and the total noise variance can be expressed as

$$\sigma_n{}^2 = \langle I_s{}^2\rangle + \langle I_d{}^2\rangle + \langle I_a{}^2\rangle\ . \tag{3.43}$$

A more detailed investigation of the receiver noise has been presented by Personick [53].

3.5 SUMMARY

The linewidth of the transmitting LD can cause significant broadening of the IF. The non-flat frequency response of DFB LDs also contributes to the wide spectral spread of the IF, although this effect can be compensated for by using a phase tunable or multi-electrode DFB laser. In this chapter, the effect of the IF linewidth on the BER performance was analysed. It has been reported in the literature that, for a broad linewidth transmitting LD, increasing the IF filter bandwidth lowers the error rate floor. However, this also increases the receiver noise and degrades the receiver sensitivity. For multi-channel transmission, it has

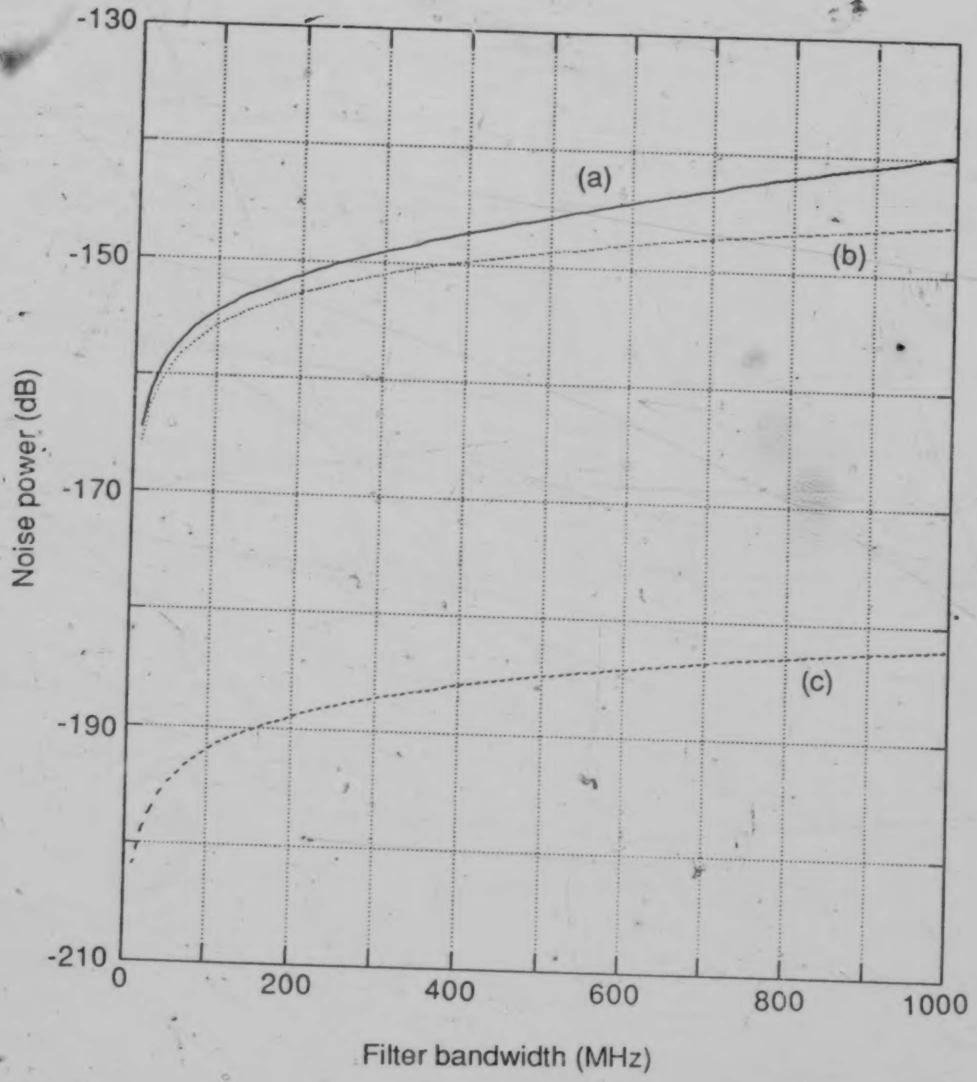

Fig. 3.6 Receiver noise components as a function of the filter bandwidth.
(a) Thermal noise.
(b) Shot noise due to the received signal.
(c) Dark current noise.

been calculated that, for a SIR of 20 dB, the minimum required channel spacing should be 15 times the bit-rate. In order to determine the signal to noise ratio as a function of the channel spacing, the receiver noise should also be taken into account. From the calculated results, it is clear that the channel spacing required in a DFSK system is more than that required in other coherent systems. This is due to the mixing of very weak and noisy signals in the direct path and the delayed path.

CHAPTER 4 - TRANSMITTER DESIGN

For a DFSK system, the transmitter can be divided into two sections; namely, the optical source and the data encoder. The optical source consists of a LD, an optical isolator and GRIN rod lenses. The data encoder, on the other hand, consists of a differential encoder and a Manchester encoder. A detailed diagram of the transmitter in the experimental setup is shown in Fig. 4.1. The NRZ data from the data generator (HP 3762A) are sent to the Manchester encoder and subsequently to the differential encoder. The encoded data are superimposed on the bias current to frequency modulate the LD. The optical signal from the LD, in each channel, is then coupled to the fiber using two GRIN rod lenses and two optical isolators. This chapter includes a description of the various transmitter components and the experimental setup used to measure the characteristics of the LD.

4.1 TRANSMITTER COMPONENTS

4.1.1 DFB LASER DIODES

In coherent optical transmission systems, the LDs at the transmitter and at the LO should oscillate in a very stable single mode and should exhibit a very narrow linewidth. The narrowest linewidth is provided by external cavity lasers in which external optical feedback is used to stabilise the frequency output. However, if the phase of the feedback is not controlled, the linewidth of such LDs may broaden under the influence of the feedback [56]. Also, due to very high cavity Q, these lasers have a very poor frequency deviation constant [57]. They are also very sensitive to temperature and to the environment. Hence, these LDs are not suitable for DFSK transmission systems.

Another method for achieving a single longitudinal mode and a narrow

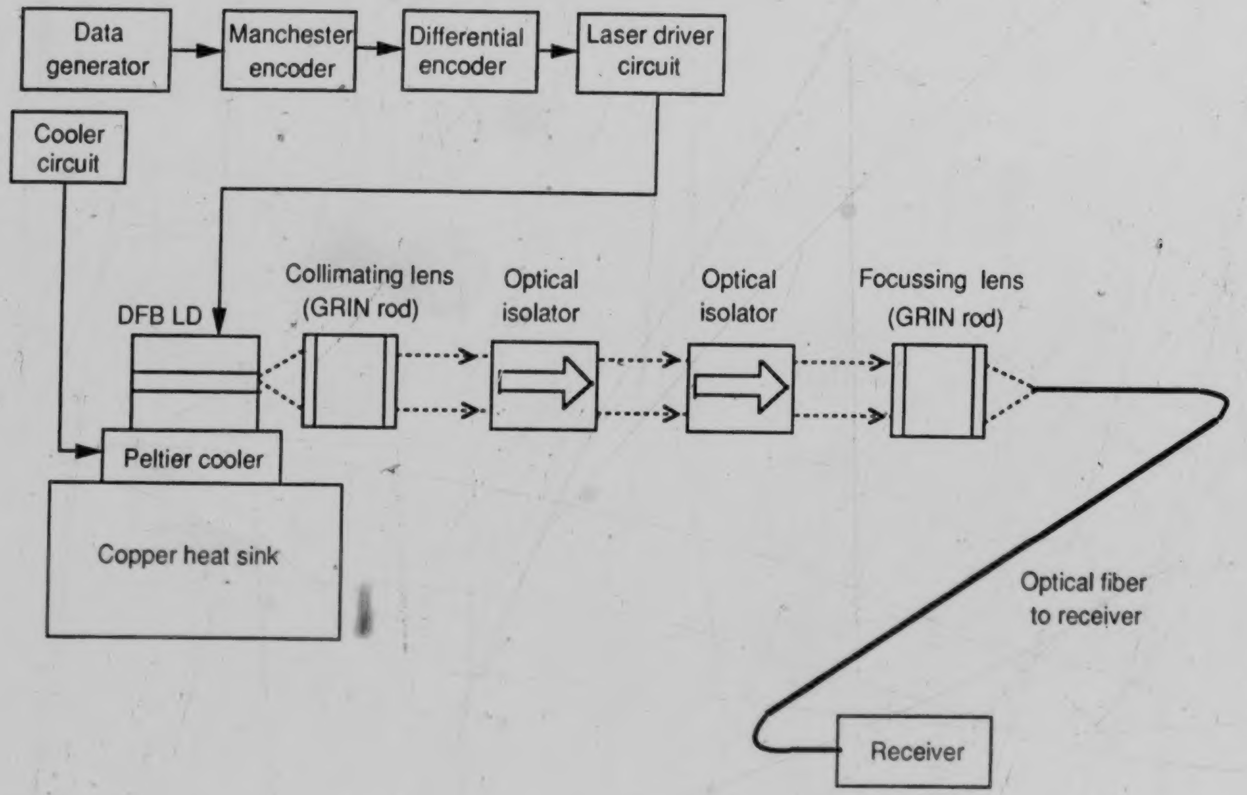
Data generator
Manchester encoder
Differential encoder
Laser driver circuit
Cooler circuit
DFB LD
Collimating lens (GRIN rod)
Optical isolator
Optical isolator
Focussing lens (GRIN rod)
Peltier cooler
Copper heat sink
Optical fiber to receiver
Receiver

Fig. 4.1 Detailed diagram of single channel DFSK transmitter.

linewidth is to provide frequency selective feedback throughout the active layer in the LD. LDs based on such a mechanism are known as distributed feedback (DFB) LDs. In DFB lasers, the feedback is not localised at the cavity facets but is distributed throughout the active region. This is accomplished by a periodic variation of the refractive index that provides feedback by means of backward-wave Bragg scattering. The change in refractive index can be realised by means of a grating formed by periodically varying the thickness of one of the active layers in the laser. If Λ is the grating period, the Bragg condition for coherent coupling between the forward and backward propagating waves is [58]

$$\Lambda = \frac{m\lambda}{2n} \tag{4.1}$$

where m is the order of coupling, n is the refractive index and λ is the wavelength. For a first order grating, the Bragg wavelength can be expressed as $\lambda_B = 2n\Lambda$. Hence, by selecting Λ properly, the feedback is provided only at certain selected wavelengths. These LDs often exhibit side mode suppression ratios of about 30 to 35 dB. DFB lasers will mode-hop between two longitudinal modes, which are situated symmetrically around the Bragg wavelength [59]. However, if a phase shift of π is introduced in the centre of the corrugation, the resonance occurs at the Bragg wavelength. This phase shift can be achieved by shifting the phase of the corrugation by $\Lambda/4$.

For the experimental DFSK system, we used two DFB LDs at the transmitter. In channel 1, a NEC quarter wave shifted DFB laser was used while in channel 2, a Fujitsu DFB laser was used. The wavelength and the linewidth measurements for these LDs are presented in section 4.2.

4.1.2 GRIN ROD LENS

In each channel, two NSG GRIN rod collimating lenses are used to launch light into optical fiber. The first lens, near the LD, collects as much light from the LD as possible and converts the divergent optical beam to a parallel beam, and acts as a collimating lens. As the GRIN rod lens is placed next to the laser, the reflected light from this collimating lens will result in optical feedback to the LD. Reflections to the LD are reduced using a plano-convex lens which is anti-reflection coated for 1300 nm. Also, to capture the maximum amount of light from the LD, the lens should have a large numerical aperture. The numerical aperture and the focal length of the lens used in this system are 0.6 and 280 μm, respectively. The distance between this lens and the LD is adjusted to obtain a collimated beam.

Another lens is used to focus the collimated beam, after it has passed through the optical isolator, into the optical fiber. The numerical aperture for this focussing lens is not as critical as that for the first lens and hence a lens with a numerical aperture equal to 0.46 is used. The focal length of this lens is 260 μm. This lens is also anti-reflection coated for 1300 nm wavelength.

4.1.3 OPTICAL ISOLATOR

The frequency modulation characteristics as well as the linewidth of the LD are adversely affected by optical feedback caused by reflections from the fiber. Optical feedback signal levels as low as -55 dBm can cause detrimental effects on the LD linewidth [60], [56]. To minimise the level of the optical feedback due to the fiber surface, an optical isolation of 60 dB is provided in the path between the fiber and the LD. This isolation is achieved using two optical isolators (NEC 0D8313 B and FUJI YD-103-9-130), which together provide an isolation of about 60 dB. Optical isolation also helps in suppressing the external cavity modes, which may develop due to the formation of a cavity between the LD and the fiber. In an external cavity configuration, the modes are separated by frequencies equal to c/2nL, where c is the velocity of light in free space, n is the refractive index, and L is the cavity length. These modes, if present, will severely degrade the performance of the system.

4.1.4 MANCHESTER ENCODER

The circuit diagram for the Manchester encoder is shown in Fig. 4.2. The

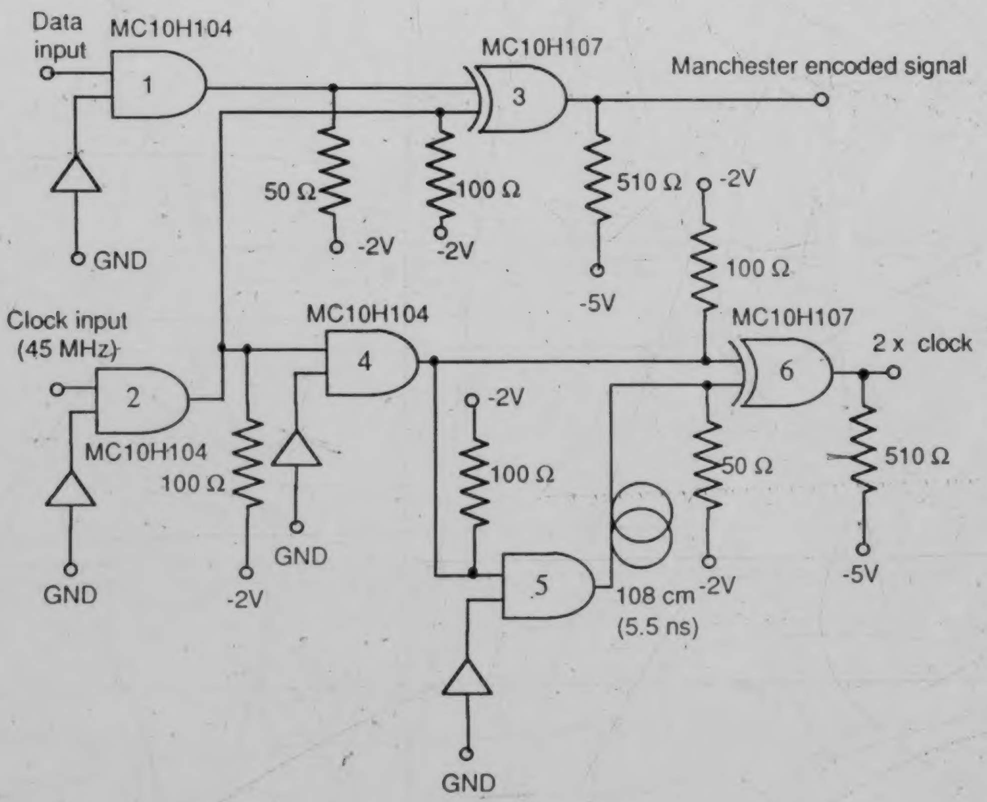
Data input
MC10H104
1
GND
MC10H107
3
Manchester encoded signal
50 Ω
-2V
100 Ω
-2V
510 Ω
-5V
-2V
100 Ω
Clock input (45 MHz)
2
MC10H104
GND
100 Ω
-2V
MC10H104
4
GND
-2V
100 Ω
5
GND
108 cm (5.5 ns)
MC10H107
6
2 x clock
50 Ω
-2V
510 Ω
-5V

Fig. 4.2 Manchester encoder and clock doubler circuit.

clock (44.7 MHz) and the data (44.7 Mb/s) are sent to two AND gates, which act as buffer stages. The outputs of gate 1 and of gate 2 are then coupled to an XOR circuit (gate 3) to obtain a Manchester encoded signal. The rising edge of the clock and of the data signal should occur at the same time at the input of gate 3. Therefore, the length of the coaxial cables carrying the data and the clock from the data generator to the Manchester encoder should be exactly the same. Since Manchester encoding increases the effective bit rate by a factor of 2, the frequency of the clock also needs to be doubled. To increase the frequency of the clock from 44.7 MHz to 89.4 MHz, an XOR gate is used. As shown in Fig. 4.3(a), The received clock is divided into two parts and one part is delayed by 5.5 ns (one quarter of the clock period) with respect to the other part. The delayed and the direct parts are then sent to an XOR gate, which generates a clock at 89.4 MHz. The timing diagram for this circuit is shown in Fig. 4.3(b). The delay introduced by the delay line should be exactly equal to 5.5 ns. The output of the Manchester encoder and of the clock doubler circuit are shown in Fig. 4.4(a) and (b), respectively.

4.1.5 DIFFERENTIAL ENCODER

The differential encoder is designed using a J-K flip-flop, as shown in Fig. 4.5. The AND gates are used to prevent any loading from the preceding or the succeeding stage. The J and K input pins of the flip-flop are tied together and the NRZ data are applied to this input, while the clock signal is connected to the clock input. When a '1' bit is received, the output of the flip-flop toggles or changes from its previous value whereas when a '0' bit is received, the output remains the same as in the previous bit. These transitions occur only at the positive edge of the clock. Fig. 4.6 depicts the input and the output signal obtained from the differential encoder.

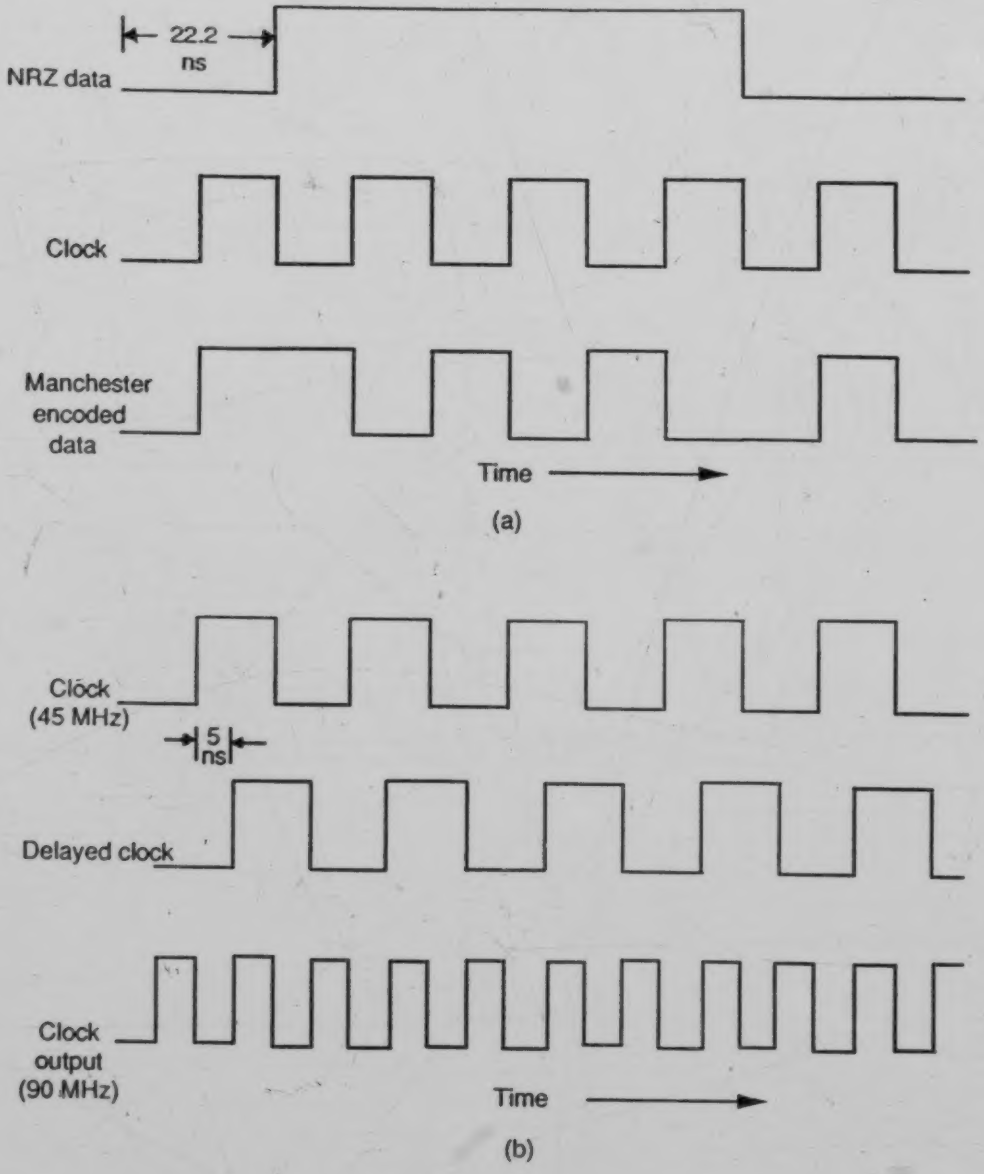
22.2 ns
NRZ data
Clock
Manchester encoded data
Time
(a)
Clock (45 MHz)
5 ns
Delayed clock
Clock output (90 MHz)
Time
(b)

Fig. 4.3 Timing diagram for

(a) Manchester encoder.

(b) Clock doubler.

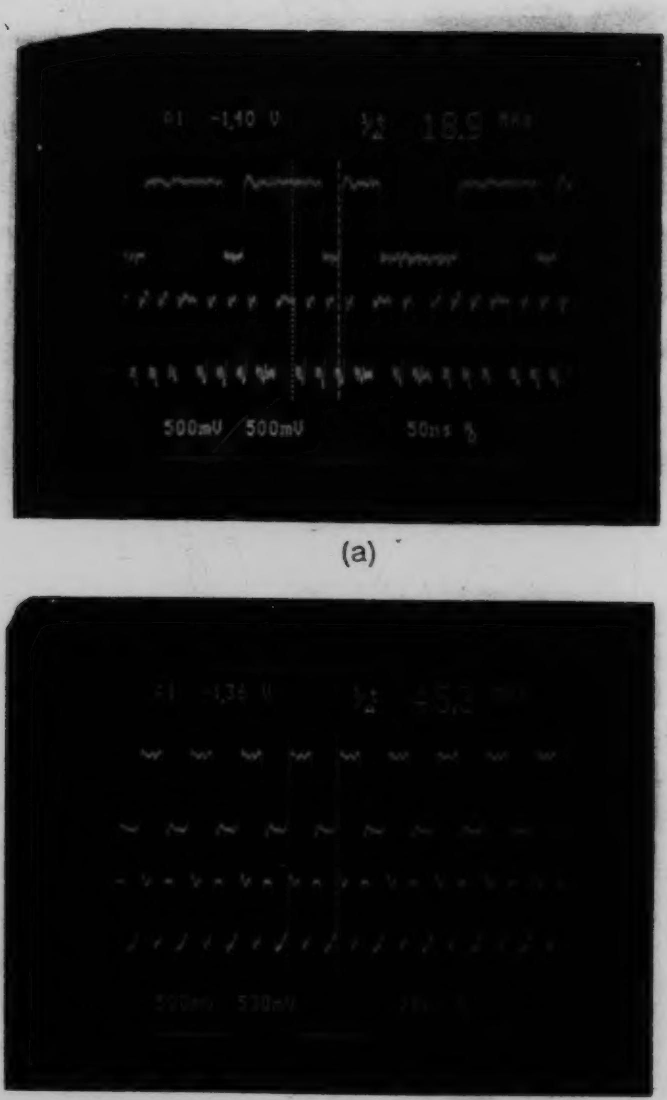

(a)

(b)

Fig. 4.4 Signal waveforms at the transmitter

(a) The NRZ data (upper trace) and the Manchester encoded signal (lower trace) for a data sequence of 1111011110110000. The Manchester encoded signal is delayed by about two bit periods as compared to NRZ data.

(b) The clock signal for a 45 Mb/s data rate (upper trace) and the clock signal at the output of the clock doubler circuit.

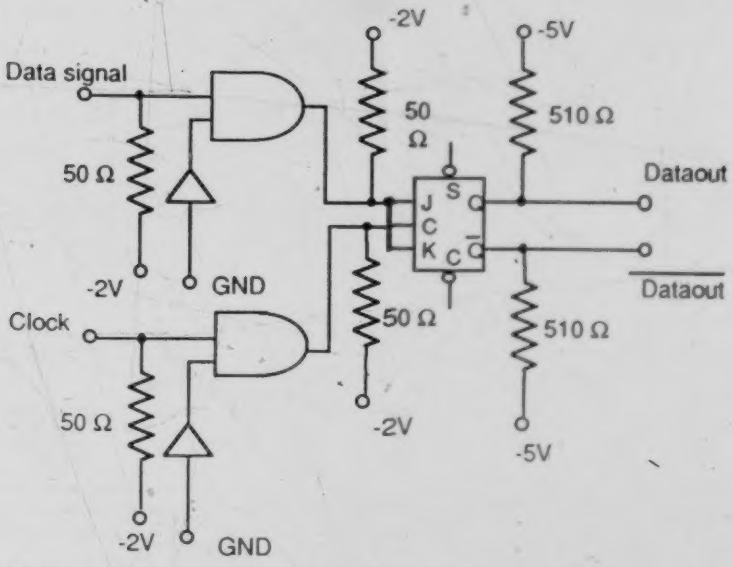
-2V
-5V
Data signal
50
Ω
510 Ω
50 Ω
Dataout
S
J
C
K
C
Q
Q̄
-2V
GND
Dataout
Clock
50 Ω
510 Ω
50 Ω
-2V
-5V
-2V
GND

Fig. 4.5 Circuit diagram of the differential encoder.

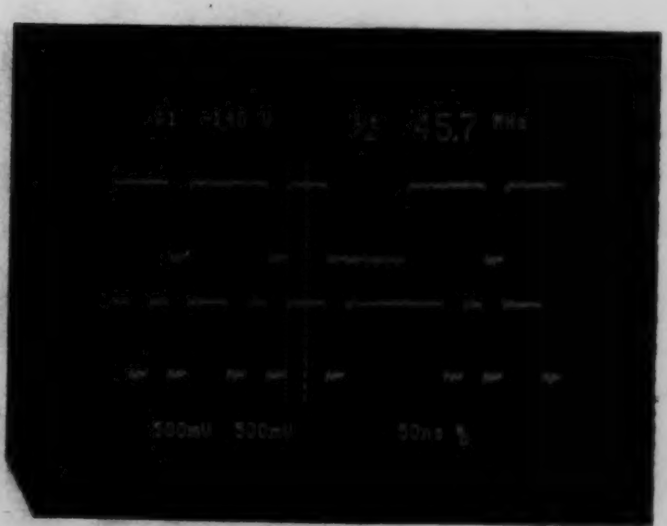

Fig. 4.6 The input signal (upper trace) and the differentially encoded output signal (lower trace) for a data pattern of 111101100001111O.....
The differentially encoded signal is delayed by two bit periods as compared to the input signal.

4.1.6 LASER DRIVER CIRCUIT

To modulate the LD at high bit rates, the laser driver circuit should be capable of operating at high frequencies. The LD driver circuit designed for the experimental system is shown in Fig. 4.7. This circuit uses a differential input and the switching is achieved by two Schottky diodes (HP 5082-2209), D1 and D2. These diodes are capable of very fast switching and can operate at frequencies as high as 10 GHz. The data and data signal, from the differential encoder, are sent to transistors T_4 and T_5. When the data signal is high, data is low and hence, diode D1 is on and diode D2 is off, and vice-versa. This switching of diodes causes the modulation current to flow in the LD. Hence, the rise time and the fall time of the signal will depend on the switching time of these diodes. The peak-to-peak amplitude of the ac modulating current can be adjusted by changing the value of the variable resistor R_{11}. The dc bias current through the LD can be monitored by measuring the voltage across the 10Ω resistor, R_3, and can be adjusted by a variable resistor R_{10}. The maximum ac and dc current that are allowed to pass through the LD are determined by resistances R_8 and R_9 respectively.

During the first stage of the experiment, when the Manchester encoder was not incorporated into the system, the switching was achieved by transistors T_4 and T_5. However, these transistors were not found to be suitable for switching at a data rate of 90 Mb/s. Therefore, when the Manchester encoder was added to the system, switching was accomplished by Schottky diodes instead of transistors.

The LD chip was mounted on a micro-positioner and was connected to the laser driver circuit through two jumper wires. These jumper wires can introduce lead inductances at high frequencies and hence cause distortion in the modulating signal waveform. The problem of lead inductance can be alleviated

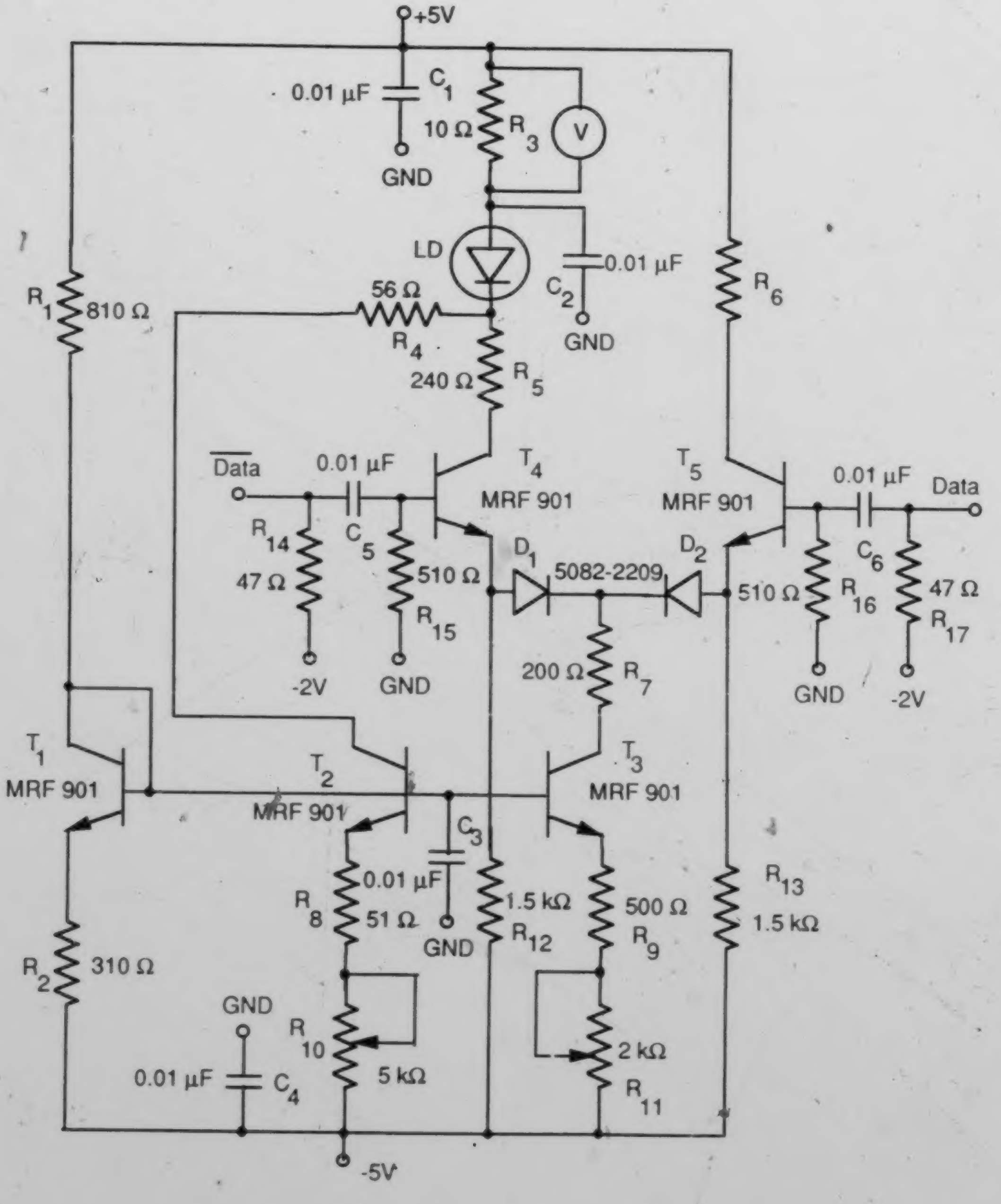
+5V
0.01 µF
C_1
10 Ω
R_3
V
GND
LD
0.01 µF
C_2
GND
56 Ω
R_4
240 Ω
R_5
R_1
810 Ω
R_6
$\overline{\text{Data}}$
0.01 µF
C_5
T_4
MRF 901
T_5
MRF 901
0.01 µF
Data
R_{14}
47 Ω
510 Ω
R_{15}
-2V
GND
D_1
5082-2209
D_2
510 Ω
R_{16}
C_6
47 Ω
R_{17}
GND
-2V
200 Ω
R_7
T_1
MRF 901
T_2
MRF 901
T_3
MRF 901
C_3
0.01 µF
GND
R_8
51 Ω
1.5 kΩ
R_{12}
500 Ω
R_9
R_{13}
1.5 kΩ
R_2
310 Ω
GND
0.01 µF
C_4
R_{10}
5 kΩ
2 kΩ
R_{11}
-5V

Fig. 4.7 Circuit diagram of laser driver circuit.

by a packaged DFB LD, which can be mounted directly on the circuit board. However, the package capacitance of such LDs should be very low, so as to avoid any modulation bandwidth limitations.

To ensure that the bandwidth of the laser driver circuit was sufficiently large to transmit a 90 Mb/s signal, a test was performed by modulating the injection current of the LD with the Manchester encoded signal. The amplitude modulated optical signal was then detected directly at the receiver. The received signal waveform at the output of the photodetector for a received data sequence of 11011000100110011... is shown in Fig. 4.8. The voltage spikes at the positive and the negative transition could be due to the lead inductance of the jumper wires. These spikes are not desirable in a DFSK system, as they will cause IF noise. The rise time and the fall time of the transmitted pulses should be smaller than 10% of the bit period in order to avoid any significant broadening of the IF.

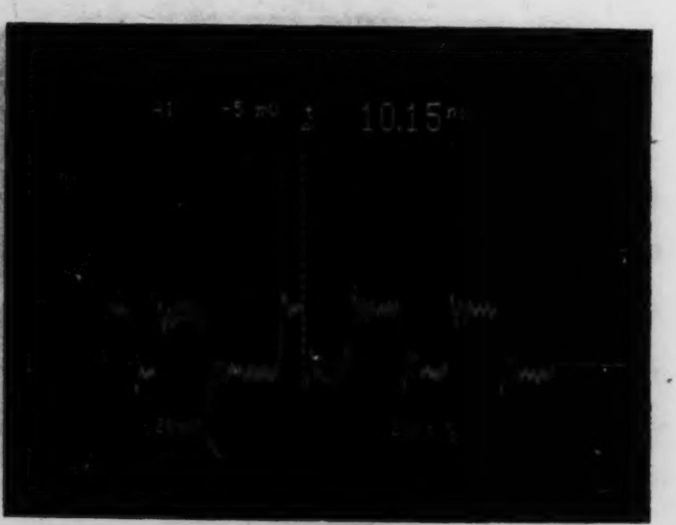

Fig. 4.8 Optical pulses received from the LD.

Also, since the modulating current is generated by the switching of the Schottky diodes, this bias circuit can only be used for square wave modulation or digital signal transmission.

4.1.7 COOLING CIRCUIT

The frequency of emmision from an LD depends on its operating temperature. In our experimental system, as shown in Fig. 4.1, the LD rests on a Peltier cooler, which constantly stabilises the temperature. The current in the cooler is controlled by a feedback control circuit, shown in Fig. 4.9. A thermistor is used to sense the temperature of the LD, which also provides the feedback signal. The equivalent resistance of the thermistor as a function of its temperature is shown in Appendix B. The variable resistance R_g is used to set the reference temperature. As the temperature of the LD rises or falls, the resistance of the thermistor is no longer equal to the reference resistance R_g and the bridge is unbalanced. The output of the differential amplifier thus causes the current through the cooler to increase or decrease accordingly.

4.2 EXPERIMENTAL MEASUREMENTS

4.2.1 WAVELENGTH MEASUREMENTS

For the DFSK system, it is essential that the wavelengths of all the transmitting stations should be different from each other. If the two stations have the same operating wavelength, there will be interference between the transmitted signals and data will be lost. Hence, to ensure that the wavelengths of the two transmitting LDs are different, a scanning monochromator was used to measure the respective wavelengths. For both LDs, the side mode suppression ratio (SMSR), as shown in Fig. 4.10, was greater than 30 dB. The operating wavelengths of the NEC and Fujitsu DFB LDs were measured to be 1302 nm and

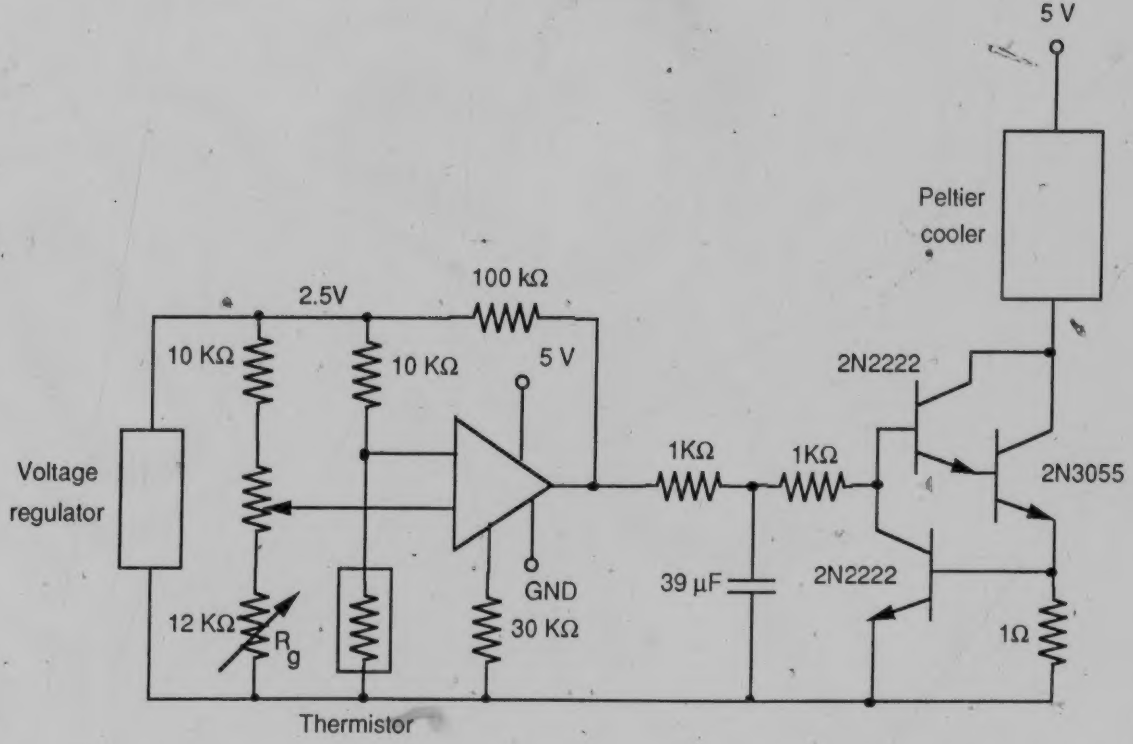
5 V
Peltier cooler
2N2222
2N3055
2N2222
1Ω
1KΩ
1KΩ
39 μF
2.5V
100 kΩ
10 KΩ
10 KΩ
5 V
GND
30 KΩ
Voltage regulator
12 KΩ
R_g
Thermistor

Fig. 4.9 Circuit diagram of the laser cooler circuit.

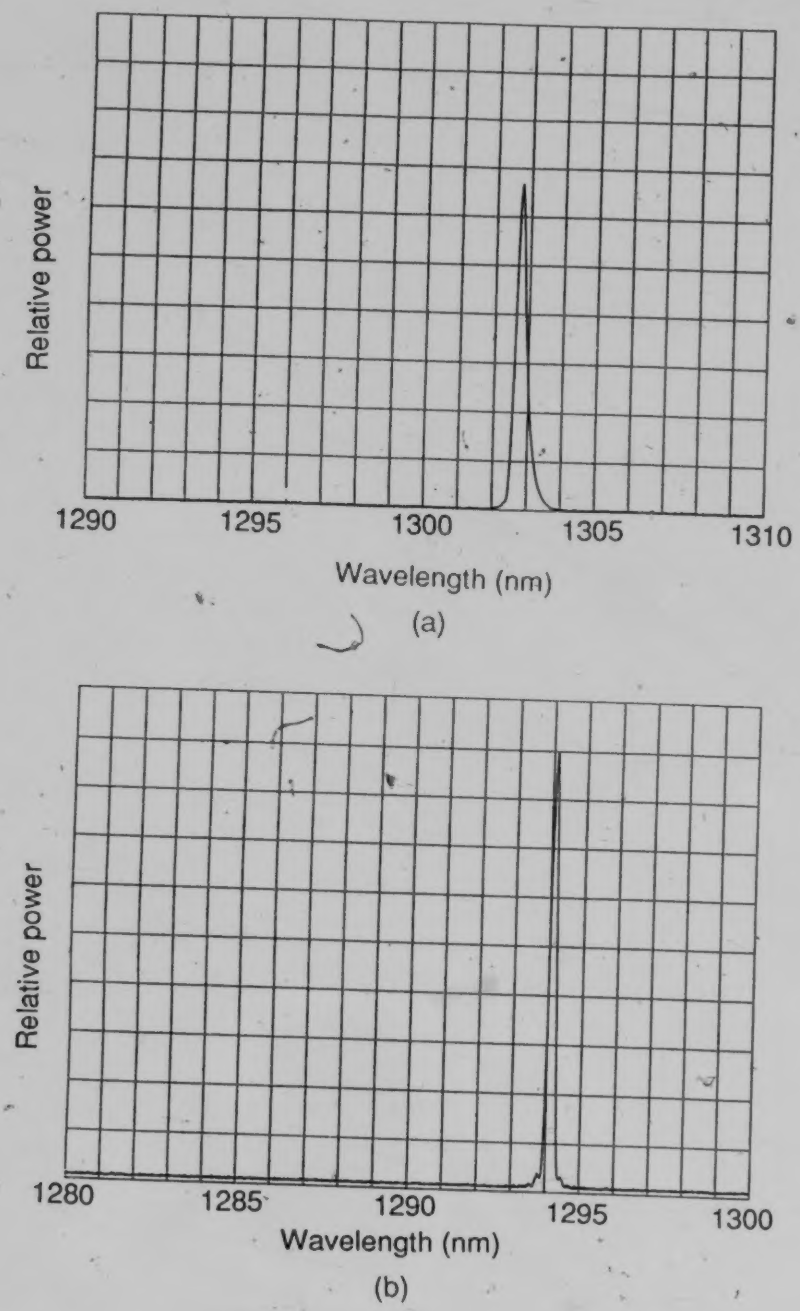

Fig. 4.10 Laser output spectrum of the LDs measured by a scanning monochromator.

(a) NEC quarter wave shifted DFB laser.

(b) Fujitsu DFB laser.

1297 nm respectively. At 1300 nm, a 1 nm difference in wavelength corresponds to a 175 GHz difference frequency. Hence, at the detector the intermodulation frequency generated by these two carriers will be around 875 GHz and will not cause any interference. The wavelengths of the LDs were observed to be stable for different bias currents and no mode hopping was observed.

The scanning monochromator has a resolution of about 4 A, which corresponds to 70 GHz frequency separation, and hence was not suitable for observing the sidemodes. Therefore, a Fabry-Perot (FP) interferometer, which has better resolution than that of a monochromator, was used to measure the side modes of the LD; the plots are shown in Fig. 4.11. The free spectral range and the finesse (defined in Section 4.1.3) of the FP interferometer were about 150 GHz and 30 respectively. As can be inferred from the plots, the side modes levels were very low.

4.2.2 LINEWIDTH AND FREQUENCY-DEVIATION MEASUREMENTS

Because of the relatively broad resolution of both the scanning monochromator and the Fabry Perot interferometer, neither of these methods are suitable for linewidth measurements. Hence, a delayed self-heterodyne method (explained in section 4.3) was used to measure the linewidths of the NEC as well as Fujitsu LDs. These measurements were carried out for different bias currents and the results are shown in Fig. 4.12 and Fig. 4.13. As expected, the linewidths of the LDs decreased with an increase in the bias current and the facet power.

The frequency deviation constant (frequency shift/unit current) can also be measured by the self-heterodyne method but, in this case the LD is modulated by a sine wave, and the spectrum of the beat signal between the direct and the delayed signal is observed. This power spectrum can be represented as follows [61]

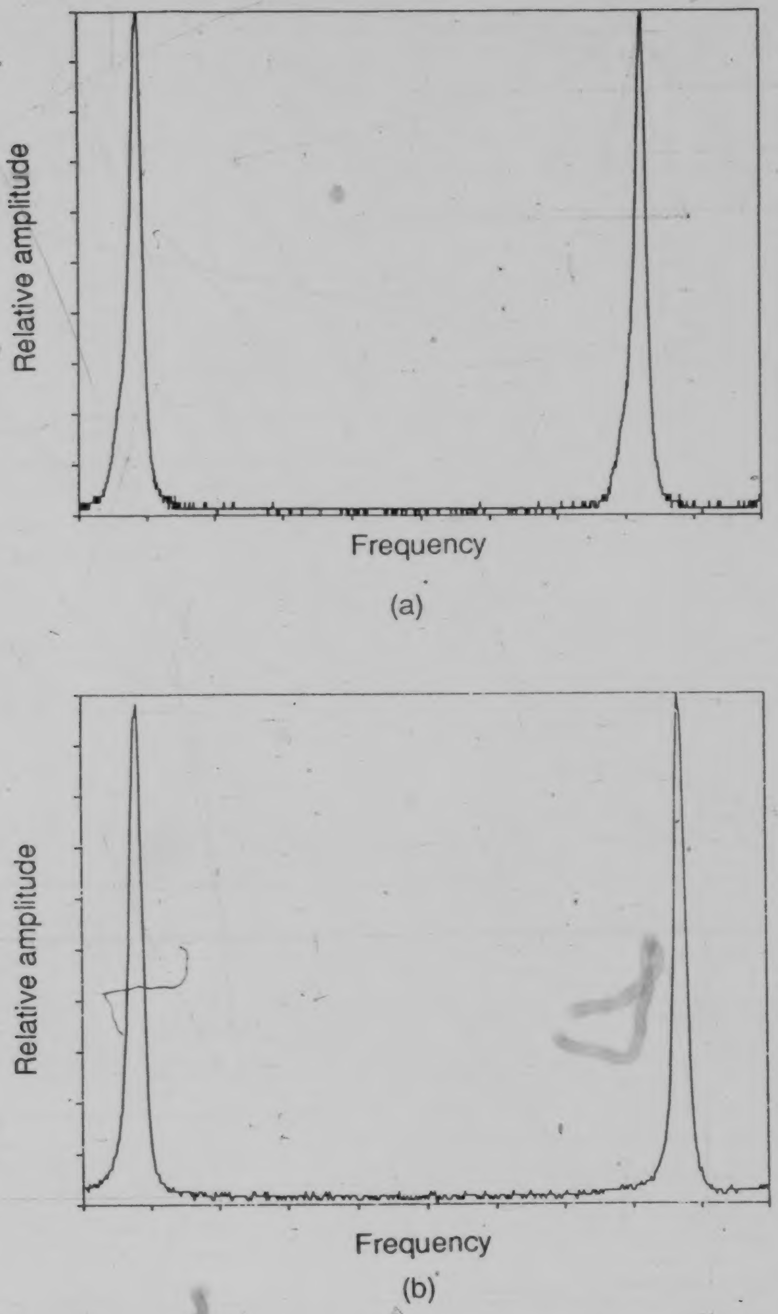

Fig. 4.11 Output power spectrum of the LDs measured by a Fabry-Perot interferometer.

(a) NEC quarter wave shifted DFB laser.

(b) Fujitsu DFB laser.

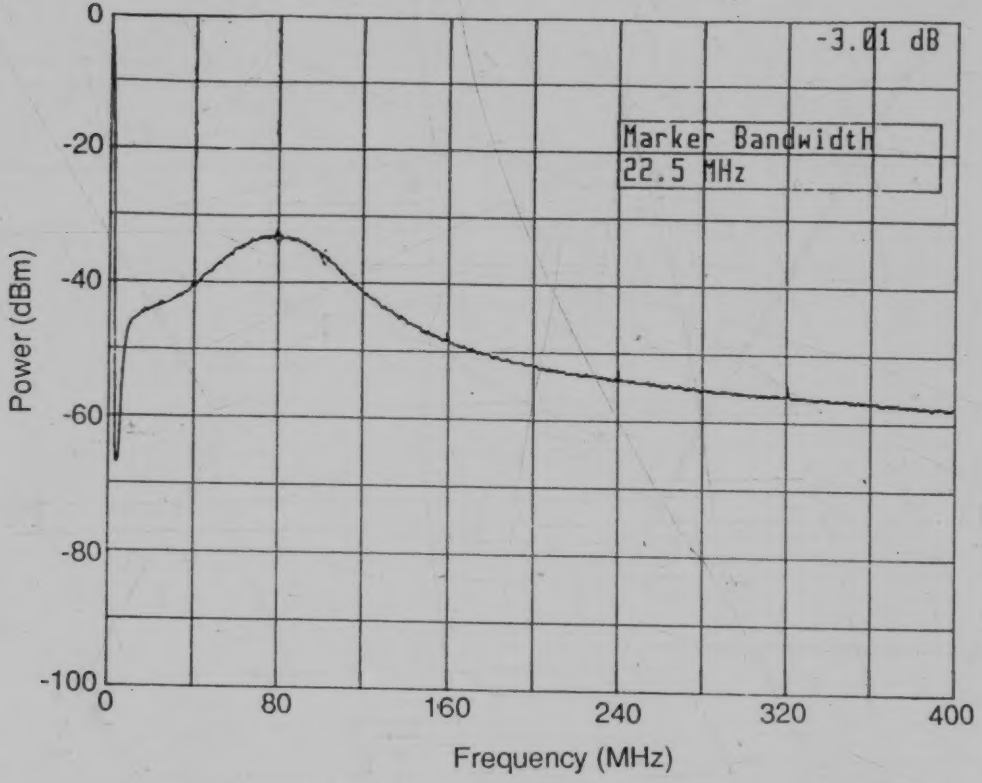

Bias current = 35 mA Linewidth = 22.5 MHz

Bias current (mA)	Facet power (mW)	Linewidth (MHz)
22. 5	2	35
29	4	29
35	6	22.5

Fig. 4.12 Linewidth of the NEC quarter wave shifted DFB LD for different bias currents measured by the delayed self-heterodyne setup.

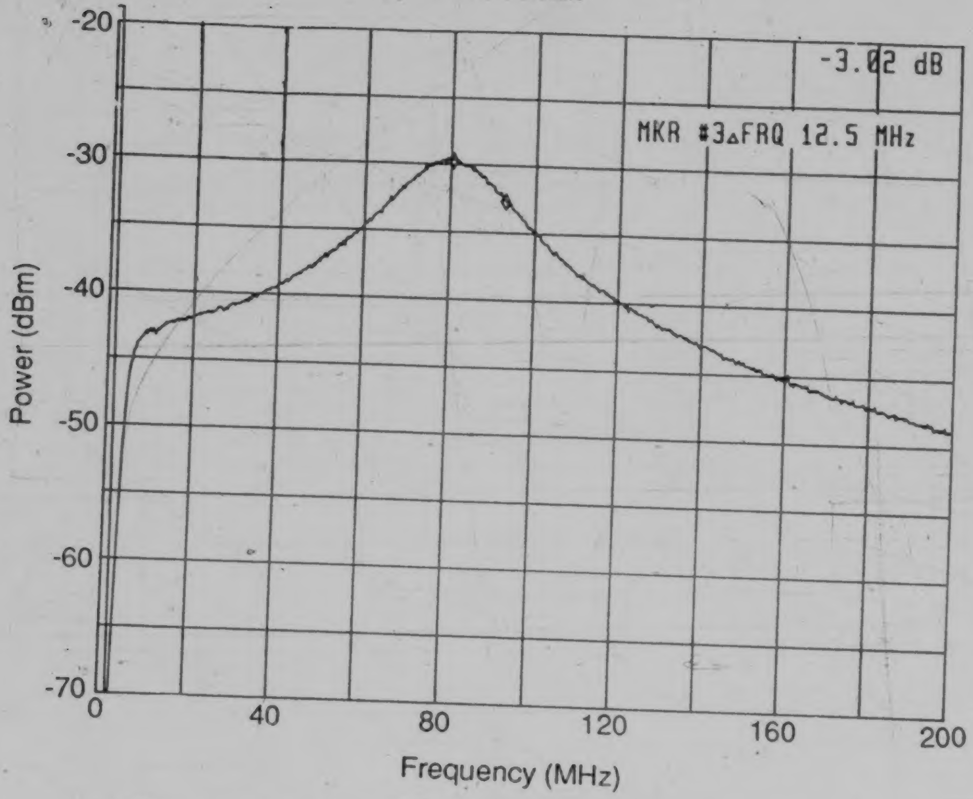

Bias current = 37 mA Linewidth = 12.5 MHz

Bias current (mA)	Facet power (mW)	Linewidth (MHz)
20	2	29
27	4	20
37	6	12.5

Fig. 4.13 Linewidth of the Fujitsu DFB LD for different bias currents measured by the delayed self-heterodyne setup.

$$S(f) = \frac{1}{\pi} \cdot \sum_{n=-\infty}^{n=+\infty} \left| J_n \left[2m \cdot \sin \left\{ \frac{\omega_m \tau_d}{2} \right\} \right] \right|^2 \cdot \frac{2\Delta\nu}{(f-nf_m)^2 + (2\Delta f)^2} \tag{4.2}$$

where t_d is the delay time, J_n is Bessel function of nth order, f_m is the modulation frequency, $L_m = 2\pi f_m$, and m is the frequency modulation constant of LD.

The power spectrum in Eq. 4.2 can be interpreted as that for a frequency modulated wave with a modulation index equal to $2m \cdot \sin\ (\omega_m \cdot \tau_d/2)$. This modulation index can be obtained from the ratio of the peak amplitude of the carrier to that of the first side band. The frequency deviation constant of the LD can then be determined by substituting the value of the delay time. Since the experimental LD driver circuit was only capable of modulating the LD by a square wave, sine wave modulation could not be applied. Hence, the self-heterodyne set-up could not be used to determine the frequency deviation constant of the LDs.

However, the frequency deviation constants of the LDs were determined by observing the difference frequency for different values of the modulating current. An increase in the peak amplitude of the modulating current caused the difference frequency to move further away. The frequency where the peak of the difference frequency existed was then divided by the peak amplitude of the modulating current to roughly estimate the frequency shift/mA. For the NEC LD, a frequency shift of about 500 MHz/mA was calculated, while for the Fujitsu LD, the frequency shift was calculated to be only 120 MHz/mA. Hence, the Fujitsu LD was not suitable for use in the second channel, because a very large modulating signal (more than 10 mA p-p) would be needed to obtain the desired difference frequency (about 1500 MHz). Use of this diode would have caused significant AM noise. Therefore, we were not able to modulate the output of the second channel.

4.3 MEASURING EQUIPMENT

4.3.1 SCANNING MONOCHROMATOR AND FABRY-PEROT INTERFEROMETER

The experimental setup for the scanning monochromator is shown in Fig. 4.14. At first, the slit-width of the monochromator is wide open (about 460 μm) for ease of alignment. After the initial alignment, the slit width is subsequently reduced to achieve better resolution. For the experimental measurements in this project, the slit width is reduced to 60 μm, which corresponds to 60 GHz resolution.

The experimental set-up for the Burleigh scanning monochromator is shown in Fig. 4.15. The separation between the two mirrors is set to 1 mm, which corresponds to a free spectral range (FSR) of 150 GHz. FSR is defined as the separation between the resonance frequencies of the interferometer, which is given by [62]

$$\mathrm{FSR} = \frac{c}{2nl\cdot\cos\theta} \tag{4.3}$$

where, l is the separation between the mirrors, c is the velocity of the light, n is the refractive index of the medium between the mirrors, and θ is the angle of incidence of light.

The resolution of the Fabry-Perot interferometer is limited by the quality of its mirrors, and determines the instrumental broadening of the observed spectrum. The performance of a Fabry-Perot interferometer is specified as finesse, which is defined as [62]

$$F = \frac{\mathrm{FSR}}{\Delta f} \tag{4.4}$$

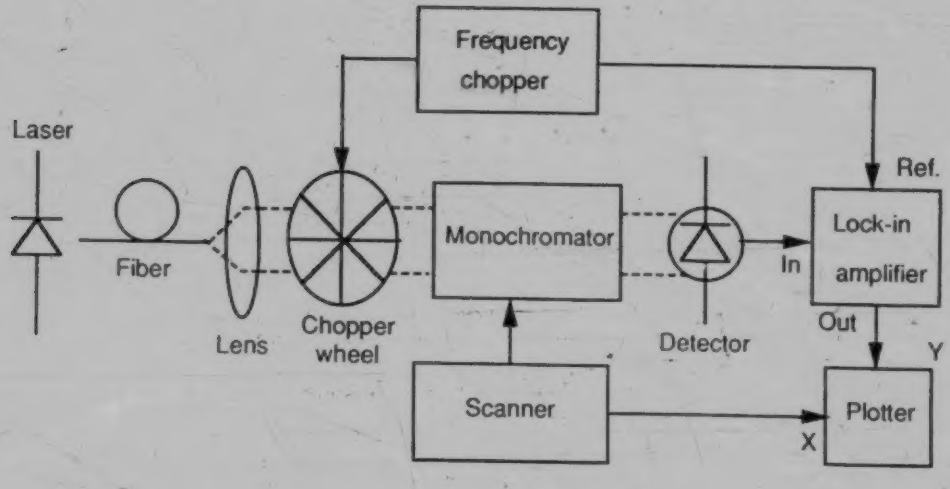
Frequency chopper
Laser
Ref.
Monochromator
Lock-in amplifier
Fiber
In
Lens
Chopper wheel
Detector
Out
Y
Scanner
Plotter
X

Fig. 4.14 Scanning monochromator set-up for laser wavelength measurements.

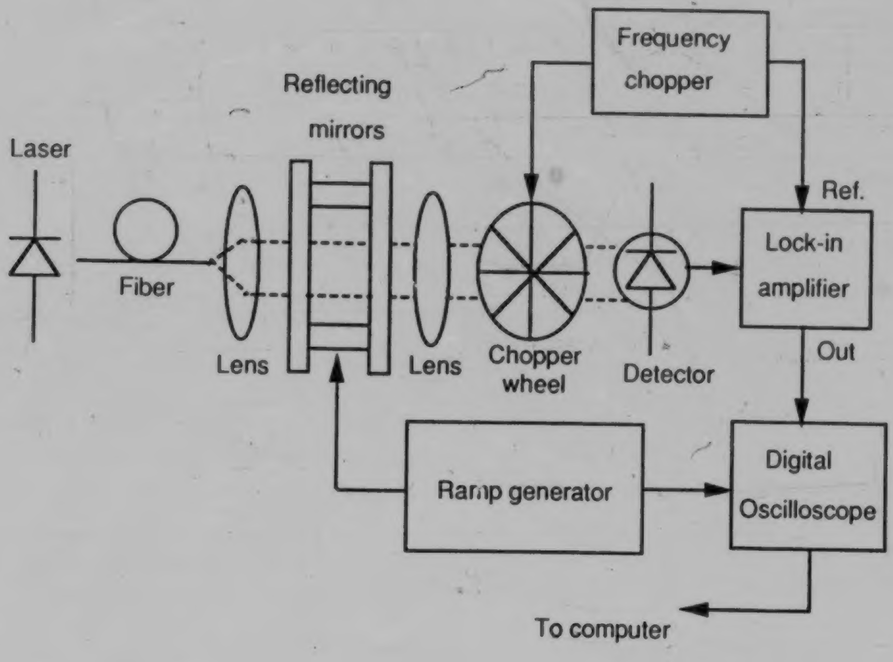
Frequency chopper
Reflecting mirrors
Laser
Ref.
Lock-in amplifier
Fiber
Lens
Lens
Chopper wheel
Detector
Out
Digital Oscilloscope
Ramp generator
To computer

Fig. 4.15 Fabry-Perot interferometer set-up for laser spectrum measurements.

where Δf is the frequency separation between the two spectral components having one half their peak value at their cross-over frequencies. The finesse can also be expressed in terms of the reflectivity of the mirrors.

$$F = \frac{\pi\sqrt{R}}{1 - R} \tag{4.5}$$

where F is the finesse and R is the relectivity of the mirrors.
The finesse of the instrument, as can be seen from Eq. 4.5, depends upon the quality of the coating on the mirrors. This setup, due to insufficient resolution, could not be used to determine the linewidth of the LD. However, it was used for observation of the intensity of multiple longitudinal modes (see Section 4.2.2).

4.3.2 SELF-HETERODYNE SET-UP

Until recent years, the linewidth of a LD was most commonly measured by a Fabry-Perot interferometer or by a Michelson interferometer. The Michelson interferometer is based on the principle of beating the optical signal with itself. This interferometer acts as a frequency discriminator and hence converts the FM noise into an AM signal. Because of the tedious alignment of the mirrors and the beam splitters, these interferometers are difficult to operate. Recently, Kikuchi and Okoshi suggested the delayed self-heterodyne method to measure the linewidth of a LD [63]. This method is based on the same principle as that of the Michelson interferometer, except that the interferometer is built with single mode optical fiber. Hence, it is very stable and no alignment procedure is required.

The block diagram of the delayed self-heterodyne method is shown in Fig. 4.16. An acousto-optic modulator (Matsushita EFL-M080-Y03) is used in the direct path to shift the beat frequency from d.c. to 80 MHz. The length of the

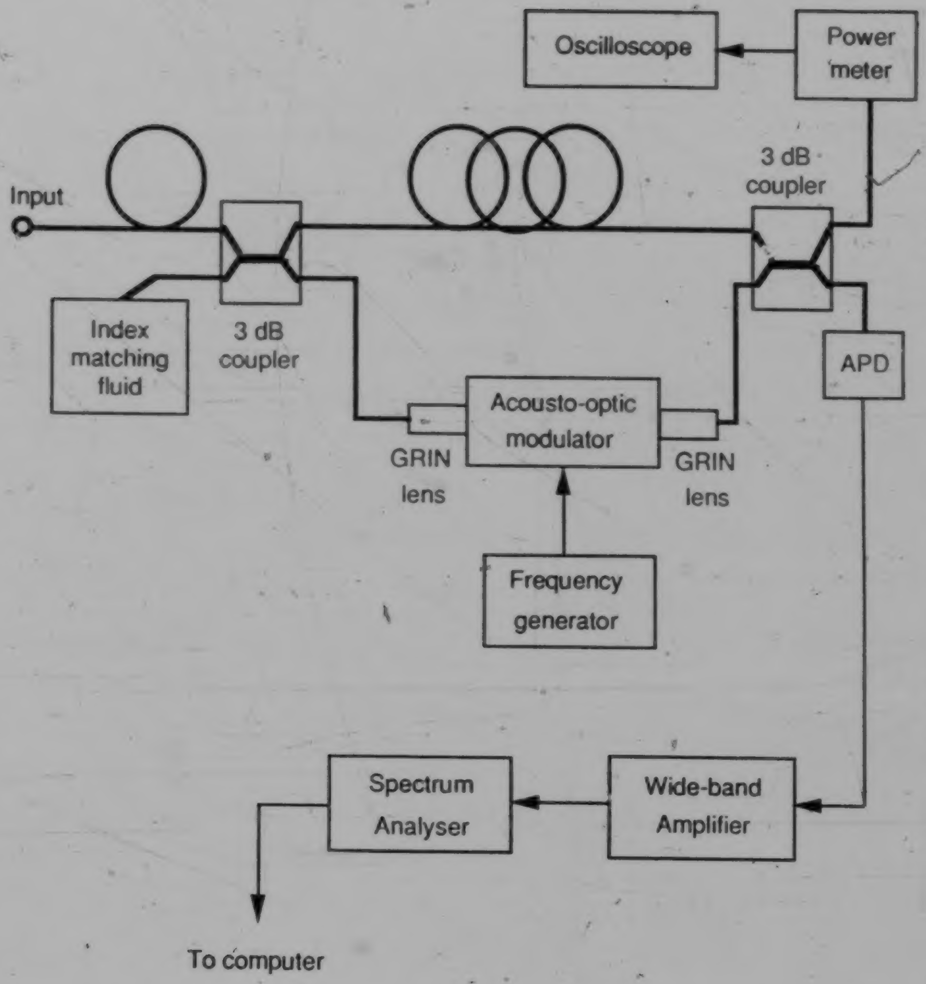
Oscilloscope
Power meter
3 dB coupler
Input
Index matching fluid
3 dB coupler
APD
Acousto-optic modulator
GRIN lens
GRIN lens
Frequency generator
Spectrum Analyser
Wide-band Amplifier
To computer

Fig. 4.16 Delayed self-heterodyne system for high resolution linewidth measurements.

delay line in the set-up is 750 m, which is large compared to the coherence length of the LD. The purpose of introducing a long delay line is to decorrelate the signal in the direct path and the delayed path. The power spectrum of the signal at the output of the photo-diode can be represented as [63]

$$S(f) = e^{-2\pi\delta f\tau_d}\cdot\delta(f) + \frac{\delta f}{\pi\cdot[f^2 + (\delta f)^2]}\cdot\left[\,1 - e^{-2\pi\delta f\tau_d}\cdot\left\{\cos(2\pi f\tau_d) + \left\{\frac{\delta f}{f} + \frac{f}{\delta f}\right\}\cdot\sin(2\pi f\tau_d)\right\}\right] \tag{4.6}$$

where δf is the linewidth of the LD and τ_d is the delay time. When the delay time is longer than the coherence time ($\tau_d > 15\tau_c$), as in this set-up, the power spectrum can be approximated by

$$S(f) = \frac{\delta f}{\pi\cdot(f^2 + (\delta f)^2)} \tag{4.7}$$

As can be noted, the 3 dB bandwidth of the above spectrum is twice as large as the linewidth of the LD. The spectral resolution for the self-heterodyne setup is approximately equal to $0.5/\tau_d$. For a 750 m length of the delay line, the resolution is equal to 200 kHz. This method provides better resolution than a Fabry-Perot interferometer.

4.4 SUMMARY

There are several considerations that should be taken into account when designing a transmitter. The modulation bandwidth of the transmitter should be large compared to the bit rate to avoid distortion in the transmitted pulses. In order to comply with high speed requirements, the laser driver circuit was designed using very fast Schottky diodes. Also, the alignment of the collimating lens and of the LD is very critical. It was observed that a slight change in the distance between the LD and the collimating lens caused the linewidth of the LD to change significantly. Hence, for commercial applications, a packaged DFB LD with a built-in optical isolator and collimating lens is desirable.

CHAPTER 5 - RECEIVER DESIGN

The main sources of noise in an optical receiver are:

1. Intrinsic quantum noise or shot noise at the photodetector.
2. Shot noise due to the detector dark current.
3. Excess noise caused by an APD.
4. Shot noise due to gate leakage current of the FET.
5. Thermal noise due to feedback or shunt load resistance.
6. Thermal noise and shot noise due to the receiver components.

For small received signal levels, the thermal noise dominates over the other noise sources. Hence for optimum receiver sensitivity, the receiver should amplify the weak received signal without introducing a significant amount of thermal noise. The block diagram of the experimental DFSK receiver is shown in Fig. 5.1. After the signal is pre-amplified, it is passed through the band pass filter. If the amplification in the pre-amplifier is large, then the insertion loss due to the band pass filter has very little effect on the signal to noise ratio. Further, the IF signal needs to be amplified before it is demodulated by the envelope detector. The desired amplification of the signal is achieved by amplifier 1 and amplifier 2. After the signal is passed through the low pass filter, the Manchester decoder decodes the received signal and the NRZ data can be recovered. This chapter includes the basis for the design of the various receiver components used in the project.

5.1 PINFET RECEIVER

Typically, the following detectors may be used for detection of the optical signal:

1. Positive-Intrinsic-Negative (PIN) diodes.
2. Avalanche photodiodes (APDs).
3. Integrated devices for photo-detection.

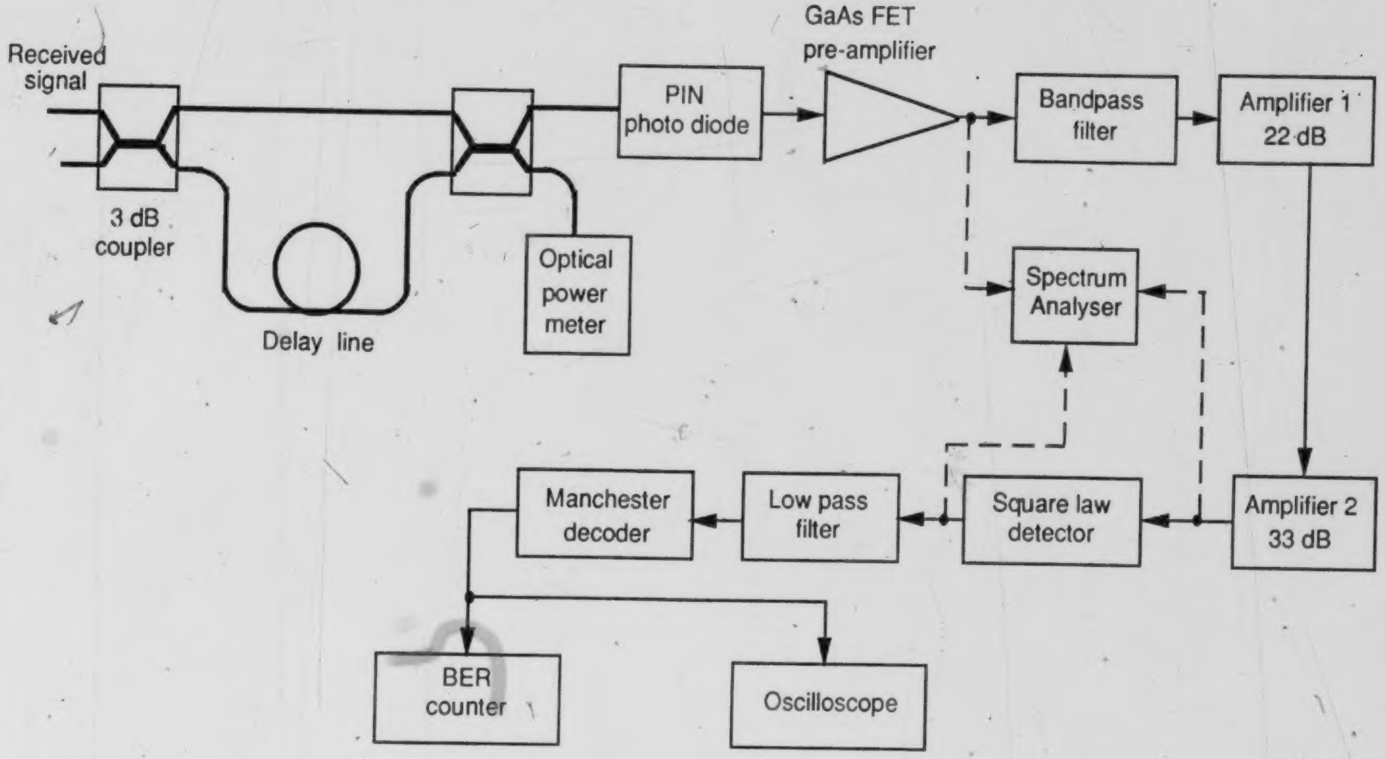
Received signal
3 dB coupler
Delay line
Optical power meter
PIN photo diode
GaAs FET pre-amplifier
Bandpass filter
Amplifier 1 22 dB
Spectrum Analyser
Amplifier 2 33 dB
Square law detector
Low pass filter
Manchester decoder
BER counter
Oscilloscope

Fig. 5.1 Block diagram of the experimental DFSK receiver.

APDs offer the advantage of avalanche gain but at the same time suffer from an excess noise penalty due to avalanche multiplication. Even with the excess noise penalty and high dark current, these photodetectors provide 3 to 5 dB higher sensitivity than that of a PIN diode at high bit rates (over 100 Mb/s) [64]. However, optical receivers using APDs need special AGC control circuitry to compensate for their temperature dependent avalanche gain. On the other hand, PIN diodes have a relatively small leakage current as compared to that of APDs and are also free from avalanche excess noise. Further, PIN diodes can exhibit lower shunt capacitances than APDs.

Recently, there has been the significant development of PIN photodiodes integrated with a microwave bipolar transistor pre-amplifier or GaAs FET pre-amplifier [65]. These devices provide a considerable reduction of the stray capacitance associated with the photodiode and active components. However, these devices are still in the research stage and are not commercially available.

The two most commonly used approaches for the design of the pre-amplifier are shown in Fig. 5.2. These are:

1. Transimpedance amplifier
2. High shunt impedance amplifier.

The transimpedance amplifier has the advantages of negative feedback so that the bandwidth of these amplifiers can be extended to the desired value. Therefore, no equalising circuit is required. However, due to the thermal noise of the feedback resistor, the sensitivity of these amplifiers is lower compared to that of high impedance amplifiers. Also, these amplifiers need careful design of the feedback path to prevent oscillations from occurring.

High impedance amplifiers, on the other hand, due to their large load resistance offer very low thermal noise and high detection sensitivity. Since the RC time constant of these amplifier is large, the receiver bandwidth is limited.

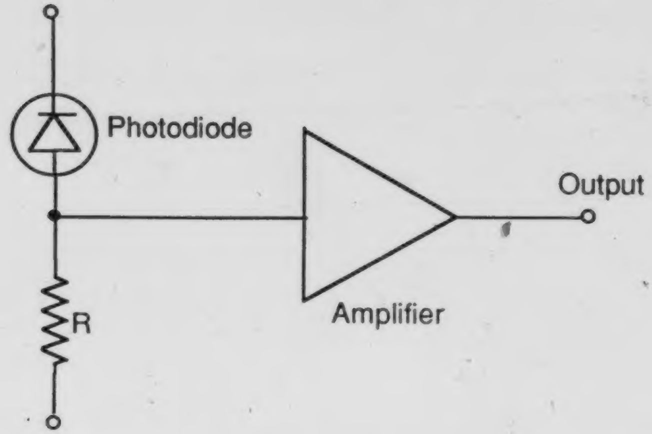
Photodiode
Output
R
Amplifier

(a) High impedance receiver amplifier.

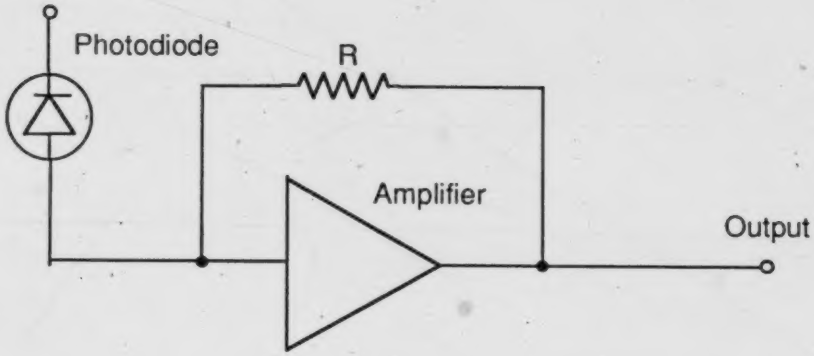
Photodiode
R
Amplifier
Output

(b) Transimpedance receiver amplifier.

Fig. 5.2 Most commonly used receivers for optical fiber systems.

Hence, an equaliser is required to extend the bandwidth to the desired value. Also, because of the large RC time constant, the receiver tends to integrate the detected signal. This causes severe baseline wander due to the integration of long strings of '0's and '1's in the input data stream [66]. This problem can be alleviated by using a dc balanced line coding scheme.

Both microwave bipolar transistors as well as GaAs FETs can be used in the pre-amplifier design. For bipolar transistors, the base-emitter and collector-base capacitance should be very small and the current gain should be large. For GaAs FETs, the gate-source capacitance should be small and the transconductance should be high. GaAs FETs suffer from 1/f noise, which can reduce the effective signal to noise ratio at low frequencies.

Due to the large receiver bandwidth and simple design requirements, a PIN diode with a high input impedance GaAs FET amplifier was considered suitable for this project. A detailed schematic diagram of the PINFET receiver is shown in Fig. 5.3. The detector diode is a Fujitsu PIN diode (FID 13S51SR), which has a

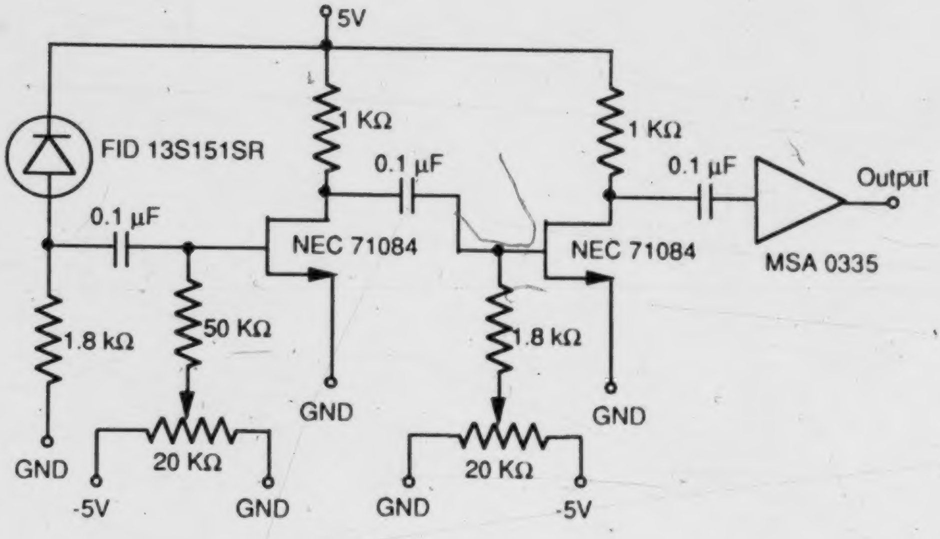

Fig. 5.3 Circuit diagram of the single detector PINFET receiver.

3 dB response bandwidth of 1.5 GHz and a capacitance of 0.4 pF. The current generated by the photo-diode passes through the 1.8 kΩ resistance and produces a voltage, which is then amplified by the GaAs FET amplifier. This amplifier stage, as mentioned earlier, should introduce very small noise and should be able to amplify high frequencies of the order of a few GHz. Hence, the stray shunt capacitances and the junction capacitances of the GaAs FET should be as low as possible. In our case, we used a GaAs FET (NEC 71084) with an input capacitance of 0.28 pF and a cut off frequency of about 20 GHz. The equivalent circuit of the FET is given in Fig. B.4 (Appendix B). To reduce the effect of stray shunt capacitances and series inductances, the components in the receiver are placed in very close proximity.

The frequency response of the GaAs FET amplifier cascaded with an Avantek power amplifier (MSA 0335) is shown in Fig. 5.4(a). The frequency response was measured by using a network analyser (HP 85046) with input and output impedances terminated to 50 ohms. As can be seen from the plot, the forward gain of the amplifier dropped by 3 dB from its maximum value at a frequency of 2.7 GHz. The bandwidth of this amplifier is determined by the Avantek 0335 transistor, which has a roll off frequency at about 4.5 GHz. Fig. 5.4(b) shows the frequency response after the PIN diode is connected. This measurement was carried out by intensity modulating the LD using a swept frequency signal, and detecting the output directly with a PIN diode. The 3 dB roll-off frequency of this amplifier was observed to be around 1.2 GHz; this is mainly due to the PIN diode, which has a bandwidth of 1.5 GHz. Since the receiver bandwidth was almost equal to that of the PIN diode, there was no need for an equaliser.

In this thesis work, a single detector is used in the receiver. However, a dual detector receiver can be designed to detect the power from both ports of the

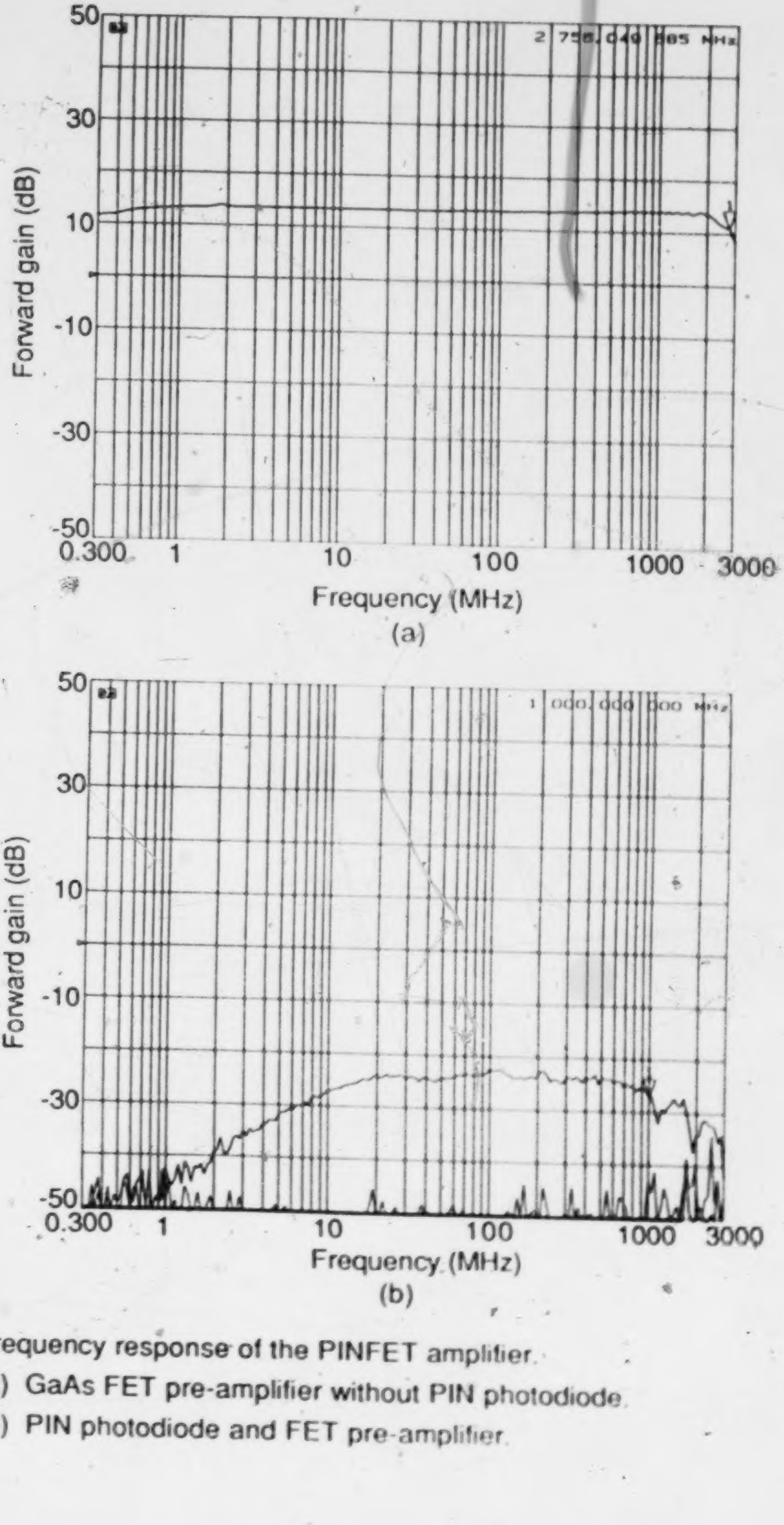

Fig. 5.4 Frequency response of the PINFET amplifier.
(a) GaAs FET pre-amplifier without PIN photodiode.
(b) PIN photodiode and FET pre-amplifier.

optical coupler [67]. A schematic diagram of a dual detector balanced receiver is shown in Fig. 5.5. Due to time constraints, we were not able to implement this receiver structure. Since the current generated by the two photo-detectors is added, the receiver sensitivity of such receivers is about 3 dB better than for single detector receivers.

5.2 BAND PASS FILTER

Due to the finite linewidth of the LD and non-uniform frequency modulation response, low frequency noise is observed whenever a '0' bit is transmitted (see Section 3.3). This noise causes inter-symbol interference and hence results in a receiver power penalty. To reject this low frequency noise and to minimise the thermal noise in the receiver, the IF is passed through a band pass filter (BPF). The bandwidth of the IF filter (BPF) should be such that it causes very small receiver noise and also allows most of the IF to pass without causing any significant power penalty. To study the bandwidth requirement for the DFSK

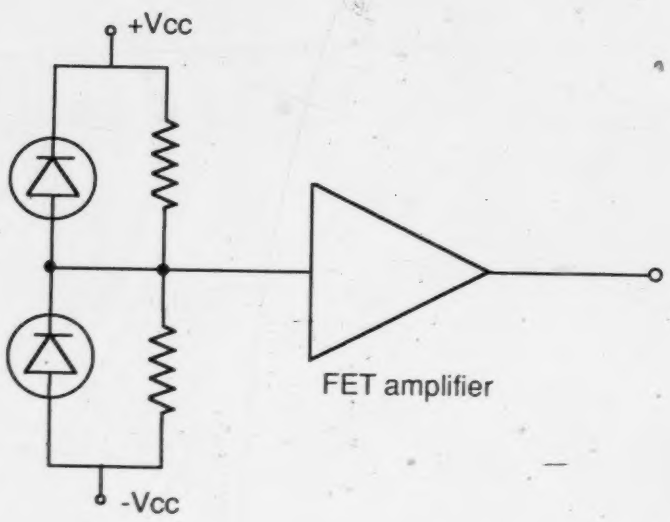

Fig. 5.5 Configuration of a dual detector receiver

system, two filters with different pass bands are used.

Fig. 5.6(a) and (b) depict the circuit design and the frequency response of filter 1, which is used for most of the measurements. The 3 dB bandwidth or pass band of this filter is about 650 MHz and the filter is tuned to a centre frequency of 1 GHz. The maximum insertion loss in the passband was about 2 dB.

Another filter, filter 2, was used to analyse the effect of reducing the filter bandwidth on the system performance. This filter was an 8 section filter with a passband of 300 MHz. As can be seen from the frequency response of the filter (see Fig. 5.7), the insertion loss of the filter is about 0.5 dB.

5.3 HIGH FREQUENCY AMPLIFIERS

To demodulate the IF efficiently, a high level signal is necessary. Hence, an amplifier with 54 dB gain is used after the BPF. To obtain such high gain, two amplifier modules, with power gains of 21 dB and 33 dB, were built. Amplifier 1, as shown in Fig. 5.8, consists of two cascaded Avantek power amplifiers (MSA 0335). Each of these amplifier modules (MSA 0335) has a gain of 12 dB at 1 GHz frequency and has a maximum usable frequency of 4.5 GHz. The frequency response of the amplifier, shown in Fig. 5.9(a), rolls off at about 2.7 GHz. Amplifier 2 was built in the same fashion as amplifier 1, except that it had three power amplifiers (MSA 0335) in cascade. The upper 3 dB cut off frequency for this amplifier occurred at around 2 GHz, as shown in Fig. 5.9(b).

The 3 dB bandwidth for n similar cascade stages can roughly be estimated as

$$f_{3dB}{}^{n} = \left[\sqrt{2^{1/n} - 1}\right] f_{3dB} \qquad (5.1)$$

where f_{3dB} is the bandwidth of each stage. For n = 2, the bandwidth of the

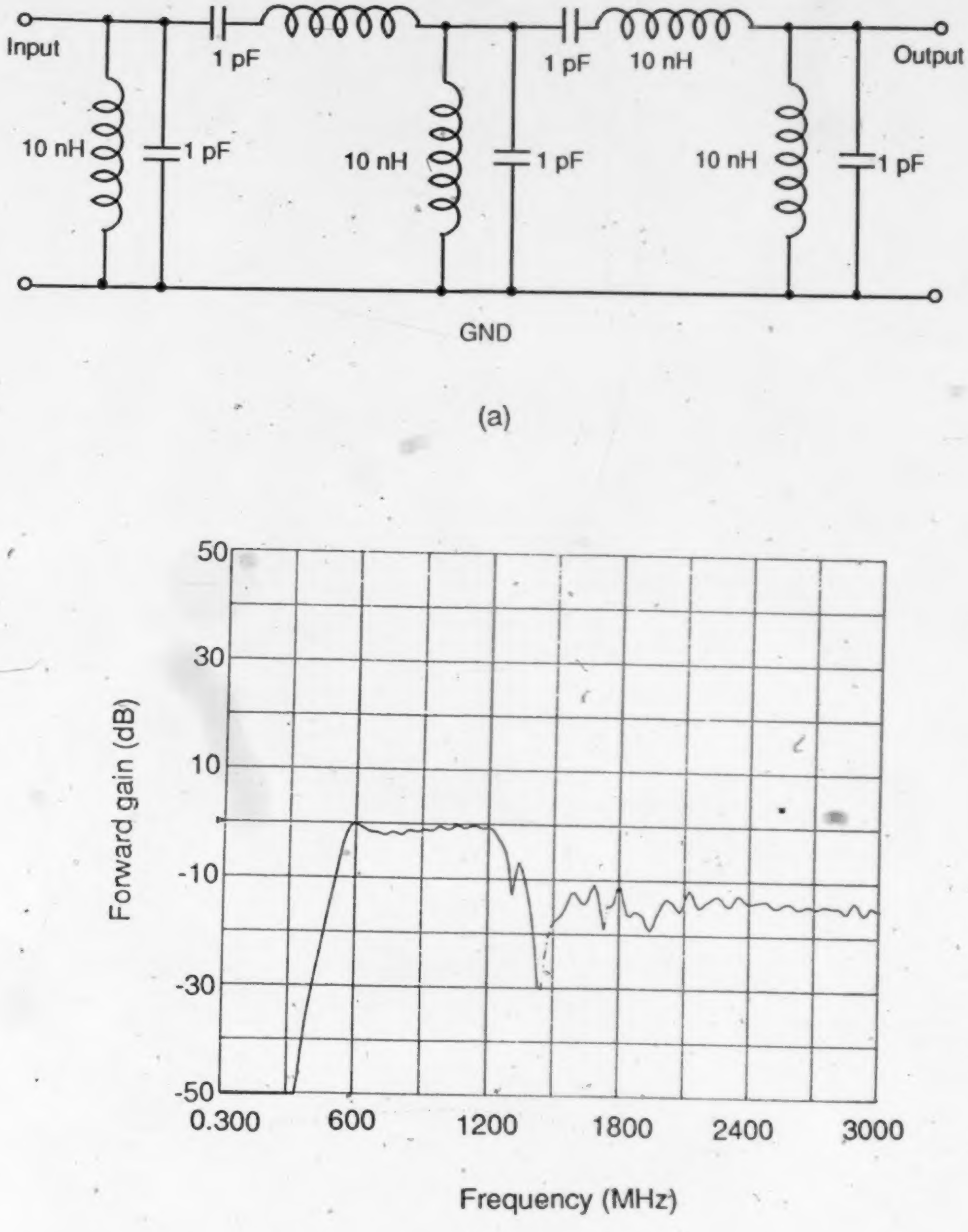
Input
1 pF
1 pF
10 nH
Output
10 nH
1 pF
10 nH
1 pF
10 nH
1 pF
GND
50
30
10
-10
-30
-50
Forward gain (dB)
0.300
600
1200
1800
2400
3000
Frequency (MHz)

(a)

(b)

Fig. 5.6 Bandpass filter with a passband of about 650 MHz.
(a) Schematic diagram.
(b) Frequency response.

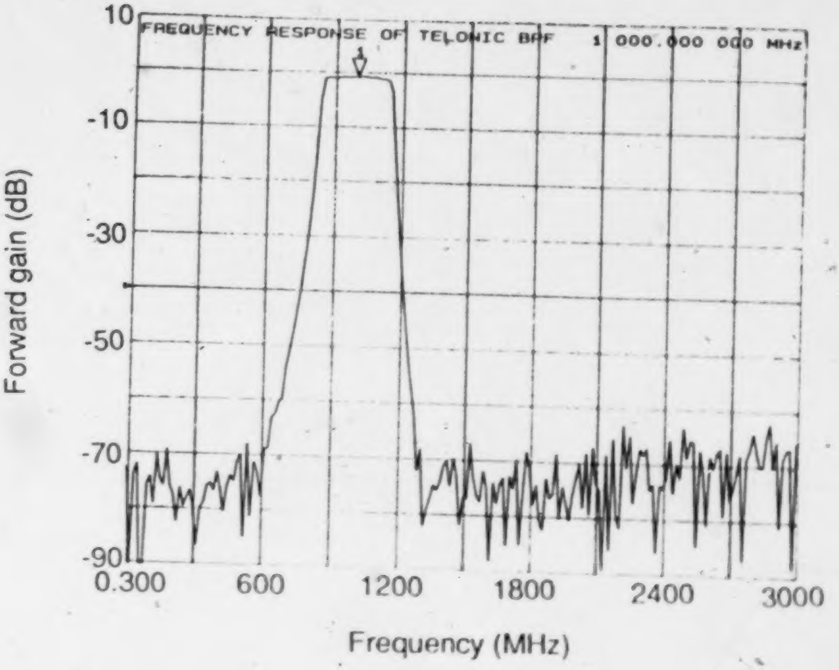

Fig. 5.7 Frequency response of filter 2 (Telonic TBP-1000-300-8SS)

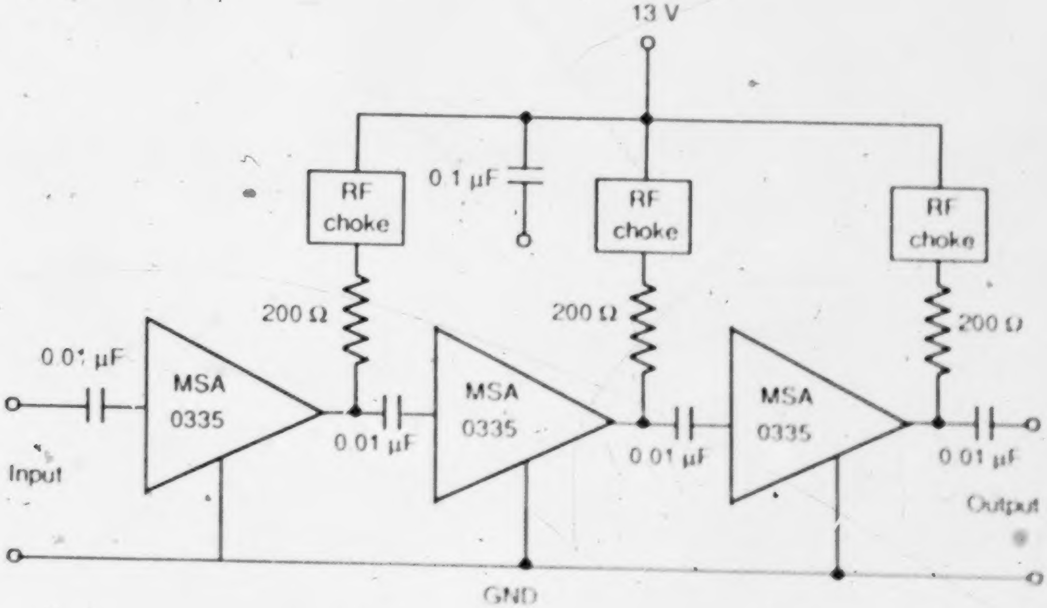
13 V
0.1 µF
RF choke
RF choke
RF choke
200 Ω
200 Ω
200 Ω
0.01 µF
MSA 0335
MSA 0335
MSA 0335
0.01 µF
0.01 µF
0.01 µF
Input
Output
GND

Fig. 5.8 Schematic diagram of high frequency power amplifier

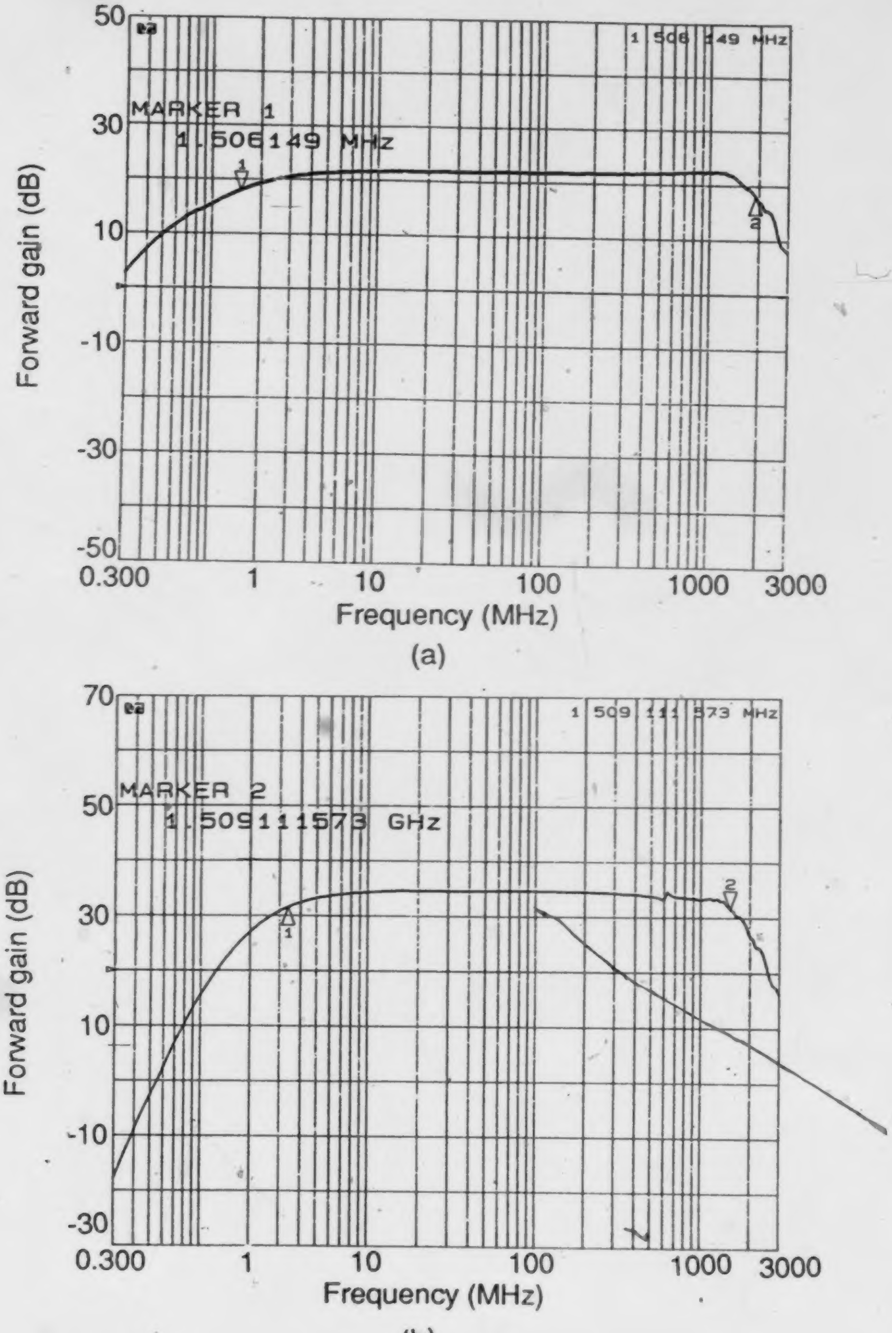

Fig. 5.9 Frequency response of the high frequency amplifiers.
(a) Amplifier 1 with a gain of 22 dB.
(b) Amplifier 2 with a gain of 33 dB

amplifier should be 2.9 GHz, whereas for $n = 3$, the 3 db bandwidth should be about 2.3 GHz. These values are quite close to what was measured for the amplifiers. However, for exact calculations, the stray capacitances and the device structure should be taken into account.

5.4 ENVELOPE DETECTOR

The most common method of demodulation, which is typically used for non-synchronous demodulation of the IF, is envelope detection. For the output of the envelope detector to be insensitive to the phase noise of the LD, it is necessary that the ratio of the bit rate to the IF frequency and the IF linewidth to IF frequency should be very small. If the IF bandwidth is too large, the system performance will degrade; in that case, a square law detector should be used as the demodulator [67].

The schematic diagram of the square law detector is shown in Fig. 5.10. The Schottky diode (HP 5082-2209), which is used as detector can be considered as a voltage source in series with a diode internal resistance. The diode equation for a Schottky diode can be expressed as

$$i = i_s \cdot (e^{v/0.026} - 1) \tag{5.2}$$

where, i_s is the saturation current and v is the junction voltage.

The junction resistance is given by the slope of the V-I curve at some value of the current. Hence, by differentiating the above equation with respect to v, we get

$$\frac{1}{0.026}\,\frac{dv}{di} = \frac{1}{\;}\,\frac{1}{i_s \cdot \exp(v/0.026)} \tag{5.3}$$

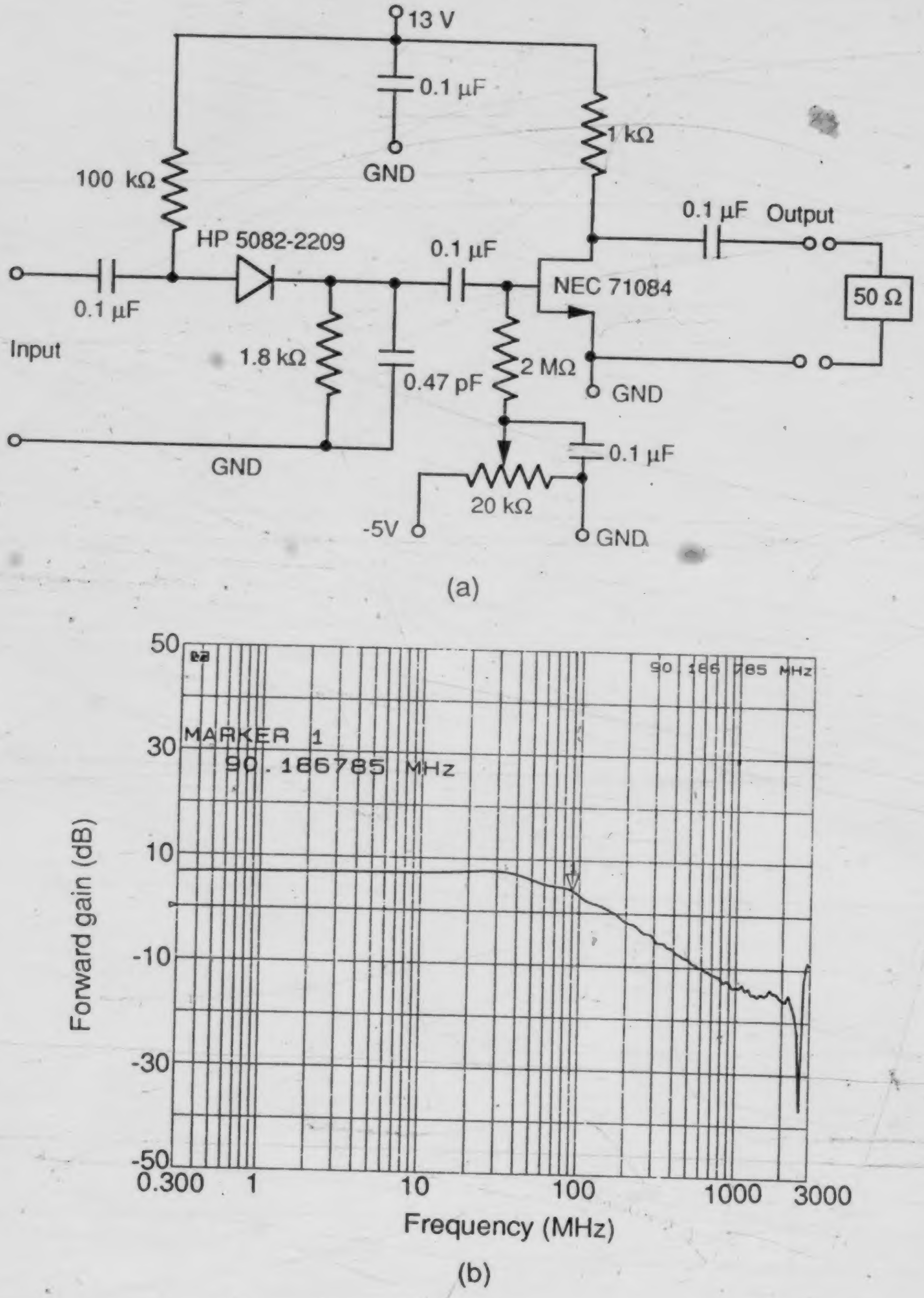
13 V
0.1 µF
GND
1 kΩ
100 kΩ
0.1 µF
Output
HP 5082-2209
0.1 µF
NEC 71084
50 Ω
0.1 µF
Input
1.8 kΩ
0.47 pF
2 MΩ
GND
0.1 µF
GND
20 kΩ
-5V
GND
(a)
50
30
10
-10
-30
-50
Forward gain (dB)
MARKER 1
90.186785 MHz
90 186 785 MHz
0.300
1
10
100
1000
3000
Frequency (MHz)
(b)

Fig. 5.10 Schottky diode square law detector.
(a) Circuit diagram.
(b) Frequency response.

or

$$\frac{dv}{di} = R_j = \frac{0.026}{i + i_s} \tag{5.4}$$

where R_j is the junction resistance.

The saturation current for Schottky diodes is of the order of 0.7 nA [68]. When no external bias is applied, the junction resistance of the diode is very high (40 MΩ). Since the detected voltage at the diode is divided between the junction resistance of the diode and the load resistance, a very large load resistance is required to detect the RF signal. This is not suitable for high speed circuits due to the large bandwidth requirement. However, as the junction resistance is inversely proportional to the bias current through the diode, a d.c. bias can be applied to operate the detector at a low junction resistance. Therefore, a d.c. bias current equal to 120 μA is passed through the Schottky diode to reduce the junction resistance to 225 Ω. A load resistance of 1.8 kΩ is used to detect the output voltage. This dc bias also causes the Schottky diode to operate in the square law region. The RF signal does not appear at the output of the detector as it is bypassed by a capacitor C_1 (0.47 pF). The frequency response of the envelope detector is shown in Fig. 5.10(b). The response bandwidth was observed to be about 90 MHz, which is sufficient for a 90 Mb/s signal. The FET stage after the envelope detector acts as a high input impedance pre-amplifier.

5.5 LOW PASS FILTER

A low pass filter (LPF) is used at the output of the envelope detector to reject the high frequency components. The circuit diagram and the frequency response of this filter are shown in Fig. 5.11(a) and (b), respectively. The upper cut off frequency of this filter is about 90 MHz, which is sufficient for a 90 Mb/s signal. The insertion loss for this filter was about 0.5 dB.

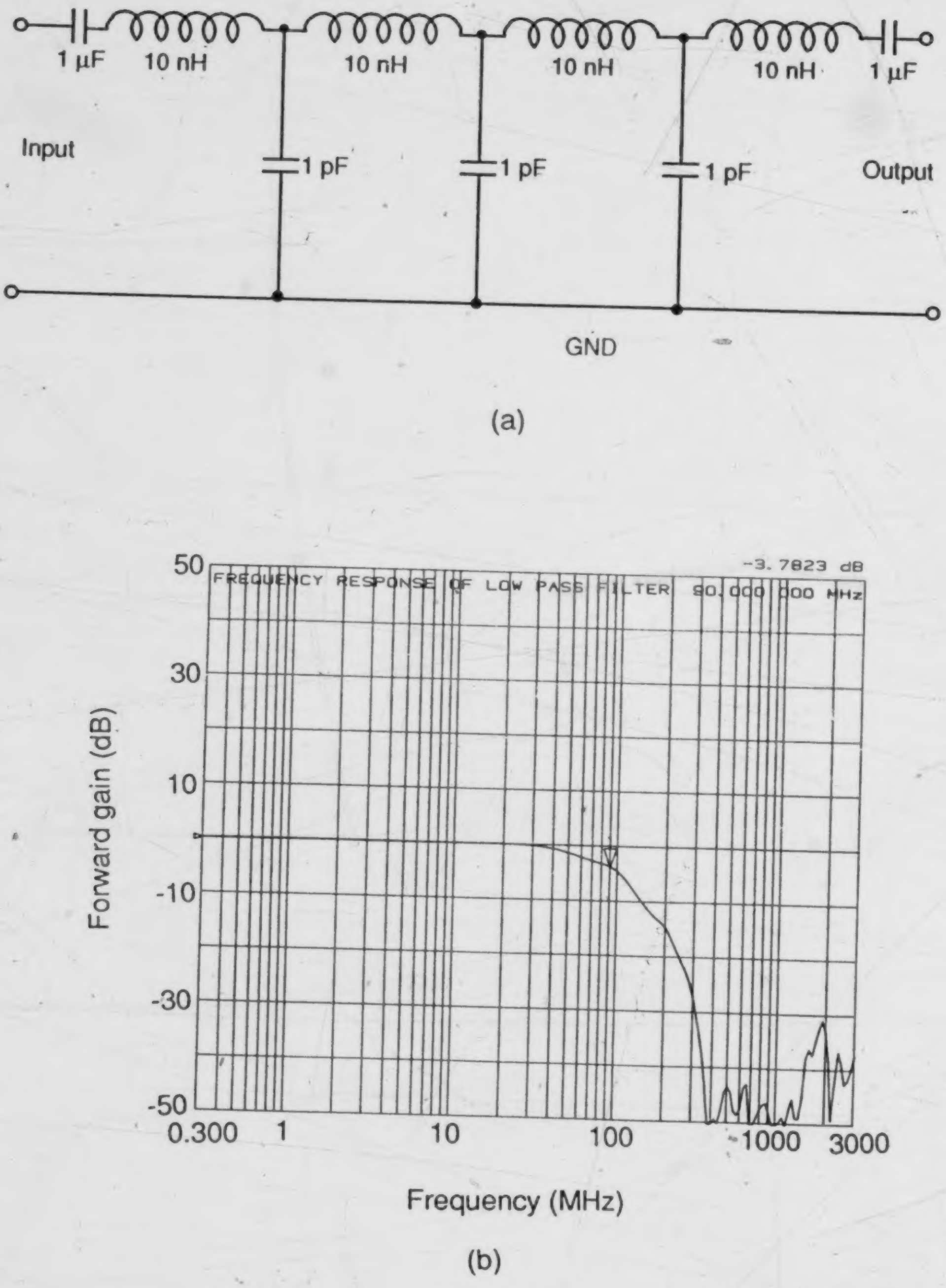
1 µF
10 nH
10 nH
10 nH
10 nH
1 µF
Input
1 pF
1 pF
1 pF
Output
GND
(a)
-3.7823 dB
FREQUENCY RESPONSE OF LOW PASS FILTER 90.000 000 MHz
50
30
10
-10
-30
-50
Forward gain (dB)
0.300
1
10
100
1000
3000
Frequency (MHz)
(b)

Fig. 5.11 Low pass filter.
(a) Circuit diagram.
(b) Frequency response.

5.6 MANCHESTER DECODER

The signal received at the output of the low pass filter is an ac signal. However, the Manchester decoder was designed using ECL chips. Hence, the signal level needs to be converted to ECL levels, where the required voltage swing is limited to between -0.9 V and -1.9 V. Therefore a TTL to ECL converter chip was used, as shown in Fig. 5.12. The required input voltage levels for this chip are 0 V for the low state and 5 V for the high state. Hence, resistances R1 and R2 were used to introduce the desired dc level at the input of the chip.

The received signal at the output of the LPF should be Manchester decoded to obtain the desired transmitted data. The Manchester decoder, as shown in Fig. 5.12, basically consists of a D flip-flop. The clock frequency is

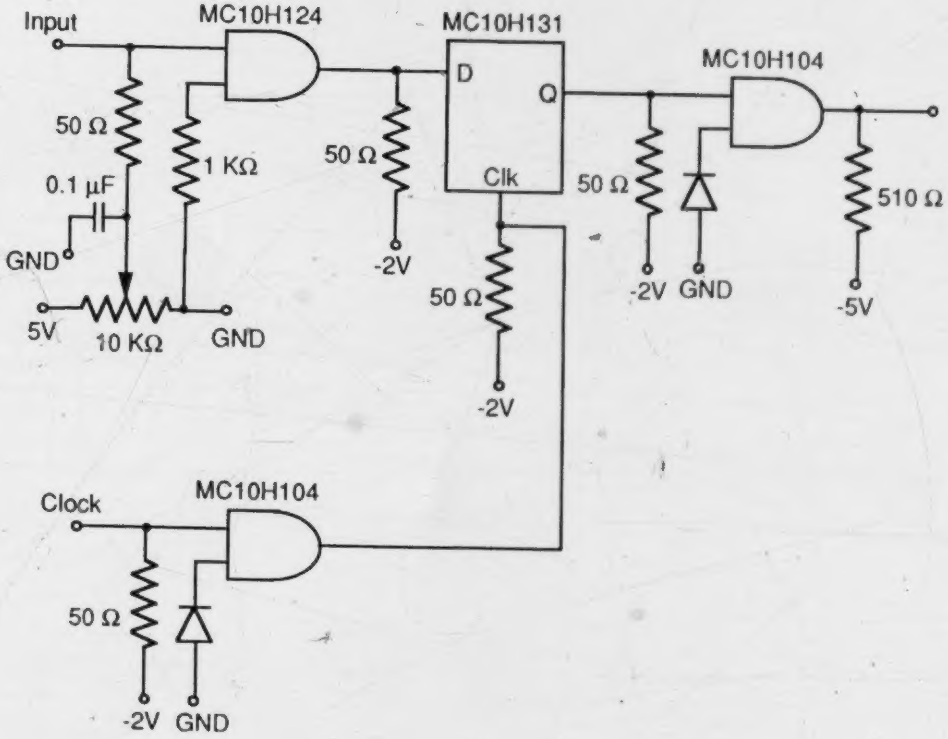
Input
MC10H124
MC10H131
D
Q
Clk
MC10H104
50 Ω
1 KΩ
0.1 μF
GND
5V
10 KΩ
GND
50 Ω
-2V
50 Ω
-2V
50 Ω
-2V
GND
510 Ω
-5V
Clock
MC10H104
50 Ω
-2V
GND

Fig. 5.12 Circuit diagram of the Manchester decoder.

44.7 MHz and the received signal is applied to the data input. The output of the flip-flop depends upon the value of the signal at the rising edge of the clock. The AND gate at the output of the flip-flop is used as a buffer stage.

5.8 SUMMARY

The circuit description of the various receiver components was presented in this chapter. Although every stage in the receiver adds to the noise in the system, it is the photodetector and the pre-amplifier stage that basically determine the signal to noise ratio. A PIN photodiode and a high input impedance FET pre-amplifier were used in the receiver. This structure was considered suitable due to the simple design and very low input capacitance of the GaAs FETs. The bandpass filter was designed using lumped capacitors and inductors, and had an insertion loss of about 2 dB.

If the IF passband is broad, then envelope detection can cause serious degradation of the received signal. For such cases, a square law detector is more suitable. Hence, a Schottky diode square law detector was used to efficiently demodulate the received signal.

The receiver performance could be improved by using micro-strip lines for interconnecting the various receiver components. Also, a band pass filter with lower insertion loss and higher stop band attenuation could be used to improve receiver performance.

CHAPTER 6 - SYSTEM MEASUREMENTS

In optical systems, system performance is normally evaluated by measuring the bit error rate (BER) as a function of the average received optical power. For coherent systems, the broad linewidth of a LD can cause serious degradation of the receiver sensitivity, which limits the achievable bit error rate. When the received signal is small, the receiver noise makes the probability of error large and the effect of laser linewidth is relatively small. But when the received signal is large compared to the receiver noise, then the phase noise or linewidth of the LD dominates and causes errors to occur. Hence, even for very large signal to noise ratios at the receiver end, a LD with broad linewidth at the transmitter may cause the occurrence of a high error rate floor (i.e. minimum achievable BER no matter how much power is received.).

This chapter provides the experimental measurements carried out for the DFSK system. In the first part of this chapter, the power spectrum of the received signal is discussed. Following this, the bit error rate as a function of the received optical power for a single channel DFSK system is considered. The chapter concludes with the analysis of the effect of a second channel on the characteristics of the first channel and measurement of the cross-talk produced by the phase noise in the second channel.

6.1 POWER SPECTRUM MEASUREMENTS

The spectrum of the received signal was measured in the electrical domain by means of a HP 71000 spectrum analyser. The measurements, discussed in the next sections, were obtained at the output of the pre-amplifier and at the output of the band pass filter.

6.1.1 RECEIVED SIGNAL AT PRE-AMPLIFIER

Curve (b) in Fig. 6.1 depicts the spectrum of the received signal when no modulation is applied to the LD at the transmitter. The Lorentzian spectrum observed for this case is due to the linewidth or the FM noise of the LD and hence represents the low frequency noise. If the coherence time of the LD is much larger than the delay time, the linewidth of this spectrum is very narrow. The ratio of the coherence time to the delay time can be increased either by using a LD with a narrow linewidth or by increasing the bit-rate. Hence, for high bit rates, the requirements for the linewidth of the LD are less stringent.

Since the low frequency noise may extend to the IF region, it will cause intersymbol interference. Fig. 6.1(b) illustrates the power spectrum of the received signal for the case when the LD is modulated. The two peaks correspond to the case when a '0' bit (low frequency peak) and a '1' bit (high frequency peak) is received. It can be inferred from Fig. 6.1 that the spectral width of the low frequency noise for a received '0' bit is more than that observed for the unmodulated LD output. It can be attributed to the non-uniform frequency modulation characteristics of the LD. The frequency deviation per unit current depends upon the modulation frequency as well as on the operating temperature of the LD. As a result, when a '0' bit is received, the direct and delayed signal may have different frequencies and hence generate a difference frequency which adds to the low frequency noise.

6.1.2 RECEIVED SIGNAL AT BANDPASS FILTER

It has been shown both theoretically and experimentally that the effect of linewidth on the broadening of the IF can be compensated for by proper selection of the band pass filter [69]. This is true only in the case of ASK and FSK systems. For PSK systems, there is a large penalty due to the linewidth of the LD and,

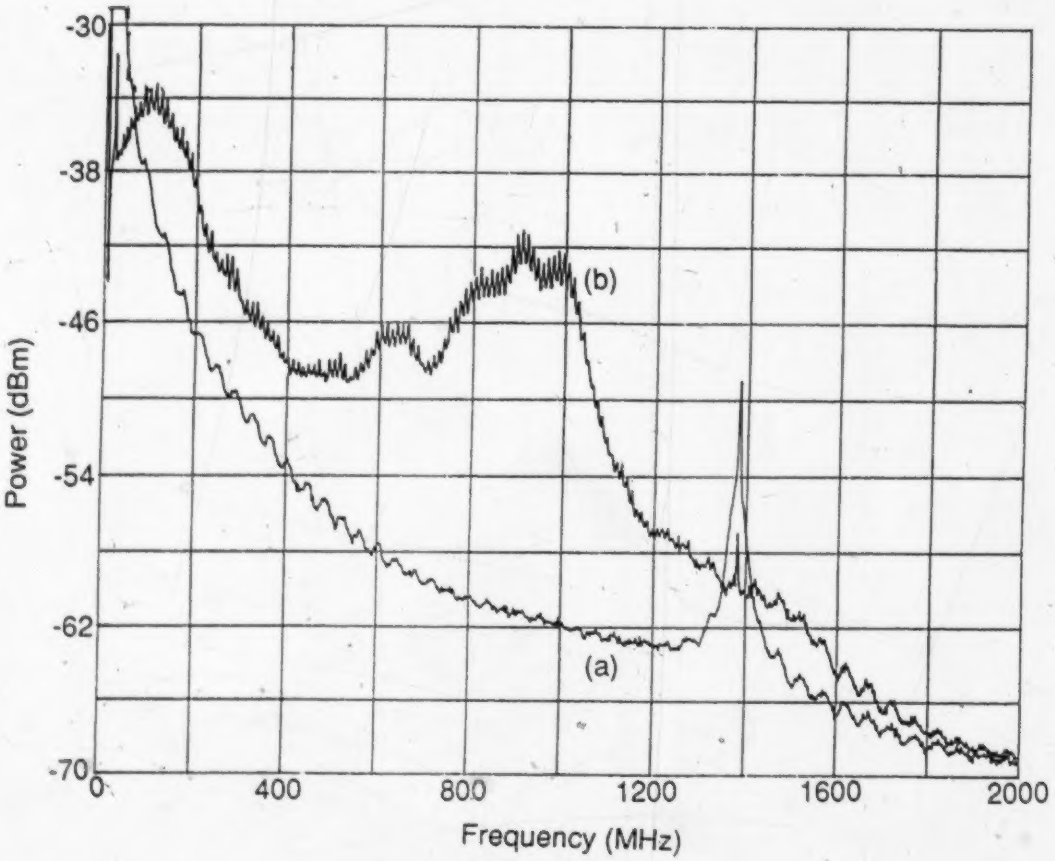

Fig. 6.1 Power spectrum of the received signal.
(a) No modulation signal applied to the LD.
(b) For 1.6 mA peak to peak modulation current.

therefore, a narrow linewidth is essential. According to Kazovsky [16], the bandwidth of the IF for an ASK modulation scheme can be approximated as

$$B_{IF} = \sqrt{(3R)^2 + B_L^2} \tag{6.1}$$

where R is the bit-rate, $B_L = 12.7 \cdot \Delta\nu$, and $\Delta\nu$ is the linewidth of the IF signal.

From Eq. 6.1, it can be calculated that, for a DFSK system, the IF filter bandwidth requirement should be 587 MHz. In the above equation, $\Delta\nu$ has been set equal to 44 MHz (twice the linewidth of the LD). In Fig. 6.2, which demonstrates the spectrum at the output of the BPF, the bandwidth of the IF can be estimated to be about 650 MHz. Hence, a fair agreement was achieved between the theoretical and the experimental results.

6.2 RECEIVED SIGNAL WAVEFORMS

Fig. 6.3 shows the transmitted and received signals for various bit patterns without Manchester encoding. The upper traces correspond to the transmitted signal which were observed at the transmitter (data generator), while the lower traces correspond to the received signal at the output of the low pass filter. In Fig. 6.3 (a), the transmitted bit sequence is 101010.... and the performance of the system is satisfactory. However, when a long string of consecutive '0' bits are transmitted, baseline wander effects are observed (see Fig. 6.3 (b)).

Fig. 6.4 depicts the transmitted and the received signals after the Manchester encoder and decoder were added to the DFSK system. The transmitted signal waveforms, as before were observed at the output of the function generator, while the received signal was observed at the output of the Manchester decoder. As can easily be seen, there is no base line wander effect

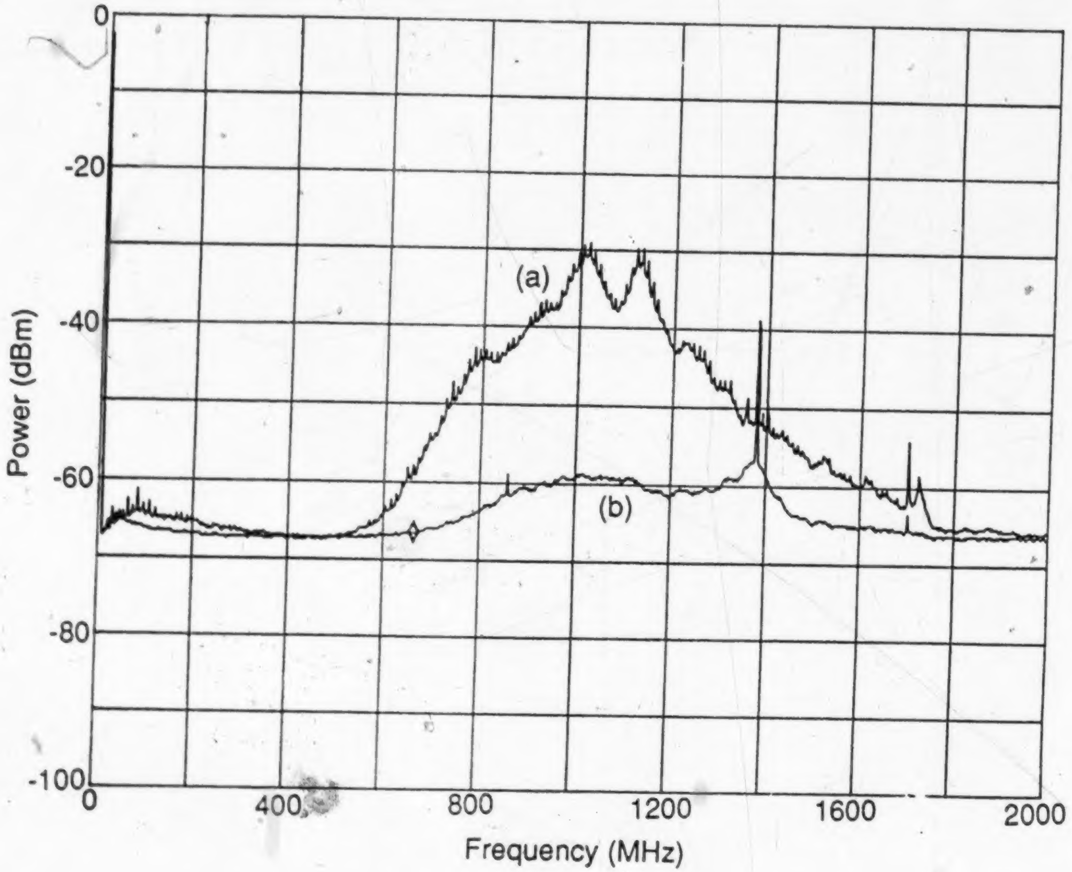

Fig. 6.2 Power spectrum of the IF signal at the output of the filter 1.
(a) With modulation signal applied to the LD.
(b) Without modulation signal.

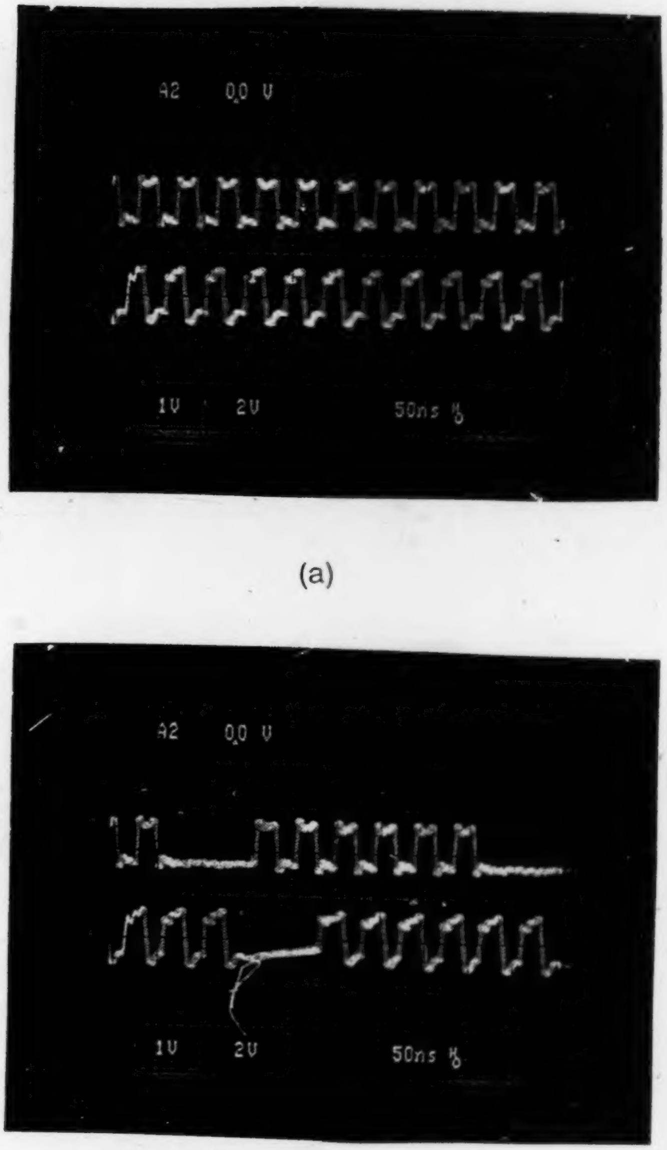

(a)

(b)

Fig. 6.3 The transmitted signal waveforms (upper traces) and the received signal waveforms (lower traces) for different data patterns.
(a) Bit pattern: 101010..........
(b) Bit pattern: 1000001010101010..........

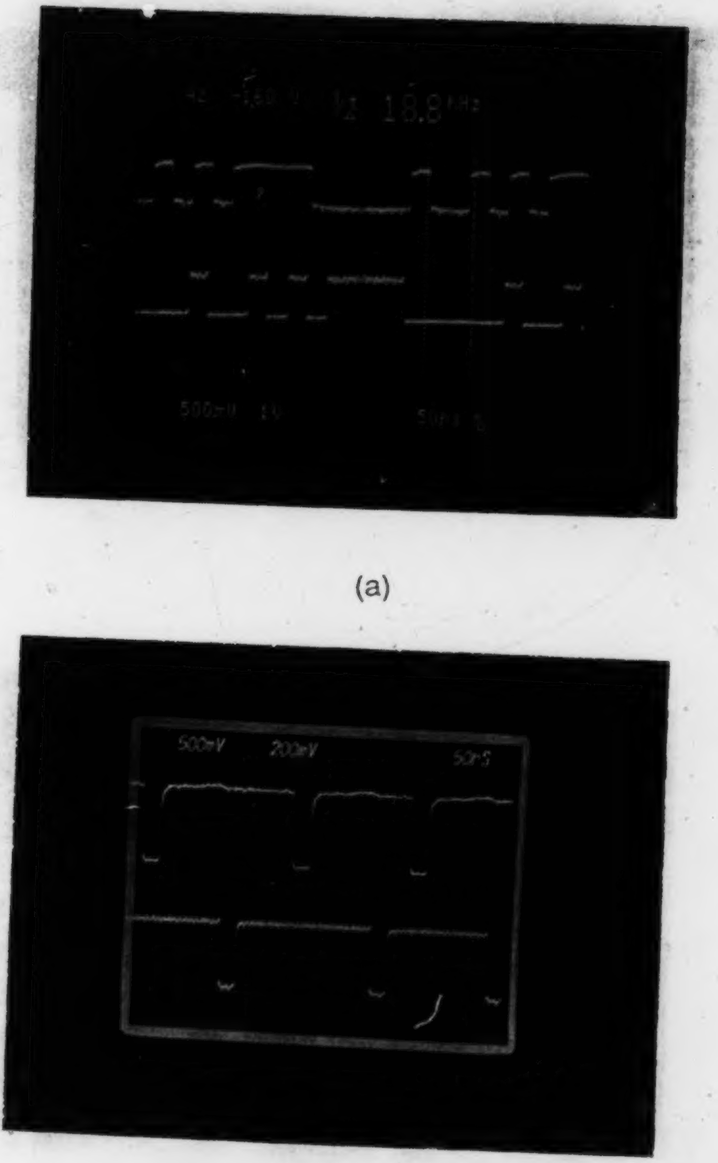

(a)

(b)

Fig. 6.4 The transmitted signal waveforms (upper traces) and the received signal waveforms (lower traces) after the Manchester encoder and the decoder were implemented.

(a) Bit pattern: 1111000001001010..........

(b) Bit pattern: 1111111101111110............

for long strings of '0' bits and '1' bits.

6.3 BIT ERROR RATE MEASUREMENTS

This section discusses the error rate performance of the DFSK system with and without incorporating Manchester encoding of the NRZ data. The BER is measured as a function of received average optical power. The received signal power was monitored at the output port of the second coupler in the receiver (refer to Fig. 2.6). The detector used for monitoring the optical power is a Germanium detector (UDT 256). Due to the slow frequency response of this detector, high frequencies were averaged out and hence the average received optical power was measured.

6.3.1 SINGLE CHANNEL DFSK SYSTEM

BER curves for different transmitted and received data patterns are shown in Fig. 6.5. These measurements were performed using a band pass filter with a 3 dB bandwidth of about 650 MHz. For a 101010... data sequence, the performance of the system was satisfactory and no error rate floor (higher than 10^{-9}) was observed. However, an increase in the number of consecutive '1' bits and '0' bits caused an increase in the required signal power (power penalty) to achieve a BER of 10^{-9}. When the transmitted data sequence is changed to 11001100...., a power penalty of 1.7 dB was observed, while for a 111000111000... sequence, an error rate floor developed at 10^{-8}. This power penalty and the error rate floor could be due to the non-uniform frequency modulation characteristics of the LD, explained in Chapter 3.

BER measurements were also performed using band pass filter 2 (described in Section 3.2) in the IF stage; the results are presented in Fig. 6.6. It was still possible to obtain a BER of less than 10^{-9} for a 101010...transmitted bit

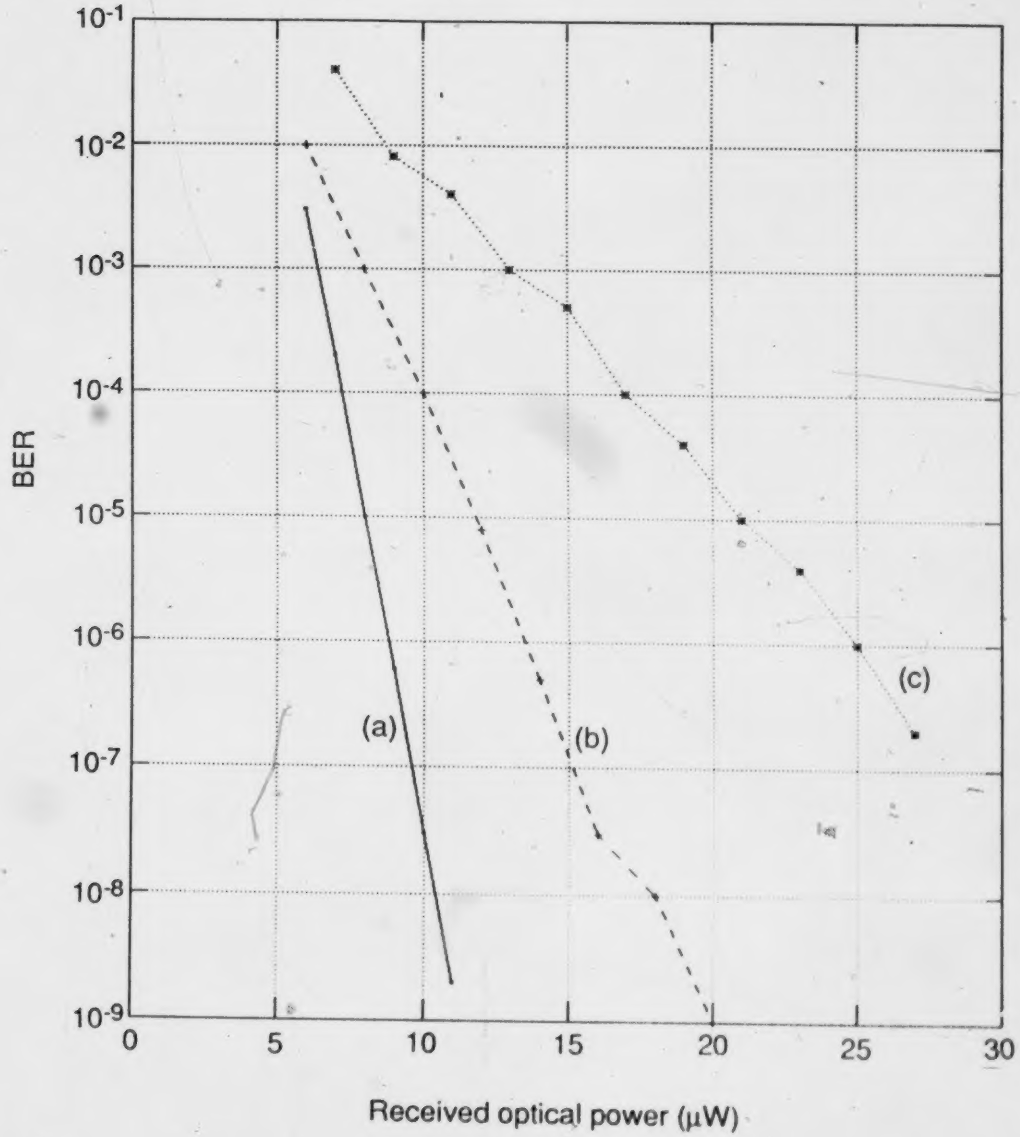

Fig. 6.5 BER as a function of the received average optical power. The bandwidth of the IF filter was 650 MHz.

(a) Bit pattern: 101010....................

(b) Bit pattern: 11001100.................

(c) Bit pattern: 111000111000........

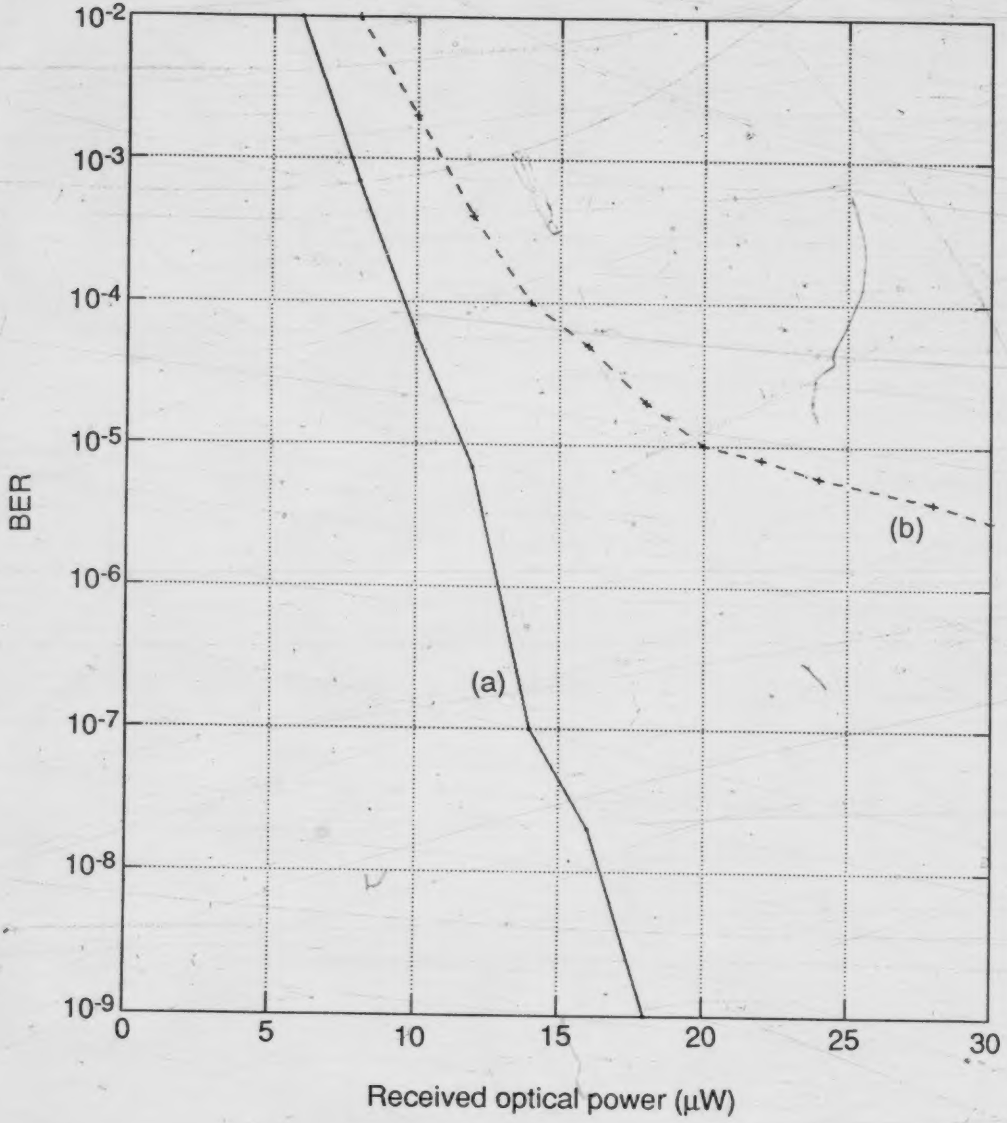

Fig. 6.6 BER as a function of the received average optical power with an IF filter of 300 MHz bandwidth.

(a) Bit pattern: 101010.............

(b) Bit pattern: 11001100........

pattern, but for two consecutive '1' bits and '0' bits in a row, an error rate floor at 10^{-5} was obtained. This clearly indicates that a part of the IF signal is rejected by the band pass filter, and that, hence, a 300 MHz bandwidth is not sufficient.

The optimum filter bandwidth requirement for an ASK system has been calculated by several authors [45], [46], [16]. The required filter bandwidth as a function of the IF linewidth to bit-rate ratio is presented in Fig. 6.7 [69]. For our case, the IF linewidth is equal to 44 MHz (twice the linewidth of the LD) and thus the linewidth to bit-rate ratio is approximately equal to 1. From Fig. 6.7 it follows that the bandwidth of the IF filter should be $12 \cdot R$ (540 MHz), where R is the bit rate. This indicates that the theoretical calculation for the bandwidth requirement agrees with the experimental value.

6.3.2 MANCHESTER-DIFFERENTIAL ENCODED SIGNAL

The performance of the DFSK system with only differential encoding was observed to degrade as the frequency of the modulation signal was decreased and therefore, it was necessary to get rid of the low frequency part of the modulating signal spectrum. Hence, Manchester encoding was used, which basically converts the NRZ data to a RZ signal. For a Manchester encoded signal, there is very little power at low frequencies and therefore, the requirement for the non-uniform frequency modulation characteristics of the LD is less stringent. Although Manchester encoding increases the effective bit rate by a factor of two, the bandwidth of the IF filter need not be increased. The BER curve for the DFSK system after Manchester encoding/decoding is incorporated is shown in Fig. 6.8. This measurement is carried out for a pseudo random bit sequence (PRBS) of length 2^{23}-1, and no error rate floor was seen to develop. Due to insufficient bandwidth of filter 2 (300 MHz), it was not used for any subsequent measurements.

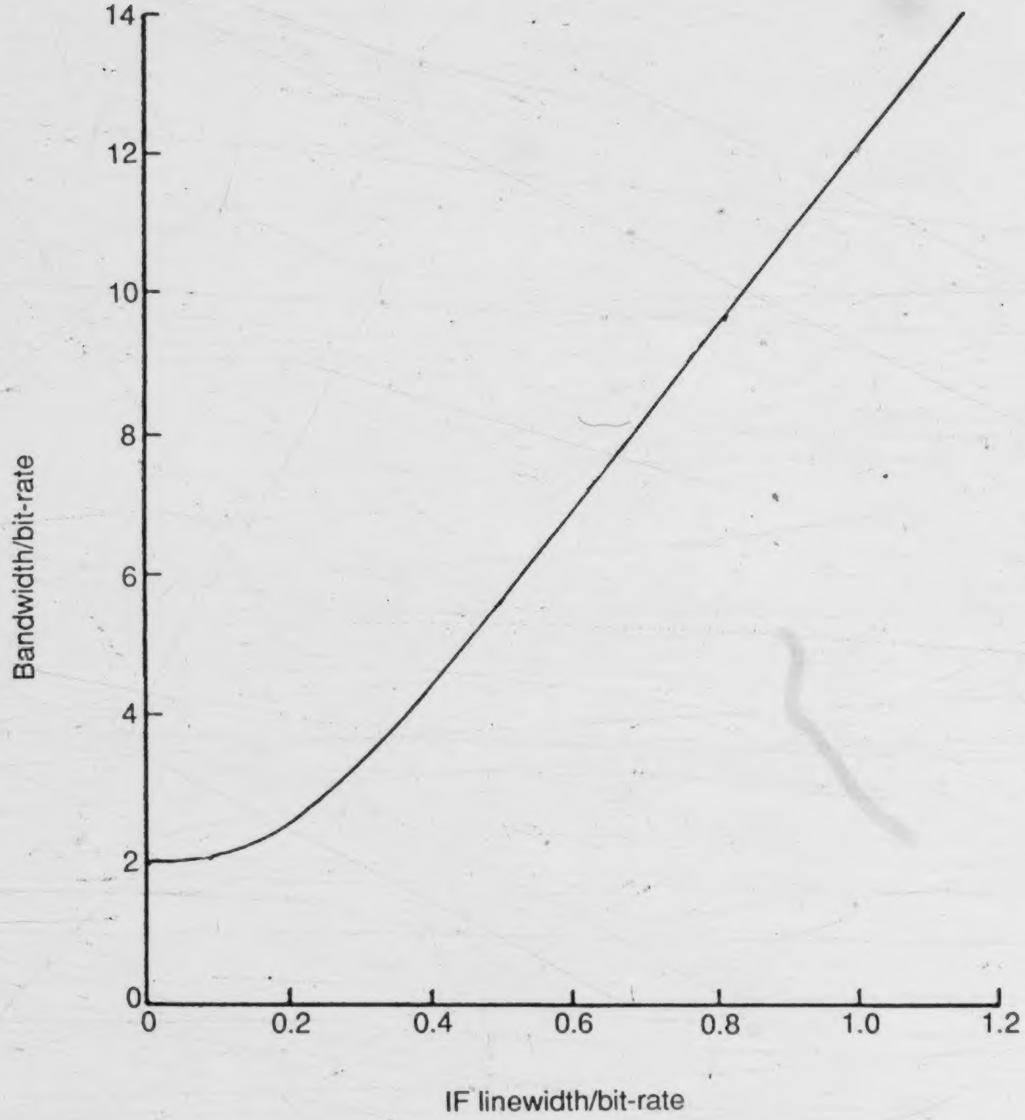

Fig. 6.7 Filter bandwidth requirements as a function of the IF linewidth to bit-rate ratio.

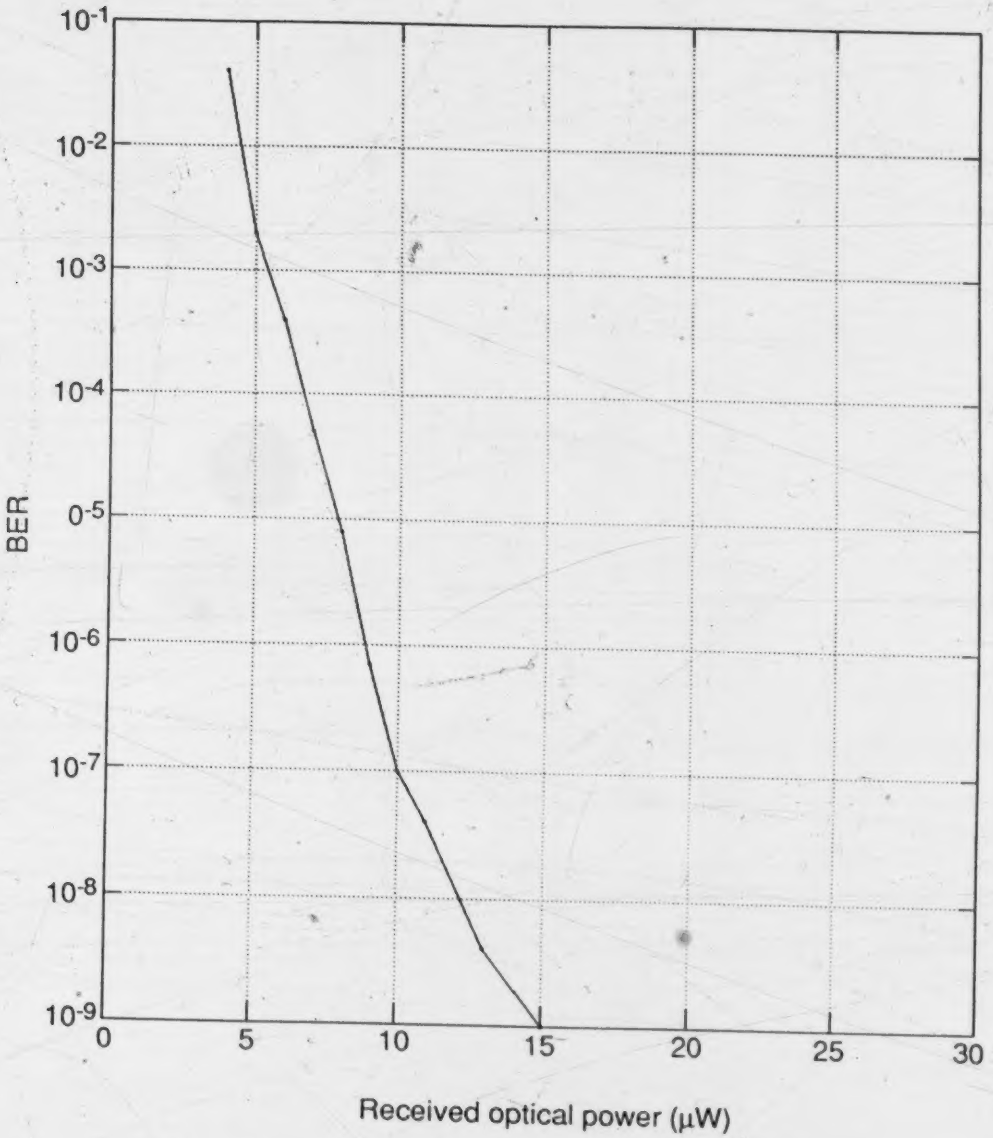

Fig. 6.8 BER as a function of the received average optical power for a pseudo random bit sequence of $2^{23} - 1$. These measurements were carried out after the Manchester encoder was incorporated in the experimental system.

6.3.3 TWO CHANNEL TRANSMISSION

When several channels are transmitted using the DFSK scheme, inter-channel interference needs to be considered. This interference occurs mainly due to the spectral spread of the IFs at the receiver. The separation between the channels should be sufficiently large to minimise this interference. On the other hand, increasing the channel spacing causes a decrease in the number of channels that can be transmitted, because of the limited receiver bandwidth.

In order to analyse the inter-channel interference, a second channel was added to the DFSK system. This channel was multiplexed optically using a 3 dB optical coupler. It was ensured that the operating wavelength of the second LD (1296 nm) was different from that of the first LD (1304 nm). The frequency separation of the two optical carriers can be calculated by the following formula

$$\Delta f = \frac{c\cdot(\lambda_1 - \lambda_2)}{\lambda_1\cdot\lambda_2} \quad . \qquad (6.2)$$

If λ_1 and λ_2 are 1296 nm and 1304 nm and c is the velocity of light in the fiber ($2\cdot10^8$ m/sec), the frequency separation is found to be equal to 946 GHz. Hence, there will not be any intermodulation interference.

The first channel is centered at an IF of 1 GHz and thus, in order to transmit the second channel without significant power penalty, it should be placed higher in frequency than the first channel (around 1.5 GHz). For our experimental system, it was not possible to place the second channel at 1.5 GHz, due to the limited receiver bandwidth (1.3 GHz). Also, the frequency modulation capability of the second LD was poor. Therefore, no modulation signal was applied to the LD in the second channel. The effect of the second channel, when not modulated, would be to increase the shot noise in the receiver, and also cause an increase in the low frequency interference noise. The inter-channel interference will depend upon the signal power and the linewidth of the LD in the second channel. Fig. 6.9 shows the degradation in the performance of the first channel when the second channel is operated at different power levels. When the optical power in the second channel is 1.5 dB lower than that in the first channel (required to obtain a BER of 10^{-9}), a penalty of 0.5 dB is observed in the received optical power. This power penalty is increased to 2.5 dB when the power in the second channel is 2.5 dB higher than in the first channel. To explain the power penalty caused by the second channel, the output of the bandpass filter is observed in the absence of the first channel and in the presence of the second channel. Fig. 6.10(a) and (b) show the power spectrum of the received signal at the output of the BPF when only the second channel is transmitted. In both figures, the lower trace corresponds to the receiver noise in the system when both channels are off, and the upper trace shows the increase in noise due to interference arising from the second channel. In Fig. 6.10(a), the received optical power in the second channel is 10 μW (1.5 dB lower than that in first channel). The interference signal in this case was measured at the output of the bandpass filter. As can be seen from Fig. 6.10(a), there is a 1.5 dB increase in electrical noise power. In the optical receiver, the photocurrent generated by the photodiode is directly proportional to the received optical power, while the electrical power is proportional to the square of the signal current. Therefore, a 1.5 dB increase in the electrical noise power will result in 0.75 dB optical power penalty. Further, when the signal power in the second channel was 1.5 dB higher than that in the first channel, the increase in noise was found to be 4 dB, which suggests that the power penalty in received optical power should be about 2 dB. Hence, the calculated power penalties in received optical power by observing the electrical spectrum agree well with the measurements in Fig 6.9.

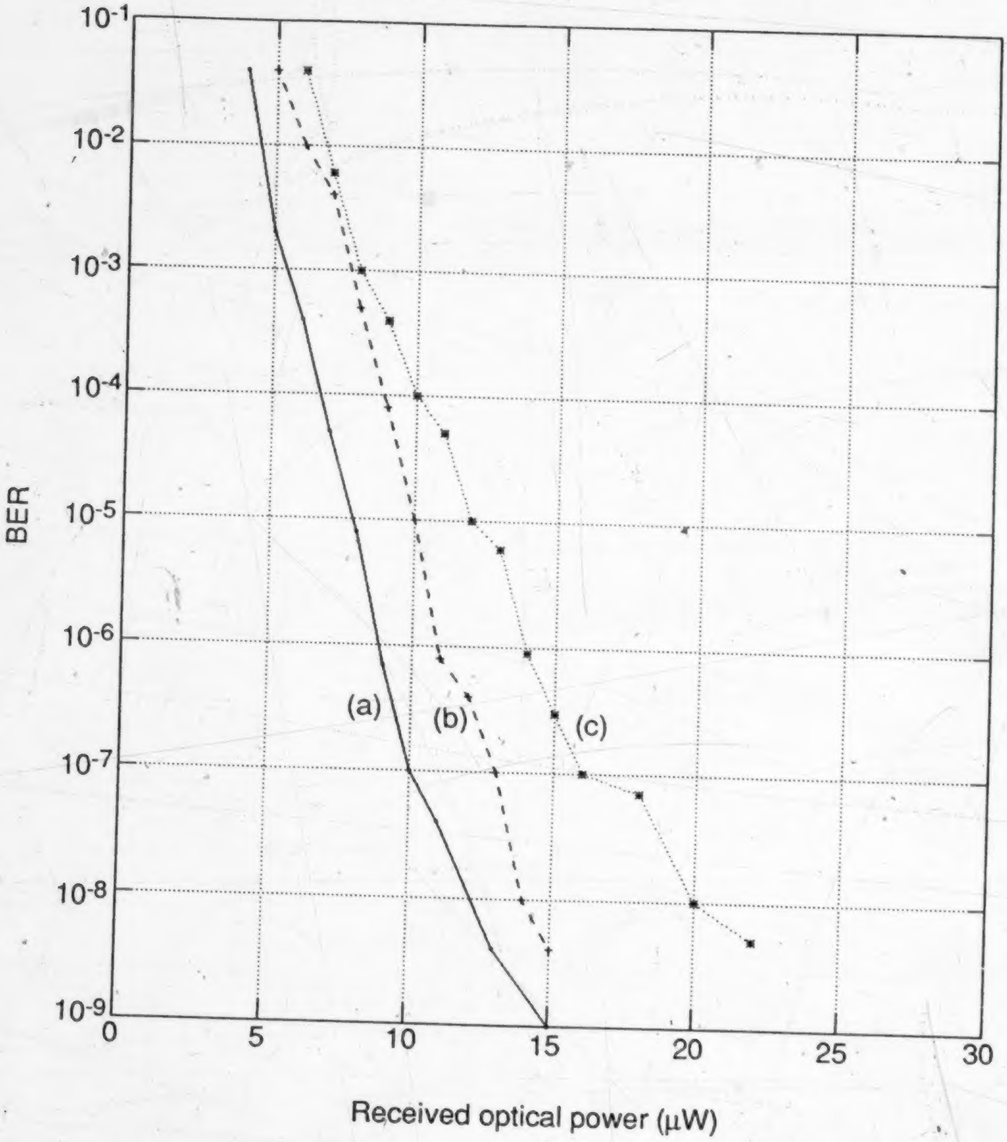

Fig. 6.9 BER as a function of the received average optical power for two channel transmission.

(a) Second channel off.

(b) Average optical power in second channel = 10 µW

(c) Average optical power in second channel = 20 µW

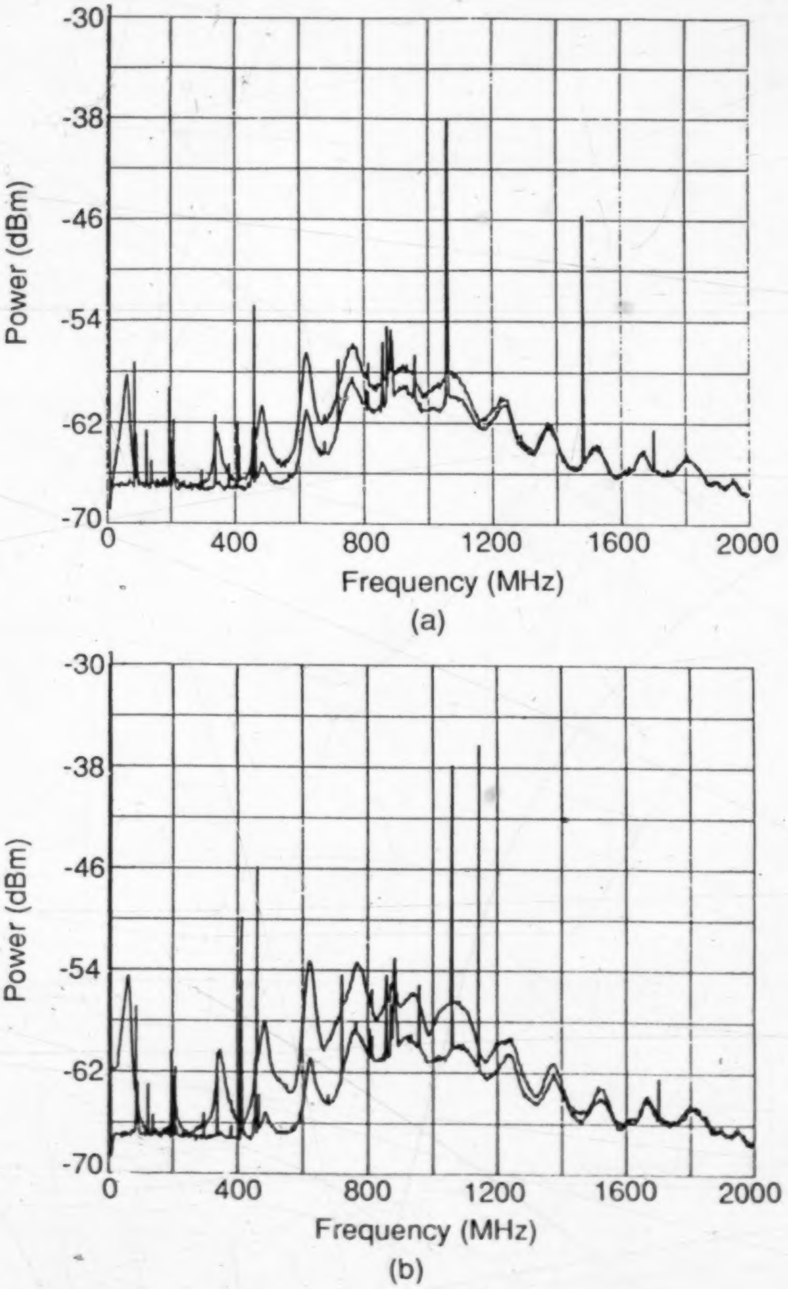

Fig. 6.10 Power spectrum of the interference signal caused by the second channel (upper trace). The lower trace corresponds to the receiver noise when both the channels are off.

(a) Average optical power in second channel = 10 μW

(b) Average optical power in second channel = 20 μW

6.4 SUMMARY

In this chapter, the performance of the DFSK system was studied. It was observed that the bandwidth of the IF filter should be greater than 600 MHz to efficiently transmit 45 Mb/s without any significant errors. This large IF bandwidth requirement is mainly due to the wide spectral spread of the LD at the transmitter. Further, it was observed that the error rate was pattern dependent, and that the baseline wander effect degraded the BER when more than two consecutive '1' bits or '0' bits were transmitted. The baseline wander effect at low modulation frequency was caused by the non-uniform frequency modulation characteristics of the LD and by the large RC time constant of the receiver pre-amplifier. Manchester encoding was used to alleviate this problem. Manchester encoding significantly improved the BER performance and no error rate floor was observed for a pseudo-random bit sequence of length 2^{23}-1.

The effects of interference and shot noise due to a second optical channel did not have any significant effect on system performance. However, this conclusion applies only to the case where the second channel was not modulated, due to receiver bandwidth constraints. To fully determine the inter-channel crosstalk, further measurements for different channel spacings are necessary. These measurements could be carried out using either an external modulator or a phase tunable DFB LD in the second channel.

CHAPTER 7 - SUMMARY AND CONCLUSIONS

Coherent systems, being capable of transmitting several wavelength division multiplexed channels, are the main focus of present research in optical communications. These systems can make maximum use of the enormous available fiber bandwidth. However, due to the unavailability of narrow linewidth lasers operating in a stable single mode, coherent systems have not yet been employed commercially. It is likely that, with the rapid developments in optical components technology, coherent systems will be deployed in the not too distant future.

In this thesis, we have described a DFSK system which uses optical delay line- or self-heterodyne detection. The concept of self-heterodyne detection originated from the Michelson interferometer, which is commonly used for the measurement of the linewidth of a LD. The interferometer consists of two optical paths with unequal lengths. When the optical signals in the two arms of the interferometer are combined, an intensity noise spectrum corresponding to the frequency noise spectrum is obtained. Recently, a self-heterodyne method was proposed, which basically consists of a fiber interferometer. In a DFSK system, the same principle is used, and the frequency modulated signal is converted into an amplitude modulated signal at the receiver. This is achieved by differentially encoding the output frequency of the LD, and adjusting the two arms such that the relative delay between the two paths is equal to one bit period. Since by using self-heterodyne detection the optical frequencies are converted into RF, an optical LO (laser) is not required at the receiver. This results in a low cost and simple receiver structure.

DFSK systems have some advantages and disadvantages in comparison with coherent systems. The main advantages are low receiver cost and simple transmitter and receiver design. However, coherent FSK systems, which use a tunable laser (LO) at the receiver, can transmit over a frequency range of thousands of GHz, whereas DFSK systems are limited to the bandwidth of the detector (about 10 to 20 GHz). In coherent systems, the maximum usable system bandwidth depends upon the tunability and spectral purity of the LO. The operating frequency of tunable LDs is difficult to stabilise to the required precision, and these devices are still in the research stage. On the other hand, a DFSK system does not require a LD at the receiver, so it can be built with commercially available components. Coherent FSK systems can detect lower levels of received optical power than DFSK systems. For a 100 Mb/s system, a coherent FSK system can detect about -46 dBm of received optical power, whereas the best receiver sensitivity for a DFSK receiver would be -38 dBm [20].

In DFSK systems, the bandwidth occupied by each channel is very much dependent on the laser linewidth. Broad linewidth LDs at the transmitter increase the required IF bandwidth, thus increasing (in a multi-channel system) the required channel spacing; this, in turn, decreases the number of possible channels. As for the case of IMDD systems, the number of possible channels can be greatly increased by using optical WDM.

The main objective of this thesis was to study the performance of the DFSK system. Therefore, an experimental system operating at 45 Mb/s was developed as a part of this project. It was observed that, for an IF linewidth to bit-rate ratio of 1.0, the bandwidth of the IF filter should be 13.5 times the bit-rate. Such a wide spectral spread of the IF signal will significantly reduce the number of channels that can be transmitted within the receiver bandwidth.

The BER of the DFSK system was observed to be pattern dependent. As the modulation frequency was decreased, the bit error rate became worse. These results suggest that the non-uniform FM characteristics and the base-line wander effect can cause severe degradation of receiver performance. One alternative to this problem is to use phase tunable or multi-electrode DFB lasers, which have a flat frequency response up to 1 GHz. The other alternative is to use line coding with very low dc content. Since phase tunable or multi-electrode DFB LDs are not commercially available, we used Manchester encoding to alleviate the detrimental effects of the non-uniform FM response. The performance of the system was satisfactory after the Manchester encoder and decoder were incorporated into the experimental system. A BER of 10^{-9} was achieved for a pseudo-random bit sequence of length 2^{23}-1. The lowest BER that could be obtained by the error detector was 10^{-9}. However, the BER curve in Fig. 6.8 indicates that no error rate floor occurred at 10^{-9}. Although Manchester encoding increased the effective bit period by a factor of two, the bandwidth of the IF filter did not need to be increased. This indicates that the frequency deviation index of the LD was almost constant over the range of modulating frequencies.

The effect of interference caused by a second channel on the performance of the first channel was also studied. A theoretical calculation suggested that the minimum required channel spacing should be 15 times the bit rate (700 MHz in our case). However, due to the limited receiver bandwidth and poor frequency modulation sensitivity of the LD, we could not apply the modulating signal. However measurements were carried out to observe the interference due to the presence of a second unmodulated channel. The power penalty was measured in the electrical domain as well as in the optical domain, and the results indicate that there was very little interference. When channel 2 was operated at a power level 1.5 dB higher than channel 1, a power penalty of 2 dB was observed.

In conclusion, an experimental DFSK system has been successfully implemented and tested. These systems can tolerate very broad LD linewidths at the transmitter without causing an error rate floor. It has been shown in this thesis that multi-channel DFSK systems are feasible. However, a relatively large bandwidth is required for each channel (13.5 times the bit-rate). Narrow linewidth LDs are required to maximise the number of channels that can be transmitted.

The following topics are suggested for further investigation in order to more fully explore DFSK systems:

(1) Use of a narrow linewidth DFB LD and an external modulator in each channel to eliminate the detrimental effects due to the broad linewidth and the non-uniform FM response of the LD.

(2) Determine if opto-electronic mixing at the receiver is suitable for a DFSK system and obtain the receiver sensitivity penalty.

(3) Carry out a detailed calculation of the effect of noise and cross-talk on the performance of DFSK systems. Develop a computer model for the receiver and determine the effects of laser frequency fluctuation.

(4) Set up a complete two-channel system in order to investigate more fully the effect of crosstalk between the two channels.

REFERENCES

[1] J.L. Gimlet, M.Z. Iqbal, C.E. Zah, J. Young, L. Curtis, R. Spicer, C. Caneau, F. Favire, S.G. Menocal, N. Andreadakis, T.P. Lee, and N.K. Cheung, "A 94 km, 11 Gb/s NRZ transmission experiment using a 1540 nm DFB laser with an optical amplifier and a PIN/HEMT receiver," in *Post deadline paper - Optical Fiber Communications OFC'89*, Houston, Texas, paper-PD16, 1989.

[2] S. Fujita, N. Henmi, I. Takano, M. Yamaguchi, T. Torikai, T. Suzaki, S. Takano, M. Ishihara, and M. Shikada, "A 10 Gb/s 80 km optical fiber transmission experiment using a directly modulated DFB-LD and a high speed InGaAS-APD," in *Post deadline paper - Opt. Fiber Communications OFC'88*, New Orleans, 1988.

[3] P.S. Henry, "Introduction to lightwave transmission," *IEEE Commun. Magazine*, vol. 23, no. 5, pp. 12-16, May 1985.

[4] R.C. Hopper, J.E. Midwinter, D.W. Smith, and I.W. Stanley, "Progress in monomode transmission techniques in the United Kingdom," *J. Lightwave Technol.*, vol. LT-1, no. 4, pp. 596-611, Dec. 1983.

[5] S.Y. Wang and D.M. Bloom, "100 GHz bandwidth planar GaAs Schottky photodiode," *Electron. Lett.*, vol. 19, pp. 554-55, 1983.

[6] J. Schlaper, C.B. Su, W. Powazinik, and R.B. Lauer, "20 GHz bandwidth InGaAs photodetector for long wavelength microwave optical links," *Electron. Lett.*, vol. 21, no. 11, pp. 469-70, May 1985.

[7] E.E. Basch and T.G. Brown, "Introduction to coherent optical fiber transmission," *IEEE Commun. Magazine*, vol. 23, no. 5, pp. 23-29, May 1985.

[8] T.E. Darcie, "Subcarrier multiplexing for multiple access lightwave networks," *J. Lightwave Technol.*, vol. LT-5, no. 6, pp. 1103-10, Aug. 1987.

[9] C. Desam, "Optical interference in lightwave subcarrier multiplexing systems employing multiple optical carriers," *Electron. Lett.*, vol. 24, no. 1, pp. 50-51, Jan. 1988.

[10] T.E. Darcie, R.M. Jopson, and R.W. Tkach, "Intermodulation distortion in optical amplifier from carrier density modulation," *Electron. Lett.*, vol. 23, no. 25, pp. 1392-94, Dec. 1987.

[11] T. Kimura, "Coherent optical fiber transmission," *J. Lightwave Technol.*, vol. LT-5, no. 4, pp. 414-27, Apr. 1987.

[12] T. Okoshi, "Recent advances in coherent optical fiber transmission," *J. Lightwave Technol.*, vol. LT-5, no. 1, pp. 44-51, Jan. 1987.

[13] B. Glance, "Polarisation independent coherent optical receivers," *J. Lightwave Technol.*, vol. LT-5, no. 2, pp. 274-76, Feb. 1987.

[14] L. Kazovsky, "Recent progress in phase and polarisation diversity coherent optical techniques," in *Proc. 13th European Conf. Opt. Commun. ECOC'87*, Helsinki, Finland, vol. 2, pp. 83-90, 1987.

[15] "Tutorials" *Opt. Fiber Commun. OFC'88*, New Orleans, 1988.

[16] L.G. Kazovsky, "Impact of laser phase noise on optical heterodyne communication systems," *J. of Optical Comm.*, vol. 7, no. 2, pp. 66-78, 1985

[17] M.J. Creaner, R.C. Steele, I. Marshall, G.R. Walker, N.G. Walker, J. Mellis, S.A. Chalabi, I. Sturgess, M. Rutherford, J. Davidson, and M. Brain, "Field demonstration of 565 Mb/s DFSK coherent transmission system over 176 km of installed fiber," *Electron. Lett.*, vol. 24, no. 22, pp. 1354-56, Oct. 1988.

[18] S. Saito, Y. Yamamoto, and T. Kimura, "Optical FSK heterodyne detection experiments using semiconductor laser transmitter and local oscillator," *IEEE J. Quantum Electron.*, vol. QE-17, no. 6, pp. 935-41, June 1981.

[19] R.S. Vodhanel, J.L. Gimlett, N.K. Cheung, and S. Tsuji, "FSK heterodyne transmission experiment at 560 Mb/s and 1 Gb/s," *J. Lightwave Tech.*, vol. LT-5, no. 4, pp. 1022-23, Apr. 1987.

[20] E. Emura, M. Shikada, S. Fujita, I. Mito, H. Honmou, and K. Minenural, "Novel optical FSK heterodyne single filter detection system using a directly modulated DFB laser diode," *Electron. Lett.*, vol. 20, no. 24, pp. 1022-23, Nov. 1984.

[21] E.J. Bachus, R.P. Braun, C. Casper, H.M. Foisel, E. Grobmann, B. Strebel, and F.J. Westphal, "Coherent optical multicarrier system," *J. Lightwave Tech.*, vol. 7, no. 2, pp. 375-85, Feb. 1989.

[22] R.E. Wagner, N.K. Cheung, and P. Kaiser, "Coherent lightwave systems for inter-office and loop feeder applications," *J. Lightwave Tech.*, vol. LT-5, no. 4, pp. 429-39, Apr. 1987.

[23] C.H. Henry, "Phase noise in semiconductor lasers," *J. Lightwave Technol.*, vol. LT-4, no. 3, pp. 298-311, Mar. 1986.

[24] T.E. Darcie, "Differential frequency deviation multiplexing for lightwave networks," *J. Lightwave Tech.*, vol. 7, no. 2, pp. 314-23, Feb. 1989.

[25] S. Kobayashi, Y. Yamamoto, M. Ito, and T. Kimura, "Direct frequency modulation in AlGaAs semiconductor lasers," *IEEE J. Quantum Electron.*, vol. QE-18, no. 4, pp. 582-95, April 1982.

[26] D.K.W. Lam and R.I. MacDonald, "GaAs optoelectronic mixer operation at 4.5 GHz," *IEEE Trans. Electron. devices*, vol. ED-31, no. 12, pp. 1766-68, Dec. 1984.

[27] C.H. Henry, "Theory of the linewidth of semiconductor lasers," *IEEE J. Quantum Electron*, vol. QE-18, no. 2, pp. 259-64, Feb. 1982.

[28] K. Kojima, K. Kayuma, and T. Nakayama, "Analysis of the spectral linewidth of distributed feedback laser diodes," *J. Lightwave Technol.*, vol. LT-3., no. 5, pp. 1048-55, Oct. 1985.

[29] U. Kruger and K. Petertmann, "The power independent part of the semiconductor laser linewidth, explained by the rate equations," in *Proc. 13th European Conf. Opt. Commun. ECOC'87*, Helsinki, Finland, pp. 131-34, 1987.

[30] W. Elsasser and E.O. Gobel, "Multimode effects in the spectral linewidths of the semiconductor lasers," *IEEE J. Quantum Electron.*, vol. QE-21, no. 6, pp. 687-92, June 1985.

[31] J.M. Osterwalder and B.J. Rickett, "Frequency modulation of GaAlAs injection lasers at microwave frequencies," *IEEE J. Quantum Electron.*, vol. QE-16, no. 3, pp. 250-52, March 1980.

[32] S. Yamazaki, K. Emura, M. Shikada, M. Yamaguchi, and I. Mito, "Realisation of flat FM response by directly modulating a phase tunable DFB laser diode," *Electron. Lett.*, vol. 21 , no. 7, pp. 283-85, Mar. 1985.

[33] Y. Yoshikuni and G. Motosugi, "Multielectrode distributed feedback laser for pure frequency modulation and chirping suppressed amplitude modulation," *J. Lightwave Technol.*, vol. LT-5, no. 4, pp. 516-22, April 1987.

[34] A.R. Chraplyvy, R.W. Tkach, A.H. Gnauck, B.L. Kasper, and R.M. Derosier, "8 Gbit/s FSK modulation of DFB lasers with optical demodulation," *Electron. Lett.*, vol. 25, no. 5, pp. 319-21, Mar. 1989.

[35] R.J.S. Pederson, I. Garrett, and G. Jacobsen, "Measurement of the statistics of DFB laser frequency fluctuations," *Electron. Lett.*, vol. 24, no. 10, pp. 585-86, May 1988.

[36] R.W. Tkach and A.R. Chraplyvy, "Phase noise and linewidth in an InGaAsP DFB laser," *J. Lightwave Technol.*, vol. LT-4, no. 11, pp. 1711-16, Nov. 1986.

[37] R.A. Linke and A.H. Gnauck, "High capacity coherent lightwave systems," *J. Lightwave Technol.*, vol. 6, no. 11, pp. 1750-69, Nov. 1988.

[38] I. Garrett and G. Jacobsen, "Theoretical analysis of heterodyne optical receivers for transmission systems using (semiconductor) lasers with non-negligible linewidth," *J. Lightwave Technol.*, vol. LT-4, no. 3, pp. 323-34, March 1986.

[39] A. Papulois, *Probability, random variables and stochastic processes,* McGraw-Hill Inc., pp. 115-118, 1984.

[40] G. Nicholson, "Transmission performance of an optical FSK heterodyne system with a single-filter envelope detection receiver," J. Lightwave Technol., vol. LT-5, no. 4, pp. 502-509, April 1987

[41] J.N. Proakis, *Digital communications*, McGraw-Hill Inc., pp. 15-16, 1983.

[42] J. Franz, "Evaluation of the probability density function and bit error rate in coherent optical transmission systems including laser phase noise and additive gaussian noise," *J. Optical Comm.*, vol. 6, pp. 51-55, 1985.

[43] K. Kikuchi, T. Okoshi, M. Nagamatsu, and N. Henmi, "Degradation of bit error rate in coherent optical communications due to spectral spread of the transmitter and the local oscillator," *J. Lightwave Technol.*, vol. LT-2, no. 6, pp. 1024-33, Dec. 1984.

[44] Y.K. Park, S.W. Granlund, C.Y. Kuo, M. Dixon, T.W. Cline, R.W. Smith, N.K. Dutta, and G. Vannucci, "Crosstalk penalty in a two channel ASK heterodyne detection system with non-negligible laser linewidth," *Electron. Lett.*, vol. 23, no. 24, pp. 1291-93, Nov. 1987.

[45] I. Garrett and G. Jacobsen, "The effect of laser linewidth on coherent optical receivers with non-synchronous demodulation," *J. Lightwave Technol.*, vol. LT-5, no. 4, pp. 551-60, April 1987.

[46] G. Jacobsen and I. Garrett, "Theory for heterodyne optical ASK receiver using square-law detection and post detection filtering," *IEE proceedings*, vol. 134, no. 5, pp. 303-12, Oct. 1987.

[47] P. Healy, "Effect of intermodulation in multichannel optical heterodyne systems," *Electron. Lett.*, vol. 21, no. 3, pp. 101-103, Jan. 1985.

[48] L.G. Kazovsky and J.L. Gimlett, "Sensitivity penalty in multichannel coherent optical communications," *J. Lightwave Technol.*, vol. 6, no. 9, pp. 1353-65, Sep. 1988

[49] L.G. Kazovsky, "Multichannel coherent optical communications systems," *J. Lightwave Technol.*, vol. LT-5, no. 8, pp. 1095-1102, Aug. 1987.

[50] Y. H. Cheng and T. Okoshi, "Effect of laser linewidth on crosstalk penalty in two channel ASK heterodyne detection system," *Electron. Lett.*, vol. 24, no. 14, pp. 830-31, July 1988.

[51] R.U. Hoffstetter, P.L. Heinzmann, and P. Gysel, "Novel multichannel transmission scheme using differential frequency shift keying modulation and optical delay line detection" in *Proc. 13th European Conf. Opt. Commun. ECOC'87*, Helsinki, Finland, vol. 1, pp. 341-44, 1987.

[52] G. Keiser, *Optical fiber communications*, McGraw-Hill Inc., pp. 150-79, 1983.

[53] S.D. Personick, "Receiver design for digital fiber optic communication systems - Part 1," *The Bell System Tech. Journal*, pp. 8443-74, July 1973.

[54] T. Okoshi, K. Emura, K. Kikuchi, and R. Th. Kersten, "Computation of bit error rate of various heterodyne and coherent type optical communication systems," *J. Opt. Comm.*, vol. 2, no. 3, pp. 89-94, 1981.

[55] G.P. Aggarwal and N.K. Dutta, *Long wavelength semiconductor lasers*, Van Nostrand Reinhold Company Inc., pp. 273-75, 1986.

[56] R.W. Tkach and A.R. Chraplyvy, "Line broadening and mode splitting due to weak feedback in single frequency 1.5 μm lasers," *Electron. Lett.*, no. 21, pp. 1081-83, Nov. 1985

[57] A. Somani, *Linewidth reduction and frequency modulation of a 1.3 micron semiconductor laser with strong frequency selective optical feedback*, M.Sc. Thesis, University of Alberta, Edmonton, Canada, 1988.

[58] G.P. Aggarwal and N.K. Dutta, *Long wavelength semiconductor lasers*, Van Nostrand Reinhold Company Inc., pp. 294-302, 1986.

[59] K. Sekartedjo, N. Eda, K. Furuya, Y. Suematsu, F. Koyama, and T. Tanbun-ek, "1.5 mm phase-shifted DFB lasers for single-mode operation," Electron. Lett., vol. 20, no. 2, pp. 80-81, Jan. 1984

[60] E. Patzak, A. Sugimura, S. Saito, T. Mukai, and H. Olesen, "Semiconductor laser linewidth in optical feedback configurations," *Electron. Lett.*, vol. 19, no. 24, pp. 1026-27, Nov. 1983.

[61] S. Ryu and S. Yamamoto, "Measurement of direct frequency modulation characteristics of DFB-LD by delayed self-homodyne technique," *Electron. Lett.*, vol. 22, no. 20, pp. 1052-54, Sep. 1986.

[62] A. Yariv, *Optical electronics*, HRW Inc., pp. 92-93, 1985.

[63] T. Okoshi, K. Kikuchi, and A. Nakayama, "Novel method for high resolution measurement of laser output spectrum," *Electron. Lett.*, vol. 16, no. 16, pp. 630-631, July 1980.

[64] K. Ogawa, "Consideration for optical receiver design," *IEEE J. on selected areas in Comm.*, vol. SAC-1, no. 3, pp. 524-32, April 1983.

[65] P. Runge, "An experimental 50 Mb/s fiber optic PCM repeater," *IEEE Trans. on Commun.*, vol. COM-24, no. 4, pp. 413-18, Apr. 1976.

[66] T. Muoi, "Receiver design for high speed optical fiber system," *J. Lightwave Technol.*, vol. LT-2, no. 3, pp. 243-67, June 1984.

[67] F. Mogensen, T.G. Hodgkinson, and D.W. Smith, "FSK heterodyne system experiments at 1.5 μm using a DFB laser transmitter," *Electron. Lett.*, vol. 21, no. 12, pp. 518-19, June 1985.

[68] B.L. Kasper, C.A. Burrus, J.R. Talman, and K.L. Hall, "Balanced dual detector receiver for optical heterodyne communication at Gbit/s rates," *Electron. Lett.*, vol. 22, no. 8, pp. 413-15, April 1986.

[69] I. Garrett, G. Jacobsen, E. Bodtker, R.J.S. Pedersen and J.X. Kan, "Weakly coherent optical systems using lasers with significant phase noise," *J. Lightwave Technol.*, vol. 6, no. 10, pp. 1520-25, Oct. 1988.

APPENDIX A

POWER SPECTRUM CALCULATION OF SELF-HETERODYNE LASER OUTPUT

The auto-correlation of the phase noise of the laser can be expressed as

$$R_{\Delta\phi}(t') = 2\pi\Delta f\cdot(T-|t'|) \qquad \text{for } |t'| \le T$$
$$= 0 \qquad \text{for } |t'| > T\ . \qquad \text{(A.1)}$$

After the laser output signal is delayed and mixed with itself, the auto-correlation function of the signal can be expressed as (see Eq. 3.12)

$$R(t') = \frac{A^2}{4}\cdot E\left[\{\exp\,(j\Delta\phi(t)) + \exp\,(-j\Delta\phi(t))\}\cdot\{\exp\,(j\Delta\phi(t + t') + \exp\,(-j\Delta\phi(t + t')))\}\right]. \qquad \text{(A.2)}$$

Simplifying the above equation we obtain,

$$R(t') = \frac{A^2}{4}\cdot E\left[\exp\,[j\{\Delta\phi(t) + \Delta\phi(t + t')\}] + \exp\,[j\{\Delta\phi(t) - \Delta\phi(t + t')\}] + \exp\,[j\{-\Delta\phi(t) + \Delta\phi(t + t')\}] + \exp\,[j\{-\Delta\phi(t) - \Delta\phi(t + t')\}]\right]. \qquad \text{(A.3)}$$

By definition, the characteristic function for two random variables x_1 and x_2 can be expressed as

$$\iota(a_1,a_2) = E\,[\exp\,\{j(a_1x_1 + a_2x_2)\}]\ . \qquad \text{(A.4)}$$

If the random variables are normally distributed and have a zero mean then the characteristic function is equal to

$$\iota(a_1,a_2) = \exp\left[-\frac{1}{2}\cdot(a_1{}^2\sigma_1{}^2 + 2r\sigma_1\sigma_2a_1a_2 + a_2{}^2\sigma_2{}^2)\right] \qquad \text{(A.5)}$$

where s_1 and s_2 are the variances of the random variables x_1 and x_2 respectively and r is the correlation coefficient defined by

$$r = \frac{C}{\sigma_1\sigma_2} \qquad \text{(C is the covariance coefficient)} . \tag{A.6}$$

If we set $\Delta\phi(t) = a_1$ and $\Delta\phi(t + t') = a_2$ in Eq. A.3, then $\sigma_1 = \sigma_2 = \sigma_\phi$, and $C = R_{\Delta\phi}(t')$.

From Eq. 3.10, ${\sigma_\phi}^2 = 2\pi\Delta\phi T$, where T is the delay time.

Substituting these values in Eq. A.2, we obtain,

$$R(t') = \frac{A^2}{4}\cdot\left[\iota(1,1) + \iota(1,-1) + \iota(-1,1) + \iota(-1,-1)\right] \tag{A.7}$$

Substituting value of ι from Eq. A.5 into Eq. A.7 we get,

$$\begin{aligned} R(t') = \frac{A^2}{4}\cdot\Bigg[&\exp\left\{-\frac{1}{2}\cdot[2{\sigma_\phi}^2 + \frac{R_{\Delta\phi}(t')}{{\sigma_\phi}^2}\cdot{\sigma_\phi}^2]\right\} + \exp\left\{-\frac{1}{2}\cdot[2{\sigma_\phi}^2\right. \\ &\left. - \frac{R_{\Delta\phi}(t')}{{\sigma_\phi}^2}]\right\} + \exp\left\{-\frac{1}{2}\cdot[2{\sigma_\phi}^2 + \frac{R_{\Delta\phi}(t')}{{\sigma_\phi}^2}\cdot{\sigma_\phi}^2]\right\} \\ &+ \exp\left\{-\frac{1}{2}\cdot[2{\sigma_\phi}^2 + \frac{R_{\Delta\phi}(t')}{{\sigma_\phi}^2}\cdot{\sigma_\phi}^2]\right\}\Bigg] \end{aligned}$$

$$= \frac{A^2}{4}\cdot 2\cdot\left[\exp\,[-{\sigma_\phi}^2 - R_{\Delta\phi}(t')] + \exp\,[-{\sigma_\phi}^2 + R_{\Delta\phi}(t')]\right] \tag{A.8}$$

Since the value of $R_{\Delta\phi}(t')$ depends upon t' (Eq. A.1), the auto-correlation of the self-heterodyned signal has to be calculated for different values of t'

Substituting the value of $R_{\Delta\phi}(t')$ and ${\sigma_\phi}^2$ from Eq. A.1 and Eq. A.7, it follows that

for $|t'| \le T$

$$R(t') = \frac{A^2}{2}\cdot\left[\exp\left(-2\pi\Delta fT - 2\pi\Delta fT + 2\pi\Delta f|t'|\right) + \exp\left(-2\pi\Delta fT + 2\pi\Delta fT - 2\pi\Delta f|t'|\right)\right]$$

$$= \frac{A^2}{2}\cdot\left[\exp\left(-4\pi\Delta fT + 2\pi\Delta f|t'|\right) + \exp\left(-2\pi\Delta f|t'|\right)\right]$$

$$= \frac{A^2}{2}\cdot\left[\exp\left(2\pi\Delta f|t'|\right)\cdot\left[\exp\left(-4\pi\Delta fT\right) + \exp\left(-4\pi\Delta f|t'|\right)\right]\right] \qquad (A.9)$$

and for $|t'| > T$, $R_{\Delta\phi}(t')$ is equal to 0. From Eq. A.8, it can be shown

$$R(t') = A^2\cdot\exp\left(-2\pi\Delta fT\right) . \qquad (A.10)$$

Normalising $R(t')$ with A^2, the Eq.A.9 and Eq. A.10 can be written as

$$R(t') = \frac{1}{2}\cdot\left[\exp\left(2\pi\Delta f\cdot(|t'| - 2T)\right) + \exp\left(-2\pi\Delta f|t'|\right)\right] \qquad \text{for } |t'| \le T$$

$$\qquad (A.11)$$

$$= \exp\left(-2\pi\Delta fT\right) \qquad \text{for } |t'| > T$$

The function in Eq. A.11 can be represented as follows

$$R(t') = \exp\left(-2\pi\Delta fT\right) + g(t') \qquad (A.12)$$

where

$$g(t') = \frac{1}{2}\cdot\left[\exp\left(2\pi\Delta f\cdot(|t'| - 2T)\right) + \exp\left(-2\pi\Delta f|t'|\right) - 2\cdot\exp\left(-2\pi\Delta fT\right)\right] \qquad \text{for } |t'| \le T$$

$$= 0 \qquad \text{otherwise} . \qquad (A.13)$$

It can be deduced from Eq. A.13 that $g(t')$ is a symmetric function. Therefore, its Fourier transform can be expressed as

$$F\{g(t')\} = G(f) + G(-f) \; . \tag{A.14}$$

$G(f)$ is the Fourier transform of $g(t')$ in the interval $0 < t' < \infty$.

Taking the Fourier transform of Eq. A.12 gives the power spectral density, which can be denoted as

$$S(f) = F\{R(t')\} = \exp\{-2\pi\Delta fT)\cdot\delta(f) + F\{g(t')\} \; . \tag{A.15}$$

$\delta(f)$, in the above equation, represents the dirac delta function.

In the next few steps, an expression for $G(f)$ is obtained.

By the definition of the Fourier transform

$$G(f) = \int_{-\infty}^{\infty} g(t')\cdot\exp\,(-j2\pi ft')\cdot dt' \; . \tag{A.16}$$

However, function $g(t')$ is defined between the limits $0 < t' < T$, therefore the above integral reduces to the following

$$G(f) = \int_{0}^{T} g(t')\cdot\exp\,(-j2\pi ft')\cdot dt' \tag{A.17}$$

$$G(f) = \frac{1}{2}\cdot\int_{0}^{T}\left[\exp\{2\pi\Delta f(t' - 2T)\} + \exp\{-2\pi\Delta ft'\} - 2\cdot\exp\{-2\pi\Delta fT\}\right]\cdot\exp\,(-j2\pi ft')\cdot dt'$$

$$= \frac{1}{2}\cdot\left[\int_0^T \exp\,(-4\pi\Delta fT)\cdot\exp\,\{2\pi\cdot(\Delta f + jf)\}\cdot dt' + \right.$$

$$+ \int_0^T \exp\,\{-2\pi\cdot(\Delta f + jf)t'\}dt'$$

$$\left. - \,2\cdot\int_0^T \exp\,\{-2\pi\Delta fT\}\cdot\exp\,\{-2j\pi ft'\}dt'\right]$$

$$= \frac{1}{2}\cdot\left[\exp\,(-4\pi\Delta fT)\cdot\left|\frac{\exp\,\{2\pi\cdot(\Delta f + jf)t'\}}{2\pi\cdot(\Delta f + jf)}\right|_0^T\right.$$

$$+ \left|\frac{\exp\,\{-2\pi\cdot(\Delta f + jf)t'\}}{-2\pi\cdot(\Delta f + jf)}\right|_0^T$$

$$\left. - \,2\cdot\exp\,(-2\pi\Delta fT)\cdot\left|\frac{\exp\,\{-j2\pi ft'\}}{-j2\pi f}\right|_0^T\right]$$

$$= \frac{1}{2}\cdot\left[\exp\,(-4\pi\Delta fT)\cdot\frac{\exp\,\{2\pi\cdot(\Delta f - jf)\cdot T\} - 1}{2\pi\cdot(\Delta f - jf)}\right.$$

$$+ \frac{1 - \exp\,\{-2\pi\cdot(\Delta f + jf)T\}}{2\pi\cdot(\Delta f + jf)}$$

$$\left. - \exp\,\{-2\pi\Delta fT\}\cdot\frac{1 - \exp\,\{-j2\pi fT\}}{j2\pi f}\right] . \tag{A.18}$$

After simplifying the above expression, it can be shown that

$$G(f) = \frac{1}{4\pi}\cdot\left[\exp\,(-2\pi\Delta fT)\cdot\exp\,(-2j\pi\Delta fT)\cdot\left\{\frac{1}{\Delta f - jf} + \frac{1}{\Delta f + jf} - \frac{1}{jf}\right\}\right.$$

$$\left. - \frac{\exp\,(-4\pi\Delta fT)}{\Delta f - jf} + \frac{1}{\Delta f + jf} - 2\cdot\frac{\exp\,(-2\pi\Delta fT)}{jf}\right]$$

$$= \frac{1}{4\pi}\cdot\left[\exp(-2\pi\Delta fT)\cdot\exp(-2j\pi\Delta fT)\cdot\left\{\frac{2\Delta f^2}{(\Delta f^2 + f2)\cdot jf}\right\} - \frac{\exp(-4\pi\Delta fT)}{\Delta f - jf} + \frac{1}{\Delta f + jf} - 2\cdot\frac{\exp(-2\pi\Delta fT)}{jf}\right]. \qquad \text{(A.19)}$$

Therefore, $F\{g(t')\} = G(f) + g(-f)$, is equal to

$$F\{g(t')\} = \frac{1}{4\pi}\cdot\left[\frac{2\cdot\exp(-2\pi\Delta fT)\cdot\Delta f^2}{(\Delta f^2 + f^2)}\cdot\left\{\frac{\exp(-2j\pi\Delta fT)}{jf} - \frac{\exp(2j\pi\Delta fT)}{jf}\right\} + \frac{1}{\Delta f + jf} + \frac{1}{\Delta f - jf} + 2\cdot\exp(-2\pi\Delta fT)\cdot\left\{-\frac{1}{jf} + \frac{1}{jf}\right\} - \exp(-4\pi\Delta fT)\cdot\left\{\frac{1}{\Delta f + jf} + \frac{1}{\Delta f - jf}\right\}\right]. \qquad \text{(A.20)}$$

After simplifying the above equation we get

$$F\{g(t')\} = \frac{1}{2\pi}\cdot\frac{\Delta f}{\Delta f^2 + f^2}\cdot\left[1 - \exp(-4\pi\Delta fT) - \frac{2\Delta f}{f}\exp(-2\pi\Delta fT)\cdot\sin(2\pi fT)\right]. \qquad \text{(A.21)}$$

Substituting this value in Eq. A.15, the power spectrum can be represented as follows

$$S(f) = \exp(-2\pi\Delta fT)\cdot\delta f + \frac{1}{2\pi}\cdot\frac{\Delta f}{\Delta f^2 + f^2}\left[1 - \exp(-4\pi\Delta fT) - 2\cdot\sin(2\pi fT)\cdot\exp(-2\pi\Delta fT)\cdot\frac{\Delta f}{f}\right] \qquad \text{(A.22)}$$

APPENDIX B

LASER DIODES AND THERMISTOR SPECIFICATIONS.

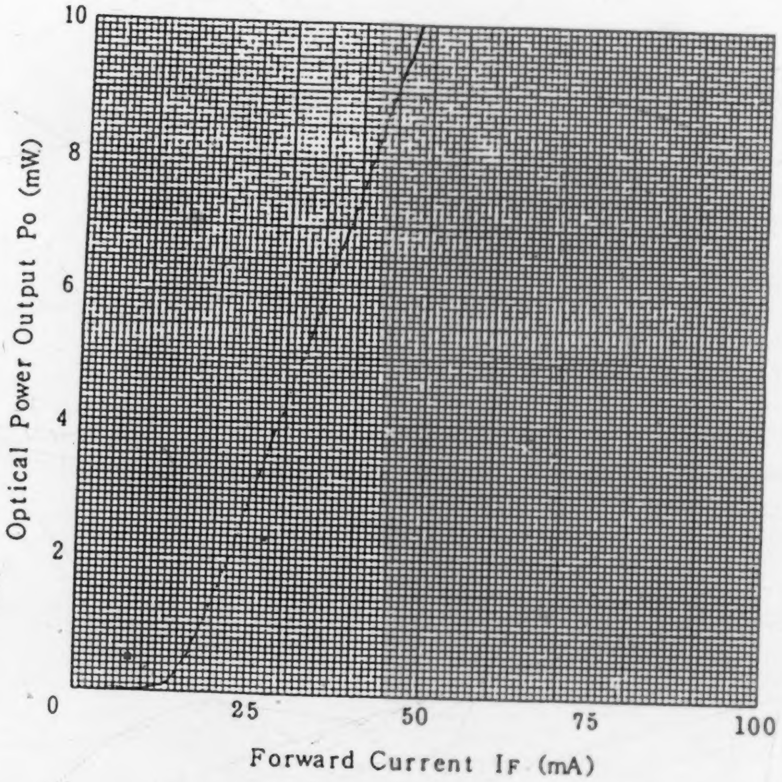

Fig. B.1 Optical output power as a function of the bias current for NEC DFB LD.

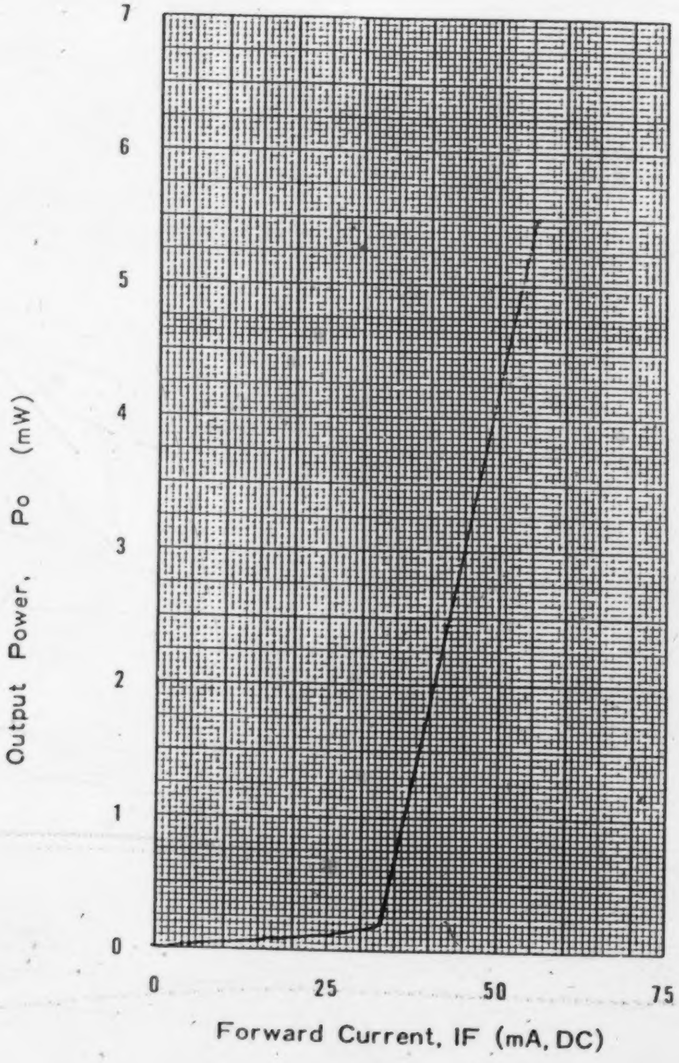

Fig. B.2 Optical output power as a function of the bias current for Fujitsu DFB LD.

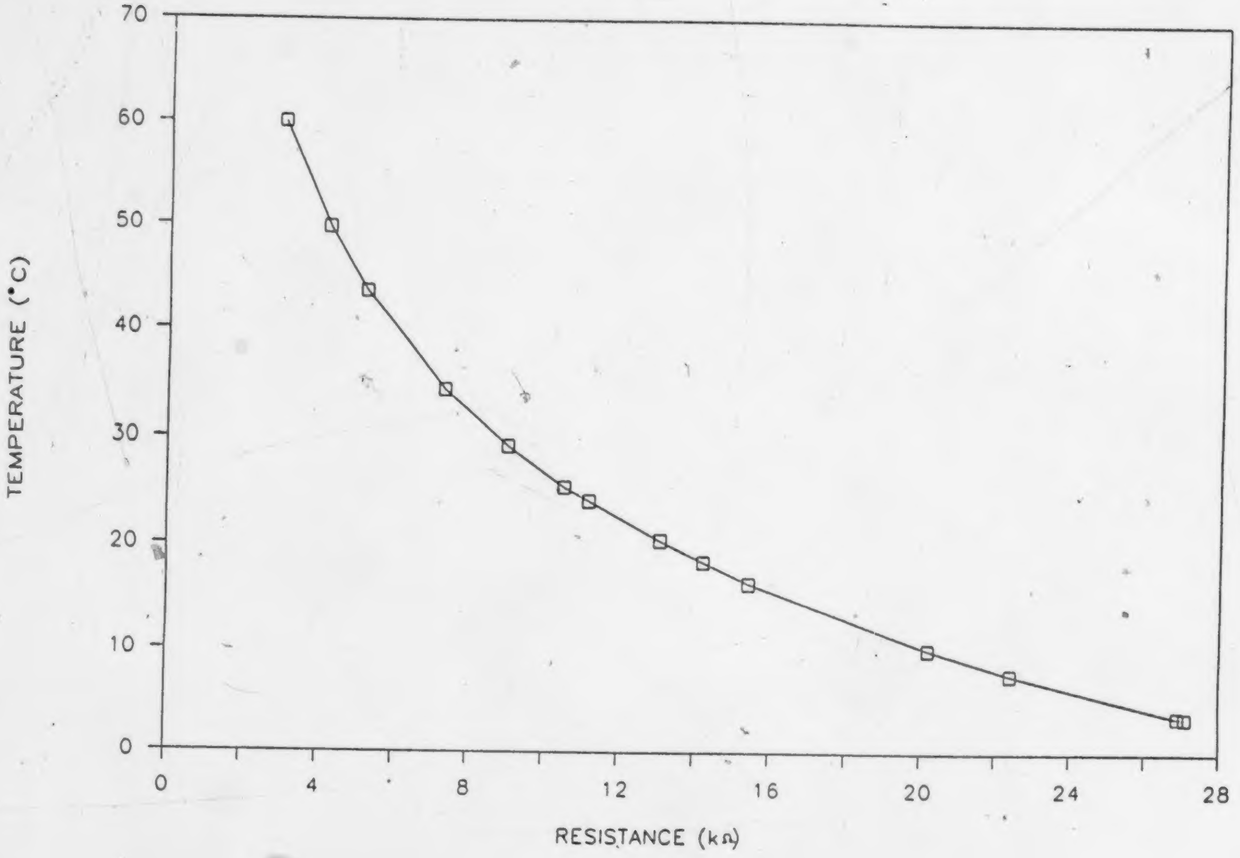

Fig. B.3 Thermistor resistance calibration.

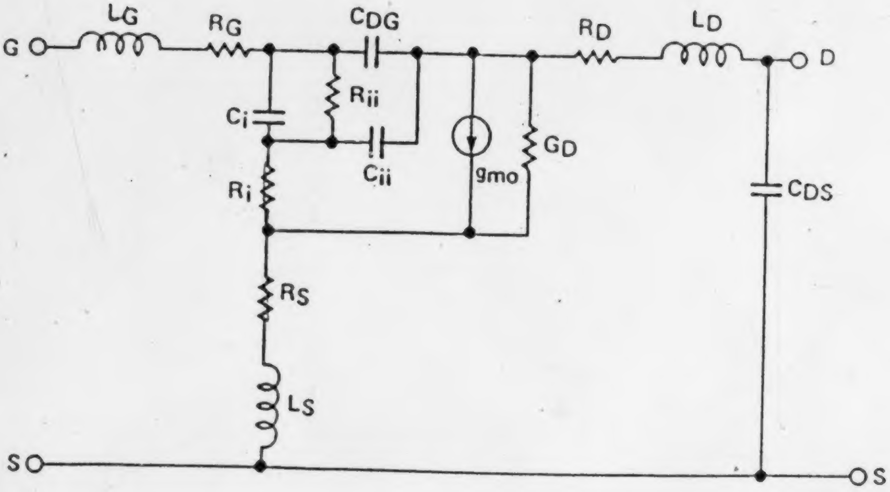
G
LG
RG
CDG
RD
LD
D
Ci
Rii
Cii
gmo
GD
CDS
Ri
RS
LS
S
S

COMPONENT	VALUE
L_G	0.005 nH
R_G	2.00 Ω
C_i	0.28 pF
R_i	1.6 Ω
C_{ii}	0.064 pF
R_{ii}	1M Ω
R_S	1.5 Ω
L_S	0.001 nH
C_{DG}	0.033 pF
R_D	1.5 Ω
L_D	0.005 nH
C_{DS}	0.03 pF
g_{mo} (mS)	-48.0 ℧
G_D (mS)	1.5 ℧

Fig. B.4 Equivalent circuit of the GaAs FET.